Experimental studies on the adsorption of SO_2 on volcanic ashes

von der Fakultät für Biologie, Chemie und Geowissenschaften
der Universität Bayreuth

zur Erlangung der Würde eines
Doktors der Naturwissenschaften
Dr. rer. nat.

Dissertation

vorgelegt von
Deborah Schmauß-Schreiner
Diplom-Geophysikerin
geboren in Zürich

Bayreuth, 2007

Vollständiger Abdruck der von der Fakultät für Chemie/Biologie/Geowissenschaften der Universität Bayreuth genehmigten Dissertation zur Erlangung des Grades eines Doktors der Naturwissenschaften (Dr. rer. nat.).

Die Arbeiten zur vorliegenden Dissertation wurden im Zeitraum von November 2002 bis Juni 2006 an der Geowissenschaftlichen Fakultät der Eberhard-Karls-Universität Tübingen und am Bayerischen Geoinstitut der Universität Bayreuth unter der Leitung von Prof. Dr. Hans Keppler durchgeführt.

Einreichung der Dissertation:	15.05.2007
Annahme der Dissertation:	23.05.2007
Tag des wissenschaftlichen Kolloquiums:	27.09.2007

Prüfungsausschuss:

Erstgutachter:	Prof. Dr. Hans Keppler
Zweitgutachter:	Prof. Dr. Friedrich Seifert
Vorsitzender:	Prof. Dr. Josef Breu
	Prof. Dr. Thomas Foken
	Prof. David Rubie, Ph.D.

Hiermit erkläre ich, dass ich die Arbeit selbständig verfasst und keine anderen als die von mir angegebenen Quellen und Hilfsmittel benutzt habe.

Ferner erkläre ich, dass ich anderweitig mit oder ohne Erfolg nicht versucht habe, diese Dissertation einzureichen. Ich habe keine gleichartige Doktorprüfung an einer anderen Hochschule endgültig nicht bestanden.

Bayreuth, Mai 2007

Danksagung

An erster Stelle will ich Herrn Prof. Hans Keppler danken für die Betreuung der Arbeit und für seine wichtigen Anregungen und hilfreichen Ideen, die mir halfen auch schwierige Arbeitsphasen zu überwinden.

Christoph Berthold (Tübingen) möchte ich für seine hilfreichen Anregungen in der Anfangsphase meiner Arbeit danken. Danken möchte ich auch Heinrich Taubald und Daniel Russ aus Tübingen, für die Durchführung der RFA-, bzw. der BET-Analysen. Dem Tübinger Werkstatt-Team um Norbert Walker und Barbara Meier, sowie dem Werkstatt-Team des BGI, Heinz Fischer und Stefan Übelhack, danke ich für die wertvolle Hilfe bei dem Aufbau und der Betreuung "meiner Apparatur" . Für die technische Hilfe in Bayreuth möchte ich mich besonders bei Detlef Krauße, Sven Linhardt und Kurt Klasinski bedanken.

Stefan Keyssner danke ich für seine unermüdliche Hilfe in organisatorischen Belangen. Bei Slava und Alexander, die meine Kollegen sowohl in Tübingen als auch Bayreuth waren, und auch bei Hubert möchte ich mich besonders für die kollegiale Unterstützung bedanken. Bei David Dolejš möchte ich mich besonders für seine Hilfe und seine große Geduld bei meinen Problemen mit der Thermodynamik bedanken und vor allem auch dafür, dass ich mit ihm das ein oder andere Ende der Welt erwandern und erradeln konnte.

An dieser Stelle möchte ich mich bei allen Kollegen, Mitarbeitern und Angestellten der Institute in Bayreuth und in Tübingen bedanken, die unerwähnt blieben, die aber mit ihrer großen Freundlichkeit und Hilfsbereitschaft die Arbeitsatmosphäre prägten.

Neben dieser kollegialen Hilfe war die "seelische Betreuung" durch meine lieben Freunde Jasmin, Jürgen und Alexander von besonderem Wert. Danke!

Zuletzt möchte ich meinen Eltern und meinen beiden Brüdern danken, dass sie mich während all der Zeit immer unterstützt und begleitet haben. Danke, dass ihr für mich da seid.

Contents

Zusammenfassung

In dieser Arbeit wurde die Adsorption von SO_2 auf synthetischen und auf natürlichen Gläsern untersucht. Die synthetischen Gläser waren rhyolithischer, dazitischer und andesitischer Zusammensetzung und wurden in einem Hochtemperaturofen bei 1600°C synthetisiert. Als natürliche vulkanische Gläser wurde Lipari Obsidian sowie Puu Waawaa Obsidian verwendet. Vor der Durchführung der Adsorptionsexperimente wurden die entsprechenden Gläser jeweils mittels einer Planetenkugelmühle unter trockenen Bedingungen zu Pulver vermahlen. Die Größe der Pulveroberfläche wurde mit einem Messgerät zur Oberflächenbestimmung durchgeführt.

Die Adsorptionsexperimente wurden bei −80°C, −20°C, 0°C, 25°C und bei 150°C durchgeführt, wobei ein Druckbereich von 0.1 bis 984 mbar abgedeckt wurde. Die Experimente bei 0°C ($p = 0.1 - 984$ mbar) und bei 25°C ($p = 38 - 938$ mbar) wurden mit andesitischem, dazitischem und rhyolithischem Glas durchgeführt. Weitere Experimente bei 150°C ($p = 118 - 538$ mbar), −20°C ($p = 75$ mbar) und −80°C ($p = 46$ mbar) wurden mit rhyolithischem Glas durchgeführt. Jeweils ein Experiment bei 0°C ($p = 31 - 949$ mbar) wurde mit dem Lipari Obsidian und dem Puu Waawaa Obsidian durchgeführt.

Die Menge an adsorbiertem SO_2 wurde volumetrisch bestimmt. Dazu wurde eine Apparatur entworfen, die aus mehreren Glasbehältern bekannten Volumens bestand. Im Vorfeld eines Experiments wurde das Glaspulver in die Apparatur eingebracht. Diese wurde dann mit reinem SO_2 geflutet. Die Menge an adsorbiertem SO_2 wurde aus dem Druckabfall in der Apparatur bestimmt, welcher aus der Adsorption von SO_2 resultierte. Der Gleichgewichtsdruck stellte sich dabei jeweils innerhalb weniger Stunden (4-5 h) ein.

Bei allen Experimenten wurde SO_2 auf der Oberfläche der Gläser adsorbiert. Die Adsorptionsisothermen der bei Zimmertemperatur durchgeführten Experimente wurden als Typ II Isotherme klassifiziert, was die Adsorption von SO_2 auf der Glasoberfläche in Multilayern nahe legt.

Die Adsorption-Desorptions Isothermen zeigten ein hysterese-artiges Verhalten,

was darauf hinweist, dass auch nach der Desorption erhebliche Mengen an SO_2 auf der Glasoberfläche verblieben. Bei den bei Raumtemperatur durchgeführten Experimenten verblieben nach der Desorption noch ca. 30 Gew% des ursprünglich adsorbierten SO_2 auf der Oberfläche. RFA-Messungen bestätigten dies. Die aus den BET-Isothermen abgeleiteten Werte für die Monolayerkapazität weisen darauf hin, dass die komplette erste Monolayer irreversibel gebunden wurde.

Die Menge an adsorbiertem Gas war stark temperaturabhängig, wobei die adsorbierte Menge mit sinkender Temperatur zunahm. Eine allgemeine Beschreibung der Temperaturabhängigkeit der Adsorption gelang mittels eines Regressionsmodells, das für jedes der synthetischen Gläser entwickelt wurde. Das Regressionsmodell wird durch folgende Gleichung beschrieben

$$\ln c = A\frac{1}{T} + B \ln p + C$$

wobei p der Druck in mbar ist, und wobei c die Menge an adsorbiertem SO_2 in mg/m^2 und T die Temperatur in Kelvin ist.

Entsprechend dem Regressionsmodell ist die Menge an adsorbiertem SO_2 proportional zu $\exp 1/T$. Die Faktoren A, B and C sind in Abhängigkeit von der Glaszusammensetzung gegeben, was darauf hinweist, dass auch die Menge an adsorbiertem SO_2 von der Glaszusammensetzung abhängig ist:

	Andesit			**Dazit**			**Rhyolith**		
	A	B	C	A	B	C	A	B	C
Wert	1644.78	0.29	-7.43	2139.52	0.29	-9.32	909.75	0.21	-4.48

Die Adsorptionsenthalpien ΔH_A der synthetischen Gläser wurden aus dem Regressionsmodell abgeleitet: Für Rhyolith ergab sich daraus ein Wert von $\Delta H_A \approx -7.6$ kJ/mol, für Dazit ein Wert von $\Delta H_A \approx -17.8$ kJ/mol und für Andesit ein Wert von $\Delta H_A \approx -13.7$ kJ/mol. Die Adsorptionsenthalpien ΔH_A der natürlichen Gläser wurden aus ihren BET-Isothermen abgeleitet. Sowohl für den Lipari Obsidian als auch für den Puu Waawaa Obsidian ergab sich ein Wert von $\Delta H_A \approx -15$ kJ/mol.

Die experimentell gewonnenen Adsorptionsdaten wurden sowohl von der BET-Gleichung für Multilayeradsorption, als auch von der Freundlich-Gleichung für Monolayeradsorption gut beschrieben. Aus den Adsorptionsexperimenten bei 0°C wurden folgende BET- und Freundlich-Konstanten bestimmt:

BET-Konstanten

	C	$\boldsymbol{V_m}$in cm^3/m^2
Rhyolith	93.4	0.32
Dazit	65.86	0.34
Andesit	72.02	0.29
Lipari Obsidian	16.00	0.33
Pu Waawaa Obsidian	20.10	0.47

Freundlich-Konstanten

	$\boldsymbol{1/a}$ in $\left(\ln\left(\frac{mg}{m^2}\right)/ln(mbar)\right)$	$\boldsymbol{\ln k}$ in$\left(\ln\left(\frac{mg}{m^2}\right)\right.$
Rhyolith	0.25	-1.01
Dazit	0.28	-1.47
Andesit	0.27	-1.37
Lipari Obsidian	0.62	-3.59
Pu Waawaa Obsidian	0.64	-3.32

Die experimentellen Ergebnisse lieferten sowohl Hinweise auf chemische (a) als auch auf physikalische (b) Adsorptionsmechanismen: (a) die Menge an adsorbiertem SO_2 scheint abhängig von der Glaszusammensetzung zu sein und die Adsorption ist teilweise irreversibel; (b) Adsorptionsmerkmale, wie beispielsweise der Isothermentyp und die Adsorptionsenthalpien, sind eher typisch für eine Physisorption.

Geologische Auswirkungen
Bei natürlichen Vulkanausbrüchen findet Adsorption von SO_2 auf vulkanischen Aschen hauptsächlich in der Region des sich horizontal ausbreitenden Plumes statt ("Umbrella Region").

Die Druck-/ Temperaturbedingungen, die dem Regressionsmodell entsprechend die Adsorption bestimmen, sind gegeben durch den in maximaler Aufstiegshöhe des Plumes herrschenden SO_2-Partialdruck, sowie durch die Temperatur der Stratosphäre in der gleichen Höhe.

Die Gesamtmenge des adsorbierten SO_2 ist abhängig von der zur Verfügung stehenden Aschenoberfläche der in dem Plume befindlichen Asche. Die zur Verfügung stehende Aschenoberfläche wiederum ist abhängig von dem anfänglichen Gas/Asche-Verhältnis $\sigma = m_{Gas}/m_{Asche}$ im vulkanischen Plume und von der Korngrößenverteilung der Asche. Es gilt, dass mit sinkendem $\sigma = m_{Gas}/m_{Ash}$ der Aschenanteil im Plume wächst. Dies wiederum hat einen Anstieg der zur Verfügung stehenden Aschenoberfläche im Plume zur Folge.

Die relative Menge an adsorbiertem SO_2, d. h die adsorbierte Menge im Vergleich zu der im Plume insgesamt vorhandenen Menge, ist abhängig von dem Anfangsgehalt an SO_2 im vulkanischen Gas ($x_{SO_2} = n_{SO_2}/n_{Gas}$): Je höher der molare Anteil an SO_2 im Ausgangsgas ist, desto geringer ist der Anteil an adsorbiertem SO_2 im Verhältnis zu der im Plume insgesamt zur Verfügung stehenden Menge. Daraus ergibt sich, dass im Falle einer starken Verdünnung des SO_2, beispielsweise durch Wasserdampf, SO_2 in erheblichem Ausmaß auf der vulkanischen Asche adsorbiert wird, so dass die Auswirkung derartiger Eruptionen auf die Umwelt eher gering sein dürfte. Wenn andererseits die SO_2-Konzentration im vulkanischen Gas hoch ist, ist es wahrscheinlich, dass das vorhandene SO_2 nur teilweise adsorbiert wird, womit ein ungleich stärkerer Einfluß auf das Klima zu erwarten ist.

Bei einem Plume Modell mit einem anfänglichen Gas/Asche-Verhältnis von $\sigma = 0.03$, mit einem Anfangsgehalt an SO_2 von 1.17 Mol%, sowie mit einer Aufstiegshöhe des Plume von 9 km und mit einer für eine Plinianische Eruption typischen Korngrößenverteilung, wird das eruptierte SO_2 komplett von der vulkanischen Asche adsorbiert. Es ist wahrscheinlich, dass das adsorbierte SO_2 bis auf die erste Monolayer wieder desorbiert wird, wenn der Partialdruck des SO_2 verdünnungsbedingt absinkt. Dieser Effekt ist vermutlich für den oftmals bei Satellitenmessungen beobachteten Anstieg der SO_2-Konzentration in der Stratosphäre 1–2 Tage nach einer Eruption verantwortlich.

Abstract

The adsorption of SO_2 on synthetic and on natural volcanic glasses was studied. The synthetic glasses were of rhyolitic, dacitic and andesitic composition and were synthesized in a high-temperature furnace at 1600°C. The natural volcanic glasses were Lipari obsidian and Puu Waawaa obsidian. Before the adsorption experiments the glasses were ground up to powder with a planetary mill under dry conditions. The surface area of the powder then was determined with a surface area analyzer.

Adsorption experiments were conducted at −80°C, −20°C, 0°C, 25°C and 150°C. The experiments covered a pressure range from $0.1 - 984$ mbar. The experiments at 0°C ($p = 0.1 - 984$ mbar) and at 25°C ($p = 38 - 938$ mbar) were performed with andesitic, dacitic and rhyolitic glass. Additional experiments with rhyolitc glass were carried out at 150°C ($p = 118 - 538$ mbar), −20°C ($p = 75$ mbar) and −80°C ($p = 46$ mbar). Two experiments were performed with Lipari obsidian and Puu Waawaa obsidian respectively, each at 0°C ($p = 31 - 949$ mbar).
During the experiments the amount that adsorbes on the surface of the respective glass powder was determined volumetrically. For this purpose a device was designed, consisting of several glass containers, each of known volume. The glass powder was stored in the device, which then was purged with pure SO_2. The amount of adsorbed SO_2 then was determined from the pressure drop in the device, that occured due to adsorption. Equilibrium pressure was reached within a few hours (4-5 h).

During all experiments SO_2 adsorbed readily on the surface of the glasses. The adsorption isotherms from the experiments at room temperature could be classified as type II isotherms, suggesting the formation of multilayers of SO_2 on the glass surface.

The adsorption-desorption isotherms showed a hysteresis-like behaviour, suggesting that remarkable amounts of SO_2 remain on the surface of the glass even after desorption. During the experiments at room temperature about 30 wt% of the originally adsorbed SO_2 remained on the surface after desorption. XRF measurements confirmed this. Moreover, the values for the monolayer capacity V_m

for SO_2, that were derived from the BET isotherms, suggest that the binding of nearly the whole first monolayer was irreversible.

The amount of adsorbed gas strongly depended on the temperature. It was shown that low temperatures promote the amount of adsorbed gas. An universal expression of the temperature dependence of adsorption was derived by developing a regression model for each of the synthetic glasses. The regression model is given as

$$\ln c = A\frac{1}{T} + B\ln p + C$$

where p is the pressure in mbar; c is the amount of adsorbed SO_2 in mg/m^2 and T is the temperature in Kelvin.

According to the regression model, the amount of adsorbed SO_2 varies with $\exp(1/T)$. The precoefficients A, B and C depend on the composition of the glass, indicating that the amount of adsorbed SO_2 also depends on the glass composition:

	Andesite			**Dacite**			**Rhyolite**		
	A	B	C	A	B	C	A	B	C
Value	1644.78	0.29	-7.43	2139.52	0.29	-9.32	909.75	0.21	-4.48

The heats of adsorption ΔH_A for the synthetic glasses were inferred from the regression model: For rhyolite $\Delta H_A \approx -7.6$ kJ/mol, for dacite $\Delta H_A \approx -17.8$ kJ/mol and for andesite $\Delta H_A \approx -13.7$ kJ/mol. The heats of adsorption ΔH_A for the natural glasses were inferred from their BET isotherms: For the Lipari obsidian and for the Puu Waawaa obsidian $\Delta H_A \approx -15$ kJ/mol.

The experimental adsorption data fitted both the BET equation, describing multilayer adsorption, and the Freundlich equation, desribing monolayer adsorption, quite well. For adsorption at 0°C the following BET and Freundlich constants were derived:

BET Constants

	C	$\boldsymbol{V_m}$ in cm^3/m^2
Rhyolite	93.4	0.32
Dacite	65.86	0.34
Andesite	72.02	0.29
Lipari obsidian	16.00	0.33
Pu Waawaa obsidian	20.10	0.47

Freundlich Constants

	$\boldsymbol{1/a}$ in $\left(\ln\left(\frac{mg}{m^2}\right)/ln(mbar)\right)$	$\boldsymbol{\ln k}$ in$\left(\ln\left(\frac{mg}{m^2}\right)\right.$
Rhyolite	0.25	-1.01
Dacite	0.28	-1.47
Andesite	0.27	-1.37
Lipari obsidian	0.62	-3.59
Pu Waawaa obsidian	0.64	-3.32

Experimental results provided evidence for both chemical (a) and physical (b) adsorption mechanisms: (a) the amount of adsorbed SO_2 appears to depend on the glass composition and the adsorption is partially irreversible; (b) adsorption relationships, like the isotherm type and the enthalpies of adsorption are more characteristic for physical adsorption.

Geological implications
Adsorption of SO_2 on volcanic ash during a natural volcanic eruption mainly occurs in the umbrella region of the volcanic plume. According to the regression model, adsorption is controlled by the partial pressure of SO_2 at the maximum ascent height of the plume and by the ambient stratospheric temperature prevailing at the maximum ascent height.

The total amount of adsorbed SO_2 depends on the total surface area of the ash suspended in the plume, which again results from the starting gas mass-fraction $\sigma = m_{Gas}/m_{Ash}$ in the eruption column and the grain size distribution of the ejected material. A decrease in $\sigma = m_{Gas}/m_{Ash}$ results in an increase of ash mass in the plume and thus in an increase of the total surface area of the ash suspended in the plume.

The relative amount of adsorbed SO_2 (e. g. the adsorbed amount, compared to the total amount in the plume) dependes on the initial SO_2 content $x_{SO_2} = n_{SO_2}/n_{Gas}$ in the volcanic gas: The higher the molar fraction of SO_2 in the starting gas, the less is the percentage fraction of adsorbed SO_2 relative to the totally available amount in the eruption column. Therefore, that if the SO_2 is strongly diluted for example by water vapour it will be adsorbed by the volcanic ash very strongly, so that the impact of such eruptions on the environment is likely to be small. On the other hand, if the SO_2 concentration in the volcanic gas is high, only part of it will be adsorbed and a much stronger impact of the eruption on climate is expected.

For a plume model with a starting gas mass-fraction $\sigma = 0.03$, an initial SO_2 content of 1.17 Mole%, an ascent height of the eruption column of 9 km and a grain size distribution typical for Plinian eruptions, the ejected SO_2 is completly adsorbed by the volcanic ash. It is likely, that the adsorbed SO_2 desorbs again, except for the first monolayer, when the partial pressure of SO_2 drops due to dilution. This effect probably accounts for the apparent increase in stratospheric SO_2 concentration 1–2 days after an eruption, which is often observed in satellite measurements.

Chapter 1

Introduction

1.1 The structure of the Earth's atmosphere

The atmosphere is divided into several regions (see Fig. 1.1). The troposphere, the stratosphere and the mesosphere are known as the homosphere. In the homosphere the mixing ratios of the trace constituents may vary greatly, but the gross composition is throughout dominated by N_2 and O_2 [25].

Troposphere:

The region closest to the earth's surface is called the troposphere. Temperature decreases with height as the solar radiation heats the Earth's surface, which warms in turn the air above it [6]. The heated air rises upwards and penetrates colder and denser air parcels. This leads to turbulent mixing of the air, eventually resulting in what we call 'weather'. The troposphere is characterised by its instability. Particles, injected into the troposphere are removed via precipitation or rainout within days or weeks.

Tropopause:

At the tropopause on top of the troposphere temperature reaches a minimum (e. g. 190 K-220 K). It serves as a 'cold trap' where water vapour freezes out, and so do gas/vapour aerosols. The height of the tropopause varies. Over equatorial regions it normally is higher than over polar regions [6]. In some regions it is difficult to locate the tropopause: stratospheric "tongues" are folded into the troposphere, allowing for mixing of tropospheric air with stratospheric air [6].

Stratosphere:

In the stratosphere temperature increases with altitude, reaching its maximum at the stratopause. This behaviour is called temperature inversion. The reason for this inversion is, that at this altitude the air mainly is heated by the absorption of ultraviolet radiation by ozone [6]. The concentration of ozone reaches its maximum in the lower stratosphere and decreases subsequently with height. The temperature inversion makes the stratosphere a very stable region, as vertical mixing hardly occurs. As it is relatively dry ($\Leftrightarrow$ 'cold trap' tropopause)

stratospheric aerosols are not rained out. Removal mechanisms are associated with stratospheric tongues. Via these tongues about 3/4 of the stratospheric aerosols are removed. The leaving 1/4 is removed by descending air at the poles. Independent from the exact mechanism, stratospheric aerosols have a residence time of several years [25].

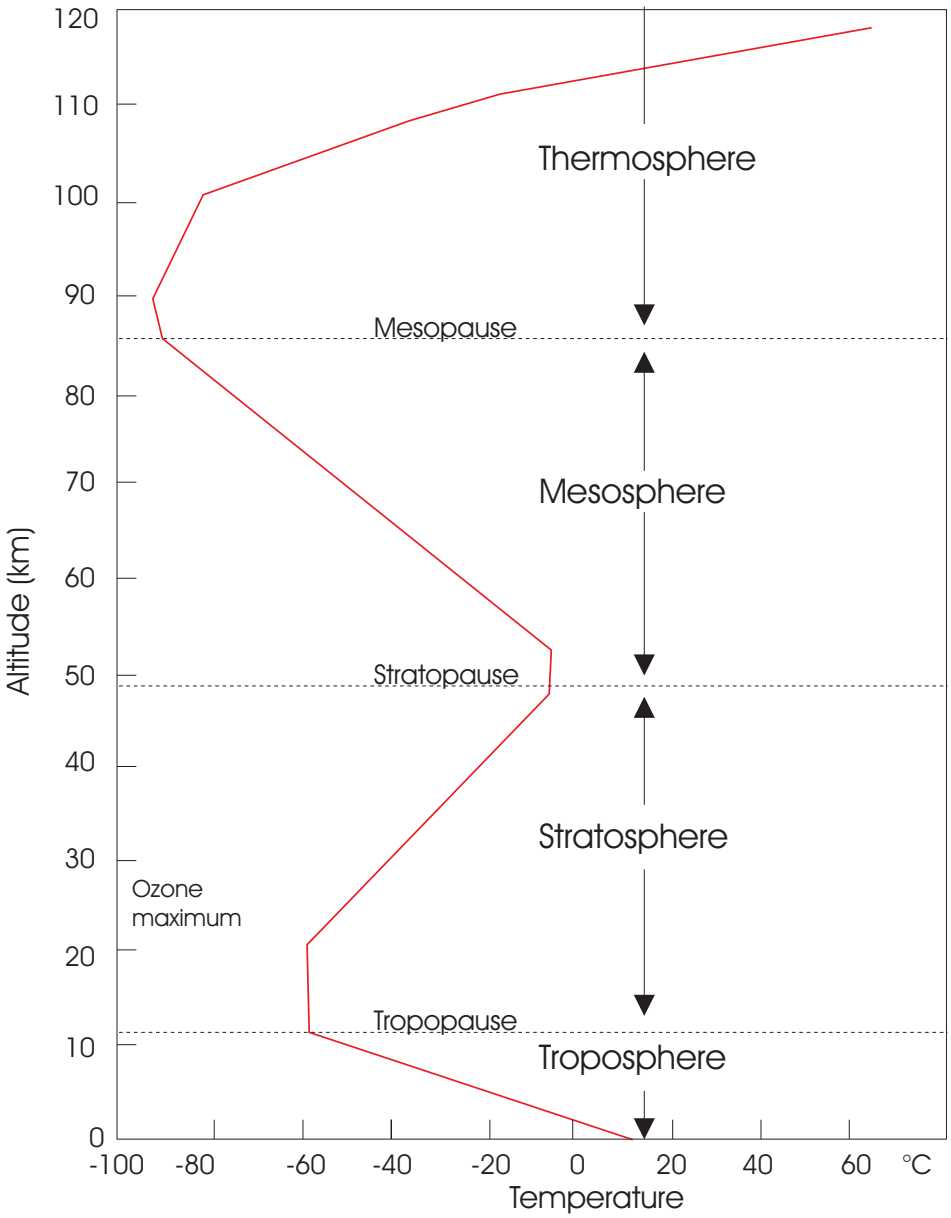

Figure 1.1: The earth's atmosphere. Redrawn after Ahrens [6], 1994.

1.2 Volcanic inputs to the atmosphere

During volcanic eruptions large quantities of ash and gases are injected into the atmosphere, affecting Earth's climate and disturbing the stratospheric chemical equilibrium [31]. The major gaseous species released are H_2O and CO_2, with smaller contributions of SO_2 and HCl (see Table 1.1).

Table 1.1: Adapted from Symonds et al. (1994) [39] and Textor et al. (2003) [42].

Characteristic composition of volcanic gases							
Species	H_2O	CO_2	SO_2	H_2S	HCl	HBr	HF
vol%	50-90	1-40	1-25	1-10	1-10	$\leq 10^{-3}$	$\leq 10^{-3}$

1.2.1 Measurement of volcanic gases

Studies of volcanic gases can deliver important information about the source of the magmas, as they directly escape from magma bodies. Modelling the global impact of individual eruptions necessarily requires information about the composition of the volcanic gases involved, as well as information about the dispersal pattern of the gases in the atmosphere.
Consequently, growing efforts are made in improving methods for gas measurements and monitoring. Data are acquired at the ground, from the air and from space with various instruments. The following section gives a brief overview on some measurement methods.

Direct measurements of volcanic gases

Directly sampling volcanic gases at high-temperature sites of volcanoes normally implies high risks. The risks are lava spraying, explosions, hot gases and the exposure to toxic gases. Accordingly sampling is not done on a continuous basis, but sporadically. The most common method for directly sampling volcanic gases is to collect them in a "Giggenbach bottle" [39] and analysing the mixture in the laboratory:
A titanium or quartz tube is inserted into the fumarole. When the hot gas is flowing through the tube it is connected to an evacuated bottle, the so called "Giggenbach bottle". It is partly filled with concentrated $NaOH$-solution. When the gas is bubbling through the solution, its acid constituents (e. g. CO_2, SO_2, HCl) are adsorbed by neutralization reactions. Gases that do not react with $NaOH$ collect in the headspace. A typical sampling setup is shown in Figure 1.2.

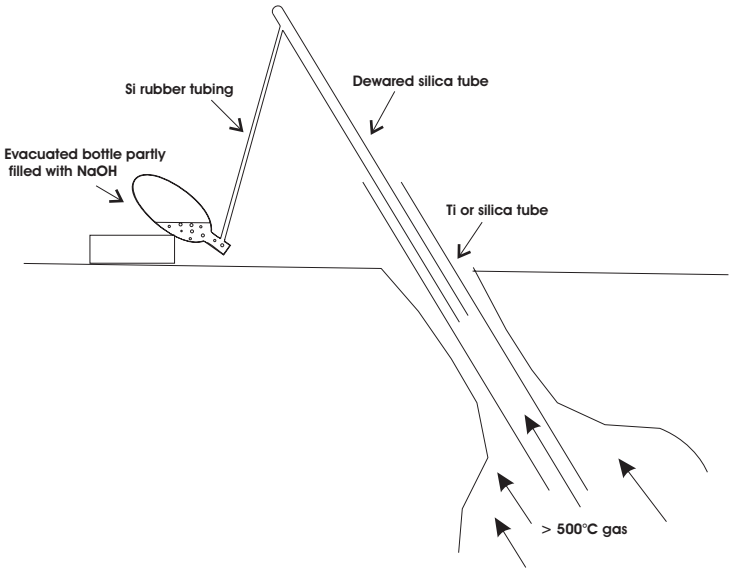

Figure 1.2: Sampling setup for collection of volcanic gas. Redrawn after [39]

Remote sensing measurements of volcanic gases

Since the last 30 years remote sensing techniques have been developed and improved. Volcanic gas can be studied by airborne and ground-based instruments and by satellite. Especially the remote determination of SO_2 has enjoyed great progress. The ground- and aircraft based COSPEC correlation spectroscopy and the total ozone mapping spectrometer (TOMS) satellite are important means for qualifying sulfur dioxide emissions from volcanic eruptions.

SO_2 measurements by COSPEC COSPEC (Correlation spectrometer) is an ultraviolet spectrometer. It measures the amount of solar ultraviolet light absorbed by sulfur dioxide in the plume and compares it with an internal standard. Light that enters the instrument travels through several mirrors, lenses and slits, eventually reaching a detector, where it is converted into electric pulses. If gas is in the pathway, COSPEC detects the amount of ultraviolet radiation adsorbed by SO_2, giving the concentration of SO_2 in the atmosphere [38]. COSPEC typically is placed in a vehicle or an aircraft which traverses the plume. Since the 1970s it has proved to be a powerful tool to estimate the total volcanic SO_2 emissions.

SO_2 measurements by TOMS The first ozone mapping spectrometer (TOMS) was launched in 1978 on board the Nimbus 7 satellite. TOMS originally was designed for mapping the distribution of the total ozone, by detecting absorption in the near UV region of the spectrum [38]. After the eruption of El Chichón in 1982, it was observed that erupted SO_2 absorbed in the same UV wavelengths as used for ozone. Subsequently TOMS was used to measure large injections of SO_2

into the stratosphere. Since then TOMS measured the SO_2 emissions from over 50 eruptions world-wide, with the Mount Pinatubo eruption being the biggest eruption with respect to the SO_2 emissions.

More remote sensing techniques COSPEC and TOMS provide fundamental data for studies on the SO_2 emissions from volcanoes. Data about other gas species, such as CO_2, H_2S, HCl and HF, on the other hand, are comparatively sparse. The ultraviolet part of the spectrum, as used by COSPEC and TOMS is not adaquate for measuring these gases. The IR region is more promissing, though IR measurements of gases may be affected by potential interferants, such as atmospheric water vapour or CO_2.
Three principal methods currently are being used:

Fourier transform infrared spectroscopy (FTIR)

Gas correlation radiometry

Thermal infrared multispectral scanner (TIMS)

An ***FTIR*** instrument works in the infrared region of the spectrum. It uses the sun or the crater as an IR source. FTIR works at a broad spectrum of absorbance, measuring gases being between the source and the instrument. The characteristic absorbance wavelength of gases makes it possible to infer the concentration of a particular gas. With the FTIR method it is possible to measure different gases at different wavelengths simultaneously.
Gas correlation radiometry is based on the same principle as the FTIR, focusing on a more narrow spectral region, rather than a broad spectrum. The gas correlation radiometry basically is used for measuring volcanic CO_2. The main problem with measuring volcanic CO_2 is the high atmospheric CO_2 background (365ppm)[38] .
TIMS also works in the infrared region of the spectrum. With TIMS, SO_2 plumes are mapped from an aircraft. TIMS establishs the possibility to make 2-dimensional maps of the SO_2 distribution and thus gives a better understanding of the heterogenous distribution of gas within the plume.

1.2.2 Volcanic ash

Tephra is the most abundant volcanic material [31]. Tephra is a general term for fragments of volcanic rock and lava of any size ejected from a volcano. The smaller grain size fraction of tephra, with a diameter less than 2 mm, is defined as volcanic ash. It basically consists of mineral fragments, glass shards, pumice grains and lithic fragments.

Grainsize distribution

Ash fall deposits are sampled shortly after ashfall has ended. As volcanic ash can travel large distances, the sampling locations range from a few kilometers to several hundred kilometers downwinds the volcano. Classically, the grains size for the coarse fractions is determined by the sieve method. For the fine fractions the pipette method, based on the "Stokes" sedimentation rates, is used. The residence time of particles in the eruption column is the lower, the larger the particles are (see Table 1.4). In general, the grainsize decreases exponentially with increasing distance from the volcano. However, the actual fallout distance of an individual particle is, amongst others, subject to the ascent height of the ashcloud, to the speed of dispersal (e. g. wind speed) and to its bulk density. Thus the grainsize distribution for a particular eruption may vary widely from the ideal exponential pattern (see Fig. 1.3).

Collecting further information, such as thickness of the accumulated ash, the textures and the maximum fragment size, makes it possible to estimate volumes of the erupted material and eruption dynamics [38].

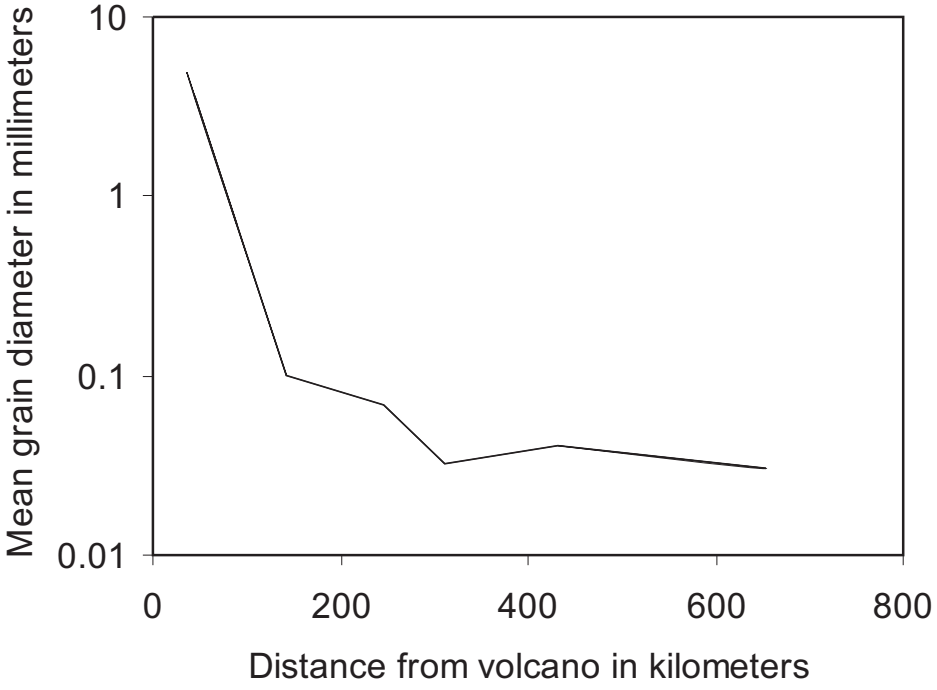

Figure 1.3: Mean grain size distribution for the Mount St. Helens eruption in 1980 [33].

Remote sensing of volcanic ash clouds

Volcanic plumes often are transported great distances, sometimes circling the globe several times. Remote sensing techniques, like the NEXRAD radar system, can be used to track eruption columns as they are transported in the atmosphere [38].

The NEXRAD system is a type of radar called C-band radar, which allows to detect ash between 1 mm and several centimeters in size up to 100 – 200 km from the volcano. For distances greater than 200 km weather satellites can observe the ash cloud, though it may be difficult to distinguish between eruption plumes and meteorological clouds [38].

1.3 Atmospheric effects of volcanic eruptions

In the past, major volcanic eruptions have produced significant cooling anomalies in the troposphere persisting for 1-3 years. An outstanding example for tropospheric cooling related to volcanic activity is the year after the eruption of Tambora (Indonesia) in April 1815, which is often referred to as the year 'without a summer' [27]. In the summer of 1816 and the subsequent summers of 1817 to 1819 an average temperature decrease of 0.4 to 0.7°C was observed throughout western Europe, ranking them among the coldest northern hemisphere summers over the last 600 years [29]. The eruption of Mt. Tambora was the most explosive eruptions of the last 10 000 years [25], having an explosivity index of 7 (see Table 1.3). The explosivity of an eruption is often expressed in terms of the **V**olcanic **E**xplosivity **I**ndex (VEI) (see Table 1.2). The VEI uses a logarithmic scale from 0 to 8, related to the volume of erupted material. It is applied to modern and ancient explosive eruptions. The VEI for ancient eruptions is mainly estimated from the volume of the deposits, and for modern eruptions mainly from the column height [25].

Table 1.2: Volcanic explosivity index. Adapted from Pyle et al. (2000) [28].

The volcanic explosivity index (VEI)									
VEI index	0	1	2	3	4	5	6	7	8
General description	Non explosive	Small	Moderate	Moderate large	Large	Very Large			
Volume of tephra (m^3)	10^4	10^6	10^7	10^8	10^9	10^{10}	10^{11}	10^{12}	10^{13}
Column height (km)	≤ 0.1	0.1-1	1-5	3-15	10-25	$\geq$25			

Another significant cooling anomaly in the troposphere following a major volcanic eruption is the cool summer in 1884. It succeeded the eruption of Krakatau (Indonesia, 1883)[27], which was an eruption of VEI=6. A similarly large eruption (VEI=6) in the younger past is the eruption of Mt. Pinatubo (Philippines in 1991). It also caused significant effects on global climate. The negative forcing after it exceeded the positive forcing associated with the 'greenhouse effect'. Consequently by mid-1992 the average global temperature dropped by about 0.5°C below the 1982-1990 average (see Fig. 1.4).

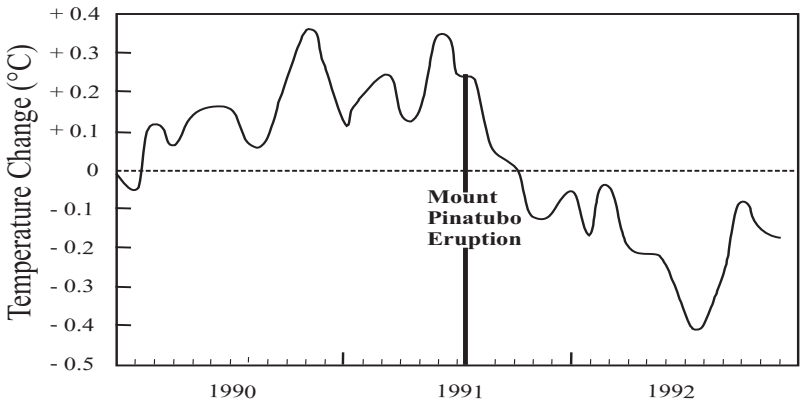

Figure 1.4: Changes in average global air temperature from 1990-1992. The dashed line depicts the 1981-1990 average. Source: C.D. Ahrens [6]

The cited eruptions were all classified as very large events, following the VEI index (see Table 1.3), e. g. they injected enormous amounts of tephra into the atmosphere (see Table 1.2). Explosive events of lower magnitude also can have significant influence on global climate. Notable in this context is the 1963 eruption of Mt. Agung in Indonesia. Though it has a comparatively low volcanic explosivity index of 4, it was one of the most important volcanic events during the twentieth century, as far as its effect on global climate is concerned [29]. The eruption of El Chichón in 1982 produced a temperature drop of 0.4 to 0.7°C in the northern hemisphere [29]. Having a VEI of 4 it hence also provides evidence that small-volume eruptions can have considerable influence on climate. Larger events like the eruption of Mt. St. Helens in 1980 (VEI=5) did not create global atmospheric perturbations [29]. In Table 1.3 the cited volcanic eruptions, among others are listed, with their VEI and the related temperature drop. Obviously, eruptions with small volcanic explosivity indices can produce climatic effects comparable to much larger events. That means, the explosivity of an eruption and the amount of ash injected into the stratosphere apparently are not the main factors in affecting Earth's climate. Considering that the stratospheric residence time of ash is relatively low, as it is removed within a few months [29], it seems plausible that it is not responsible for the long-term climatic effect of an eruption. Bursik et al. [11] estimated the residence time for ash with a grain-size distribution, typical for Plinian eruptions (see Table 1.4). For the model they present, they suggest that 95wt% of the ash precipitates within 5 days, the remaining amount within less than a month. Apparently the explosivity is not necessarily correlated with the climatic impact of an individual eruption. Instead it seems that the amount of sulfur injected into the stratosphere is crucial (see Table 1.3). Therefore it was proposed that the impact on global climate depends on the amount of sulfur (i. e. SO_2) released during an eruption [29].

Table 1.3: Stratospheric Aerosols and northern hemisphere cooling for major eruptions. Adapted from Rampino et al. 1984 [29]. Data for Pinatubo are taken from [24].

Eruption	Date	VEI	Stratospheric aerosol from optical depth (g of H_2SO_4)	Northern Hemisphere $\Delta T(^\circ C)$
Tambora (Indonesia)	1815	7	2×10^{14}	-0.4 to -0.7
Krakatau (Indonesia)	1883	6	5×10^{13}	-0.3
Santa Maria (Guatemala)	1902	6	$\leq 2 \times 10^{13}$	-0.4
Agung (Indonesia)	1963	4	$1 - 2 \times 10^{13}$	-0.3
St. Helens (USA)	1980	5	$\sim 3 \times 10^{11}$	0 to -0.1
El Chichón (Mexico)	1982	4	$1 - 2 \times 10^{13}$	-0.4 to -0.6
Pinatubo (Philippines)	1991	6	3×10^{13}	-0.7

Table 1.4: Grain size distribution of volcanic ashes. Adapted from Bursik et al. [11]. The grain-size distribution is typical of the grain-size distributions estimated for Plinian eruptions [11]. In this model the particles have a density of $2g/cm^3$ and fall from 12.9 km altitude.

Grain size (μm)	Weight percent	Residence time
1400	9.0	9.3 min
710	10.8	13.0 min
355	12.4	26.0 min
171	10.8	43.0 min
90	9.0	2.2 h
44	7.2	9.3 h
22	5.4	1.1 d
11	3.6	4.8 d
5.5	1.8	23.1 d

1.4 Volcanic aerosols

During volcanic eruptions large quantities of gases are released to the atmosphere (see Table 1.1). The most abundant gases released are H_2O and CO_2. SO_2 and HCl contribute in smaller quantities. Water vapour does not reach the stratosphere in considerable amounts as it hardly penetrates the 'cold trap' tropopause: The water condenses as the plume rises and cools, with ash particles serving as nuclei. It forms large water droplets or ice particles that eventually precipitate out of the atmosphere [25].

Direct measurements of chlorine suggest that volcanic eruptions hardly con-

tribute to the stratospheric chlorine budget [40]. Thus the increase of the global stratospheric chlorine abundance after the Mt. Pinatubo eruption, which released 4.5 Mt, was less than 1% [40]. Tabazadeh and Turco [40] proposed that supercooled water selectively scavenges HCl relative to SO_2 from the eruption column. After analyzing the physical chemistry, thermodynamics and microphysics of an eruption column, they concluded that the supercooled water dissolution mechanism is capable of reducing HCl vapour concentrations by up to four orders of magnitude [40]. This scavenging mechanism explains the absence of large volcanic injections of HCl into the stratosphere but it does not work for SO_2 [40] because of the much lower solubility of SO_2 in liquid water.
Thus only SO_2 is able to enter the stratosphere in considerable amounts. During the eruption of Mt. Pinatubo about 20 megatons of SO_2 were injected into the stratosphere, as measured by the total ozone mapping spectrometer (TOMS). In the stratosphere, SO_2 is photochemically transformed into H_2SO_4 [24] which rapidly condenses into H_2SO_4/H_2O aerosols. The conversion from SO_2 to sulphuric acid aerosol after the Mt. Pinatubo eruption took place within 30 days [24].

1.4.1 Climate effects

When reaching the Earth's atmosphere a number of interactions take place between solar radiation and the atmosphere (see Fig. 1.5). In the upper atmosphere most of the high-energy radiation is absorbed by gases. In particular, ultraviolet rays are absorbed by ozone in the stratosphere. Much of the remaining radiation is absorbed by the Earth's surface. The heated surface emitts infrared radiation, heating the air above. Some of the radiation is scattered by particles (e. g. aerosol) in the atmosphere, or is reflected from the Earth's surface, returning back to space. The albedo is a measure for the reflectivity of a surface or body. It is the ratio of radiation reflected from a surface to the amount incident upon it. The average albedo of the Earth is 30% [6]. An increase in the Earth's albedo results in a decrease of the Earth's temperature.
The albedo of an aerosol layer also depends on its optical depth [25]. In general a large number of small particles provide a greater optical depth than a small number of large particles. Tropospheric cooling after volcanic eruptions is closely related to an increase of optical depth (see Figure 1.4.1), which is due to an increase of stratospheric aerosols.

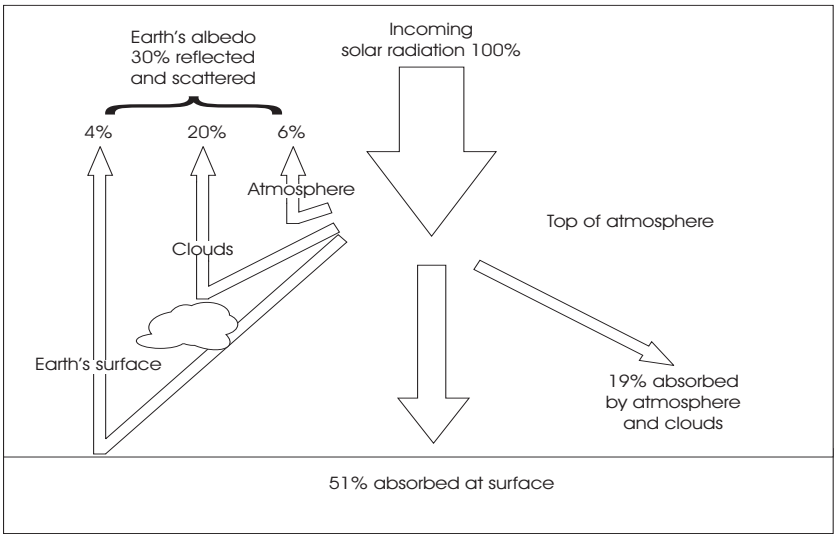

Figure 1.5: Average distribution of the solar radiation that reaches the Earth. Source: Ahrens [6].

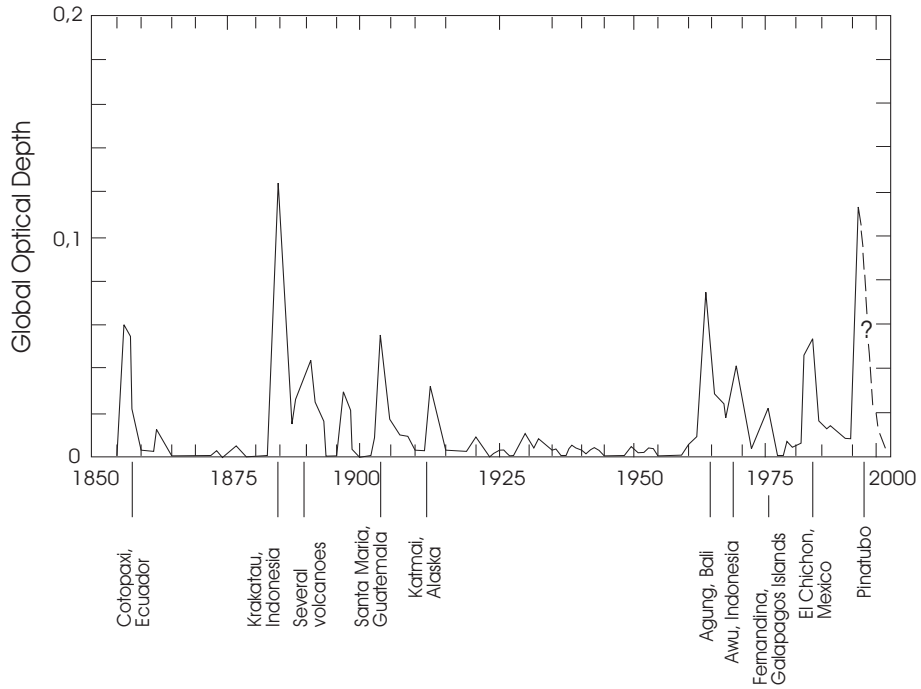

Figure 1.6: The estimated global stratospheric optical depth at $\lambda = 0.55\ \mu m$ for the period 1850 to 1993 (redrawn after S. Self et al. [36]). The peaks are the result of volcanic input of SO_2 into the stratosphere with rapid formation and subsequent decay of sulfate aerosols.

Stratospheric heating

Aerosol may absorb the infrared radiation coming from the Earth's surface, as well as solar radiation at near-infrared wavelengths. This results in heating the stratosphere. At high latitudes the surface temperature is lower, consequently there is less infrared radiation to heat the aerosol layer, making stratospheric heating typical for the tropics [25].
After the eruption of Mt. Pinatubo significant temperature anomalies in the lower tropical stratosphere were observed, where temperatures rose by nearly 2°C [25]. The warming lasted to the end of 1993.

Tropospheric cooling

In general volcanic eruptions are associated with a decrease of temperatures at the Earth's surface. Tropospheric cooling results from the injection of large quantities of sulphuric acid aerosols during volcanic events. The aerosols backscatter incident solar radiation into space, thus increasing the planetary albedo. This also involves an increase in the optical depth of the stratospheric aerosol layer as compared to before the eruption (see Fig. 1.4.1).
On one hand, volcanic aerosols absorb IR-radiation, resulting in stratospheric warming. On the other hand, they increase the Earth's albedo by reflecting incoming solar radiation. Whether the net effect of these two mechanisms is to cool or to warm the Earth depends on the particle size. The cooling effect overrides the warming effect if particles are less than 2μm in radius [25]. However, the size of stratospheric aerosols is restricted, as particles that are greater then 2μm settle out of the stratosphere within months. It therefore is unlikely, that volcanic aerosol particles are large enough to cause a long-term warming of the Earth [25]. There is significant evidence for global tropospheric cooling following volcanic eruptions (see Table 1.3). Recent major volcanic eruptions have produced significant cooling anomalies for 1 to 3 years. The Mt. Pinatubo eruption, which injected about 20 megatons of SO_2 into the stratosphere is believed to have caused the largest stratospheric perturbation of the last century. The negative forcing after it exceeded the positive forcing associated with the 'greenhouse effect'. By Mid-1992 the average global temperature dropped by about 0.5°C from the 1982-1990 average (see Fig. 1.4).

Ozone depletion

Ultraviolet radiation reaching the Earth's atmosphere is mainly absorbed by ozone (O_3) in the stratosphere. The natural destruction and formation of ozone in the stratosphere is driven by UV light. Ozone is formed when incoming ultraviolet radiation breaks molecular oxygen into atomic oxygen.

$$O_2 + \text{UV-light} \longrightarrow O + O$$

When a free oxygen atom encounters an oxygen molecule they may form ozone.

$$O_2 + O \longrightarrow O_3$$

On the other hand ozone is also destroyed by UV radiation by reverting the above reaction:

$$O_3 + \text{UV-light} \longrightarrow O_2 + O$$

Formation and destruction of ozone is a constant process maintaining an ozone layer. The ozone layer is crucial for the existence of life on Earth, as life is intolerant against UV rays. In the Mid-1980's scientists reported for the first time the development of a seasonal ozone hole over Antarctica in spring [22]. Chlorofluorocarbons (CFCs) compounds released into the atmosphere were identified as the chemical cause of this phenomenon [22]. CFCs transported to the stratosphere are broken down by UV-light to form "active" chlorine species, that destroy ozone in various catalytic cycles [25].
For the process of ozone destruction, heterogeneous chemical reactions are of special importance [22]. Heterogeneous reactions are chemical reactions occuring between atmospheric gases and solid or liquid aerosol particles. Heterogeneous chemistry responsible for the ozone hole occurs on polar stratospheric clouds (PSCs). For PSCs to form very low temperatures are needed, which occur only in the extremly cold vortex in the Southern Hemisphere [31]. With these cold temperatures H_2SO_4, HNO_3 and H_2O can freeze or exist as supercooled solutions. The resulting $H_2SO_4/HNO_3/H_2O$-ternary-solution-aerosols constitute the PSCs [31]. The polar stratospheric clouds provide active surface for heterogeneous reactions, during which relatively inactive forms of chlorine and bromine (e. g. HCl, $ClONO_2$, HBr and $BrONO_2$) are converted into active forms (e. g. Cl_2 and $BrCl$). Cl_2 and $BrCl$ break down to highly reactive Cl and Br that participate in catalytic reactions that finally destroy ozone [22].
The rate of reaction thereby is proportional to the surface area of the aerosols.

inactive	$\longrightarrow$	**active**	$\longrightarrow$	**reactive**	$\longrightarrow$	**removes**
HCl, HBr	heterogeneous	Cl_2, $BrCl$	photolysis	Cl, Br		O_3
$ClONO_2$, $BrONO_2$	reaction					

Injection of SO_2 during volcanic eruptions increases the total surface area of the polar stratospheric clouds available for heterogeneous reactions and thus enhances the ozone depletion.
The injection of 20Mt of SO_2 during the Mount Pinatubo eruption also resulted in ozone depletion:
Six months after the eruption global mean ozone began to show a significant downward trend that continued well into 1993 (see Fig. 1.7).

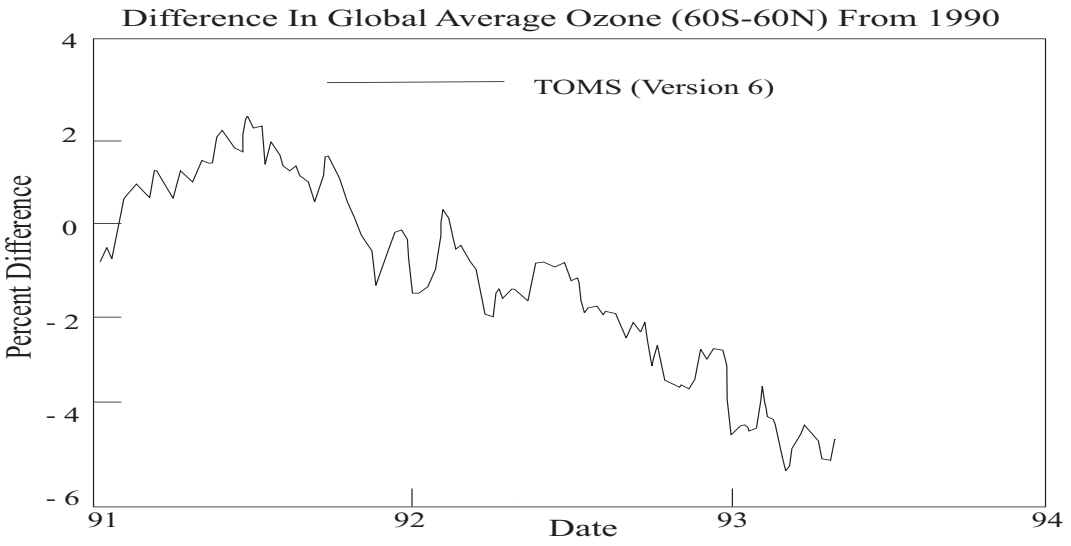

Figure 1.7: The daily differences of the globally averaged column ozone as compared to the pre-Pinatubo background. Redrawn after [35]

1.4.2 Scavenging of SO_2 by ash

The effect of volcanic activity on global climate is mainly controlled by the amount of SO_2 released into the atmosphere.
Only SO_2 has the potential to penetrate the tropopause and enter the stratosphere in considerable amounts. In the stratosphere, SO_2 forms sulfuric acid aerosols, which in turn produce an increase of the planetary albedo and so lead to a decrease of global temperatures. In addition, sulfur-bearing aerosols promote chemical reactions that result in ozone depletion.
The development of reliable climate models, that are needed to study anthropogenic effects, requires modelling the effects of volcanic eruptions. Studies on the interaction of SO_2 with ash, the most abundant volcanic product, seem to be of major importance, especially as field observations suggest that a significant fraction of SO_2 may be removed from the eruption column by adsorption on volcanic ash [32].

Volcanic ash has long been known to contain soluble salts [32]. Rose [32] showed by analyses of leachates that the salt concentrations are correlated to the surface area of the ash. Samples were mainly coated by $CaSO_4$ and $NaCl$. Rose inferred that droplets of dilute sulfuric acid/hydrochlorid acid attach themselves to ash particles, leaching soluble elements from the particle's silicate glass and minerals.

Evaluating leachate data from samples of the 1974 Fuego eruption, Rose inferred that 33% of the originally released S was scavenged by ash. In his approach Rose assumes that the conversion of SO_2 to H_2SO_4 proceeds very rapidly (half-time

for the conversion reaction: 0.07h)[32] .

However, remote measurements after the Mount Pinatubo eruption give a characteristic half-time rate of about 33 days [36].

90wt% of the ash is supposed to fall out within 5 days after the eruption [11]. Assuming a conversion rate from SO_2 to H_2SO_4 of one month, the scavenging mechanism proposed by Rose seems to be unplausible.

I propose that SO_2 is removed from the eruption column particularly by physical adsorption on volcanic ash.
In order to establish a predictive model of sulfur adsorption during volcanic eruptions I carried out the first experimental study on the adsorption of SO_2 on glasses of rhyolitic, dacitic and andesitic composition.
My study attempts to provide a basic understanding of the mechanisms by which sulfur interacts with volcanic ash. The dependence of adsorption on parameters such as the bulk chemical composition of the ash, temperature, partial pressure of the SO_2, etc. were studied.

Chapter 2

Principles of adsorption on solid surfaces

2.1 Adsorption at the solid-vapour interface

Adsorption is a process where molecules from the gas phase or from solution bind on a solid or liquid surface. The molecules that bind to the surface are called *adsorbate*, the substance, that holds the adsorbate is called *adsorbent*. The process when the molecule sticks to the surface is called *adsorption*. Removal of the molecules from the surface is called *desorption*.
There are two fundamental types of adsorption:

multilayer adsorption and monolayer adsorption

For monolayer adsorption the adsorbate covers the surface of the adsorbent with only one layer of molecules (see Fig. 2.1).
Multilayer adsorption means that several layers of the adsorbate develop onto the surface. For the formation of the first layer the attractive forces between the adsorbate and the adsorbent are decisive. The adsorption of subsequent layers is dominated by the interactions between the adsorbate molecules. Multilayer adsorption therefore basically is a condensation process. The attraction forces between the adsorbate molecules cause the gas to condense into a liquid-like film on the top of the first layer.

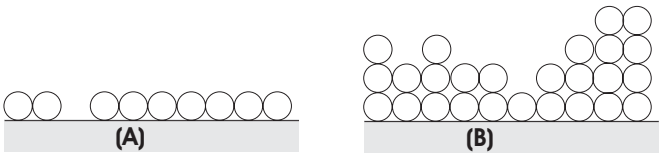

Figure 2.1: Illustration of (A) monolayer and (B) multilayer adsorption

The nature of bonding
In 1931 Taylor [41] suggested to differentiate between two radically different types of adsorption:

chemisorption and physisorption

Chemisorption involves specific chemical bonding. Physisorption does not imply specific forces, instead the adsorbate is bound by physical (e. g . van-der-Waals) forces.
Adsorption of vapour onto a solid surface is a spontaneous process, that means the Gibb's free energy change (ΔG) of the process must be negative. However, adsorption implies that the adsorbed molecules lose a degree of freedom. They become restricted to two, instead of three degrees of freedom, meaning that their entropy (S) decreases.
From the thermodynamic relationship for the Gibb's free energy

$$\Delta G = \Delta H - T\Delta S$$

it follows, that for ΔG to be negative, ΔH needs to be negative. Adsorption therefore has to be an exothermic process.

The heat of adsorption ΔH_A for physisorption generally is of the same magnitude as the heat of condensation (ΔH_L) for the gas (e. g. about -8 to $-40 kJ/mol$). For chemisorption the heat of adsorption rises to about -60 to $-400 kJ/mol$, which is comparable to chemical reaction enthalpies.
Physical adsorption normally does not require activation energy. The process is diffusion controlled, e. g. it basically occurs as soon as vapour molecules arrive at the surface. Physisorption is reversible and equilibrium will be reached rapidly.
Chemisorption generally needs some activation energy, therefore being potentially slower. The process may not be reversible and as very specific forces are involved, chemisorption always is restricted to the formation of one monolayer.

2.2 Adsorption isotherms

2.2.1 Classification of adsorption isotherms

Adsorption isotherms are plots of the amount of gas that adsorbs on a surface as a function of the pressure of the gas at constant temperature.
In 1945, Brunauer [9] established the classification of isotherms, as seen during adsorption of gases on solids, into one of the 5 different forms shown in Figure 2.2.

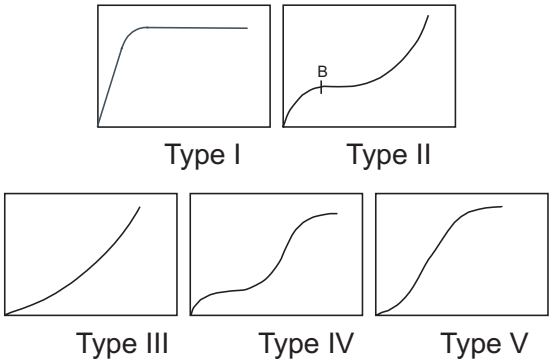

Figure 2.2: The 5 adsorption isotherms after Brunauer[9]

Type I
The amount of adsorbed gas increases with increasing pressure until some limiting value. That limiting value usually is related to the attainment of complete monolayer coverage. Type I isotherms are characteristic for monolayer adsorption and are usually denoted by *the Langmuir type* . Chemisorption always exhibits type I adsorption.
Type I isotherms are found in systems with strong interaction between the adsorbate and the adsorbent, but relatively weak nonspecific attraction between the adsorbate molecules themselves.
Type II
The first part of the isotherm corresponds to the equivalent part of type I adsorption: The amount of adsorbed gas rapidly rises with growing pressure. The isotherm starts to level off when monolayer coverage is attained. Point B on the curve is identified with complete monolayer coverage. The subsequent increase is due to multilayer formation because of strong adsorbate - adsorbate interactions.
Type II isotherms are characteristic for multilayer physisorption on nonporous solids.
Type III
These isotherms are relatively rare and correspond to systems, where the adsorbate-adsorbate interactions are much stronger than the interactions between adsorbate and adsorbent.

The initial uptake of gas molecules is slow until surface coverage is sufficient, so that the interactions between the adsorbed and the free adsorbate molecules start to dominate the process.

Type IV, Type V

Typ IV and V are modifications of type II and III, respectively, due to the presence of pores.

2.2.2 Monolayer adsorption

The Langmuir adsorption isotherm

The Langmuir isotherm is an important model for monolayer coverage [26],[23]. It has found wide application due to its simplicity .

The Langmuir model is based on the assumption that adsorption is restricted to monolayer coverage. One further assumption is, that adsorption is localized, implying specific adsorption sites. Interactions are supposed to happen between these specific sites and the adsorbate molecules. The heat of adsorption ΔH_A is supposed to be independent of the amount of adsorbed material.

In Langmuir's model the *rate of adsorption (r_A)* is proportional to the partial pressure (p) of the adsorbate and the number of unoccupied adsorption sites n_A.

$$r_A = k_A\, p\, n_A \tag{2.1}$$

$$r_A = k_A\, p\, (N - n) \qquad (with\ n_A = (N - n)) \tag{2.2}$$

N: total number of adsorption sites, n: number of occupied sites, k_A: rate constant.

The *rate of desorption* r_D is proportional to the number of occupied sites (n).

$$r_D = k_D n \tag{2.3}$$

k_D : rate constant

At equilibrium the rate of adsorption equals the rate of desorption, so that

$$k_A\, p(N - n) = k_D\, n \tag{2.4}$$

$$\Leftrightarrow$$

$$K_{eq} = \frac{k_A}{k_D} = \frac{n}{p(N - n)} \tag{2.5}$$

K_{eq} is the equilibrium constant and is defined as the ratio of k_A and k_D.
Q is the fraction of adsorption sites occupied at a given time and is given by

$$Q = \frac{n}{N} \tag{2.6}$$

Applying equation 2.5 this yields

$$Q = \frac{K_{eq}p}{1 + K_{eq}p} \tag{2.7}$$

Equation 2.7 describes the ***Langmuir adsorption isotherm***.
The Langmuir isotherm can be rearranged to the linearized form

$$n^{-1} = N^{-1} + (K_{eq}Np)^{-1} \tag{2.8}$$

A plot of n^{-1} versus p^{-1} gives a straight line, if the Langmuir model describes the adsorption process. The slope gives values of K_{eq} and the intercept yields N.

The Langmuir model describes monolayer physisorption, but it can also be applied to chemisorption.

The Freundlich Adsorption Isotherm

Another classical approach describing monolayer physisorption, especially at moderate pressures, is the ***Freundlich adsorption isotherm*** [26],[23].

$$V = kp^{1/a} \tag{2.9}$$

V is the volume of adsorbed gas, k and a are constants.
Originally, the Freundlich isotherm was derived empirically. Nevertheless, it also can be derived theoretically by assuming that the heat of adsorption is not a constant but varies exponentially with the extend of surface coverage [26]. Equation 2.9 can be linearized by taking the logarithm on both sides.

$$\ln V = \ln k + \frac{1}{a} \ln p \tag{2.10}$$

A plot of $\ln V$ versus $\ln p$ should give a straight line. Equation 2.9 fits adsorption data taken over a small pressure range quite well, but is only of little predictive value.

2.2.3 Multilayer adsorption

The Brunauer-Emmett-Teller (BET) Isotherm

The Langmuir isotherm and the Freundlich isotherm are restricted to systems, where adsorption stops at monolayer coverage.

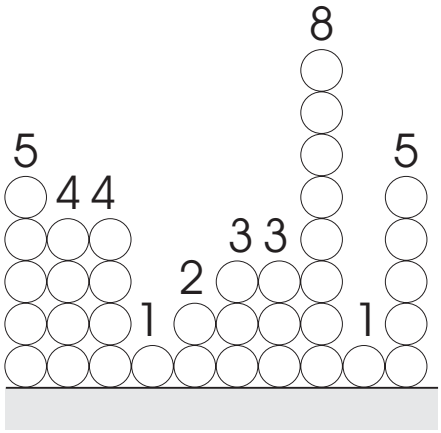

Figure 2.3: Random distribution of the various sites in the BET model

However, in most cases of physisorption, the restriction to one single monolayer is unrealistic. Monolayer adsorption is only expected, if the interactions between the adsorbate molecules are much weaker than those between adsorbate and adsorbent. In 1938 Brunauer, Emmett and Teller [10] derived the first isotherm for multilayer adsorption, the *BET Isotherm*.
In the BET model the surface of the adsorbent is divided into several types of sites:
There are empty sites, sites that are covered by one monolayer and sites that are covered by two or more layers. A random distribution of the various types of sites is assumed (see Fig. 2.3).
In the model the uppermost molecules of each adsorbed stack are in dynamic equilibrium with the vapor. Dynamic equilibrium means, that the location of the surface sites covered by one, two,..etc. layers may vary, but the number of molecules in each layer will remain constant. The first monolayer is supposed to have a characteristic heat of adsorption ΔH_A. The formation of the subsequent layers is controlled by the heat of condensation ΔH_L, of the vapour in question. The most common form of the final ***BET equation*** is

$$\frac{p}{V\,(p_0 - p)} = \frac{1}{V_m\,C} + \frac{(C-1)}{V_m\,C}\left(\frac{p}{p_0}\right) \tag{2.11}$$

V is the volume of adsorbed vapour at STP (e. g. 22.4 l/mol). STP means standard temperature (e. g. 25°C) and standard pressure (e. g. 1 atm). V_m is the monolayer capacity at STP, p is the partial pressure of the gas, p_0 is the saturation vapour pressure. C is a constant:

$$C \approx \exp\frac{\Delta H_A - \Delta H_L}{RT} \tag{2.12}$$

ΔH_A is the heat of adsorption of the first monolayer and ΔH_L is the heat of condensation of the vapor. For the graphical determination of C see equation

2.15. The BET theory primarily describes type II adsorption, but is in general capable of describing each of the five isotherm types.
Inherent to the BET adsorption model are several potential sources of error due to the assumption of the absence of lateral interactions between adsorbed molecules, the constancy of the heat of adsorption after the first monolayer and solid surface homogenity [26]. Nevertheless, it produces usefull results at pressures between $0.05p_0$ and $0.35p_0$.

Determination of surface areas from the BET isotherm

The most common use of the BET isotherm is for determining the surface area of solids. According to equation 2.11, a plot of $\frac{p}{V(p_0-p)}$ versus $\frac{p}{p_0}$ will give a straight line. The slope (S) and the intercept (I) are given with

$$S = (C-1)/(V_m\,C) \tag{2.13}$$
$$I = 1/(V_m\,C) \tag{2.14}$$
$$C = S/I + 1 \tag{2.15}$$

From the slope and the intercept you get the monolayer capacity V_m and the specific surface area A_s of the solid.

$$V_m = 1/(S+I) \tag{2.16}$$
$$A_s = V_m\,k/m_s \qquad \text{with } k = N_a A/M_V \tag{2.17}$$

In the equation m_s is the sample weight, N_a is Avogadro's number, A is the area per molecule of the adsorbed gas and M_V is the gram molecular volume of gas (22.400 l at STP). BET surface area determination generally gives good results at relative pressures p/p_0, between 0.05 and 0.35. For porous solids, or when point B on the isotherm cannot be determined accurately, results have got to be used with caution. Nitrogen is the adsorbate mostly used for the BET surface area determination as it generally gives well-defined B values.

Chapter 3

Experimental methods

Synthesis of starting materials

The purpose of this study is to provide a basic understanding of SO_2 adsorption on volcanic ashes. In order to evaluate the effect of different variables on adsorption, it is necessary to study a simple model system for the interaction of sulfur with volcanic ash.
Therefore synthetic glasses of rhyolitic, dacitic and andesitic composition (see Table 3.2, 3.3) were chosen as the adsorbent material, instead of natural ash. The starting materials for the synthesis of the glasses were the hydroxides and carbonates, listed in Table 3.1. They were mixed and homogenised with ethanol in a planetary mill for 20 minutes at 510 rotations per minute. The homogenised material then was slowly heated up to $1100°C$ in a platinum crucible and held there for 2 hours for decarbonation and dehydration.
The charge was then molten in a high-temperature furnace at 1600°C. After a run duration of 2 hours it was quenched in ice water. The glass obtained thereby was clear, partly containing bubbles.
The glass was ground up to powder with a planetary mill under dry conditions. As no liquid was added during the milling procedure, milling time was restricted to 5-10 minutes, otherwise the glass powder got 'cemented' on the walls of the grinding beacker. The surface area of the powder was then determined with a Micromeritics Gemini III 2375 Surface Area Analyzer, which works on the principle of BET surface determination (see chapter 2.2.3). The analysing gas was nitrogen. The average surface area obtained was within 2.6–4.5 $\frac{m^2}{g}$. Taking an average density of the glass of 2.3 $\frac{g}{cm^3}$ (see Table 3.4) this implies an average grain size from $0.6\mu m$ to $1\mu m$.

Table 3.1: Starting material for the synthesis of the glasses, listed in Table 3.2. Purity of all components is 99.9 % minimum.

wt%	SiO_2	$Al(OH)_3$	$Mg(OH)_2$	$CaCO_3$	Na_2CO_3	K_2CO_3
Andesite	48.24	25.85	8.87	10.09	4.95	1.98
Dacite	57.70	21.26	6.60	4.17	6.30	4.07
Ryolite	64.97	10.32	9.49	1.78	7.35	6.09

Table 3.2: Nominal composition of the glass used in the experiments.

wt%	SiO_2	Al_2O_3	MgO	CaO	Na_2O	K_2O
Andesite	59.43	20.81	7.56	6.96	3.57	1.66
Dacite	67.87	16.38	5.38	2.75	4.35	3.27
Rhyolite	76.80	12.21	3.39	0.76	3.04	3.80

Table 3.3: Composition of the glasses used for the experiments, as derived from XRF measurements.

wt%	SiO_2	Al_2O_3	MgO	CaO	Na_2O	K_2O
Andesite	56.42	20.81	7.07	7.05	3.68	1.74
Dacite	67.52	16.25	5.24	2.78	4.29	3.16
Rhyolite	77.21	12.13	3.08	0.72	2.8	3.46

Apparatus for adsorption experiments

Apparatus:
The adsorption experiments were performed in a device, which was specifically designed for the experiments (see Fig. 3.1 and Fig. 3.2). As all components had to be inert against SO_2, the device was made of glass.
The apparatus, as depicted in Figure 3.2, mainly consisted of two glass containers: a round flask, with a relatively large volume and test tube 1, with a smaller volume. The glass powder was stored in test tube 1, where it was compacted with a plug by hand. System 2 can be either connected or separated via a valve. The two washing flasks are filled with paraffin oil and are connected to the SO_2 inflow, upstream of the main apparatus. The washing flasks serve two purposes: they prevent the system from overpressure, and they allow the system to be purged with pure SO_2 (Rießner © Gase, $S0_2$ 3.8, purity 99.98%). Test tube 2 is installed for low pressure experiments. The pressure in system 1 can be lowered by connecting test tube 2 to system 1 and cooling it to the temperature of liquid nitrogen, so that the SO_2 in test tube 2 condenses and the pressure drops.
For the adsorption experiments at 150°C, 0°C, −20°C and −80°C test tube 1 is immersed in a Dewar flask filled with either hot oil, ice water or a freezing mixture.

The pressure is determined with a Vacuubrand DVR 5 vacuum gauge. The pressure transducer is made of aluminium oxide ceramics, which makes it inert to SO_2. The measurable range extends from 1100 mbar to 0.1 mbar. The DVR 5 measures the actual pressure according to the capacitive principle of measurement independent of the gas type. Electrically, the pressure transducer corresponds to a plate capacitor. A change in capacity indicates a pressure change. The uncertainty is guaranteed to be $\leq \pm$ 1mbar over the whole measuring range. For the range from 10 - 0.1 mbar I determined it to be ±0.1 mbar. The pressure gauge is directly connected to system 1 (see Fig. 3.2).
The vacuum was produced by a two-stage rotary vane pump (RZ 6 by Vacuubrand). The ultimate total vacuum it can produce is 2×10^{-3} mbar.
Calibration of the apparatus:
The amount of adsorbed SO_2 is determined from the pressure drop during adsorption by applying the ideal gas law or rather the van-der-Waals equation (see this chapter, section "Adsorption experiments"). Hence, the knowledge of the exact volumes, relevant for the calculations, is necessary.
The following volumes have been determined:
Volume of system 1 (V_1); volume of test tube 1 (V_2) and the reduced volume V_3 of test tube 1. V_3 is given by substracting the volume of the glass powder (V_{glass}) stored in test tube 1, from the V_2.
Volume V_2:
First the volume of test tube 1 was determined, by completely filling it with distilled water of known temperature. The density of the water ρ_W is determined

by its temperature. The volume of the tube then is given by the weight of the water m_W:

$$V_2 = \frac{m_W}{\rho_W}$$

$$V_2 = 18.996 \text{ ml} \pm 0.030 \text{ ml}$$

Volume V_1:
The volume of system 1 (V_1) was determined by measuring the pressure p_3 that is reached when system 1 (starting pressure p_1) is connected to the empty test tube (starting pressure p_2=0 mbar). With the known volume of test tube 1 the volume of system 1 is determined by the ideal gas equation (see equation 3.1):

$$V_1 = \frac{p_3 V_2}{p_1 - p_3}$$

$$V_1 = 616.957 \text{ ml} \pm 5.929 \text{ ml}$$

Volume V_3:
During a measurement test tube 1 is filled with glass powder, e. g. the volume available for the SO_2 gas is reduced. The reduced volume V_3 is dependent on the volume of the glass powder stored in it. For that reason I first determined the density of the glasses ρ_{glass} with a pycnometer (see Table 3.4). The amount of glass (m_{glass}) stored in the test tube during the experiments then defines the volume V_3.

$$V_3 = V_2 - \frac{m_{glass}}{\rho_{glass}}$$

Table 3.4: Density of the used glasses as determined by multiple measurements with a pycnometer.

	ρ_{glass} in g/cm^3
Andesite	2.355 ± 0.147
Dacite	2.626± 0.052
Rhyolite	2.358± 0.052

Figure 3.1: Apparatus used for the adsorption measurements.

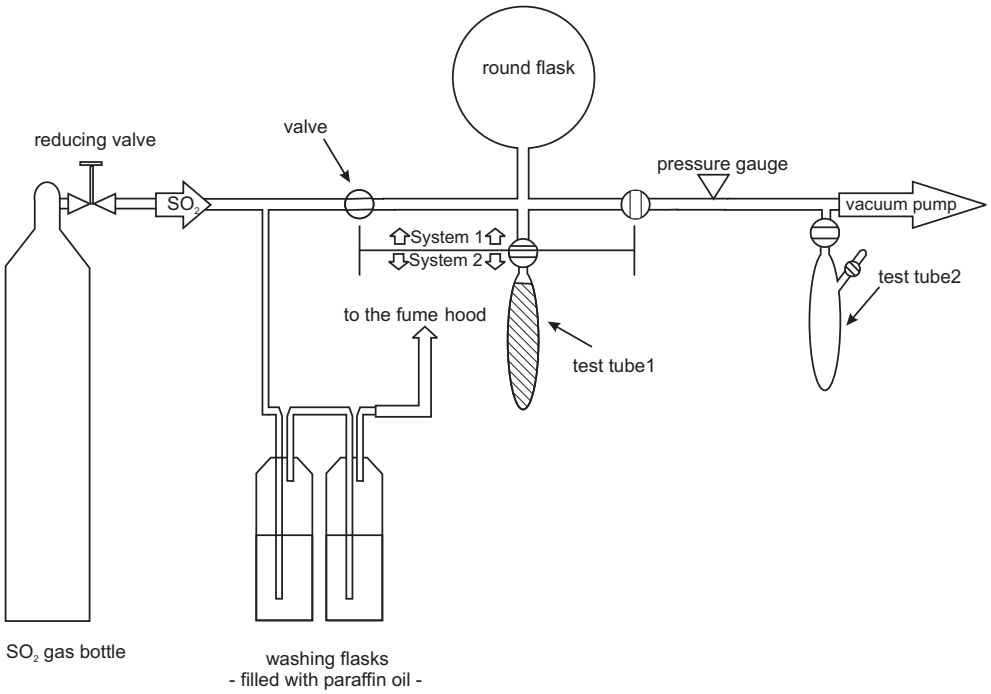

Figure 3.2: Diagram of the apparatus shown in Figure 3.1.

Adsorption experiments

At the beginning of an experiment the whole device was evacuated. Then the test tube and the gas flasket were decoupled and system 1 was filled with pure SO_2 gas up to a desired pressure. The pressure p_1 ($n = n_1$) in system 1 is determined via the pressure gauge. Initially, the pressure p_2 ($n = n_2 = 0$) in test tube 1 was 0 mbar. Connecting the test tube and the gas flask again resulted in a decreased pressure p_3.
The pressure decrease $\Delta p_1 = p_1 - p_3$ is partly due to an increase in volume ($V_1 \rightarrow (V_1 + V_3)$): pressure p_1 drops to pressure p_{22}.
This effect can be calculated with the ***ideal gas law***:

$$p\,V = n\,R\,T \qquad \text{ideal gas law} \tag{3.1}$$

p is the pressure in [Pa], V is the volume of the gas container in $[m^3]$, R is the gas constant, n is the amount of substance in [mole] and T the temperature in [K].
The amount of gas molecules in the free gas phase n_{all} in the connected system $(V_1 + V_3)$ is $n_{all} = n_1 + n_2$. Initially, the pressure in test tube 1 was 0 mbar. So, at the beginning of an experiment $n_{all} = n_1 + n_2$ reduces to $n_{all} = n_1$. Applying equation 3.1 then gives pressure p_{22}:

$$p_1 V_1 = n_1 RT \tag{3.2}$$
$$p_{22}(V_1 + V_3) = n_1 RT \tag{3.3}$$
$$p_{22} = \frac{p_1 V_1}{V_1 + V_3} \tag{3.4}$$

The remaining pressure drop $\Delta p_2 = p_{22} - p_3$ is due to adsorption of SO_2 onto the surface of the glass powder: The amount of gas molecules in the free gas phase is reduced from n_1 to n_2 as SO_2 molecules get stuck to the surface.
It is possible to calculate the amount of adsorbed gas $\Delta n = n_1 - n_2$ from the pressure drop Δp_2 applying the ideal gas law:

$$p_{22}(V_1 + V_3) = n_1 RT \tag{3.5}$$
$$p_3(V_1 + V_3) = n_2 RT \tag{3.6}$$
$$n_1 - n_2 = p_{22} - p_3 \frac{(V_1 + V_3)}{RT} \tag{3.7}$$
$$\Delta n = \Delta p_2 \frac{(V_1 + V_3)}{RT} \tag{3.8}$$

The ideal gas law implies, that the gas molecules have a negligible volume as compared to the total gas volume and that the molecules do not interact with each other. This assumption is acceptable for many gases at ambient temperature and ambient pressure (1 bar).

However, SO_2 has a relatively high boiling point of $-10°C$ at ambient pressure, so the attractive forces between the molecules need to be taken into account. So, instead of the ideal gas law, the ***van-der-Waals equation*** (Eqn. 3.9) was used for calculating the pressure decrease caused by the volume increase as well as the amount of adsorbed gas from the pressure drop caused by adsorption.
Below, the corresponding formalism for calculating the amount of adsorbed SO_2 is presented.
The ***van-der-Waals equation*** is given by

$$p = \frac{nRT}{V - nb} - \frac{an^2}{V^2} \qquad \text{van-der-Waals equation} \tag{3.9}$$

In the equation, a and b are constants for a given gas, the so-called *van-der-Waals constants*:
The parameter b is related to the size of each molecule. The volume that the molecules have to move around is not just the volume V of the container, but is reduced to $(V-nb)$. The parameter a is related to intermolecular attractive forces between the molecules. The net effect of the intermolecular attractive forces is to reduce the pressure for a given volume and temperature. As the isochore of the van-der-Waals equation has a saddle point at the critical point of a gas, it is possible to calculate the van-der-Waals constants if the critical temperature and critical volume of the gas in question is known.
For SO_2 the following van-der-Waals constants were derived from the critial point of SO_2:

$$\begin{aligned} a &= 6.9 \cdot 10^{-1} \qquad Pa\frac{m^6}{mol^2} \\ b &= 5.7 \cdot 10^{-5} \qquad \frac{m^3}{mol} \end{aligned}$$

In order to calculate the moles of adsorbed SO_2 by the van-der-Waals equation it is necessary to rearrange it. This yields an equation of third order for n:

$$abn^3 - Van^2 + abn^3 + V^2(RT + bp)n - pV^3 = 0 \tag{3.10}$$

Equation 3.10 has to be solved for n. This can be done iteratively, alternatively, the equation may be solved analytically with the ***Cardano formula***.
The principle of the Cardano formula is to rearrange the cubic equation via substitutions into quadratic equations. The number of the real solutions depend on the algebraic sign of a discriminant. In case of the van-der-Waals equation for SO_2 above the critical curve there are three real solutions, but only one is physically meaningful. For the problem of adsorption the solution is as follows:

$$n = y - \left(\frac{b}{3a}\right)$$

The variables a and b are the van-der-Waals constants for SO_2; y is given by:

$$y = -\omega \left(\cos \frac{\phi}{3} + \sqrt{3} \sin \frac{\phi}{3} \right)$$

with ω and ϕ:

$$\begin{aligned} \omega &= \left(q^2 + \left| q^2 + k^3 \right| \right)^{1/6} \\ \phi &= \arccos \left(-\frac{q}{\omega^3} \right) \end{aligned}$$

The the variables k and q are related to the pressure p and the volume V of the system:

$$\begin{aligned} 3k &= \frac{3abV^2(RT + bp) - (Va)^2}{3a^2b^2} \\ 2q &= \frac{-2V^3}{27b^3} + \frac{V^3(RT + bp)}{3ab^2} - \frac{pV^3}{ab} \end{aligned}$$

Subtracting the number of moles n before and after adsorption gives the amount of adsorbed SO_2, Δn. Figure 3.3 compares the amount of adsorbed gas as calculated from the ideal gas equation and the van-der-Waals equation, respectively. In the range of low pressure the difference is very small, but with growing pressure and decreasing temperature it becomes more obvious.

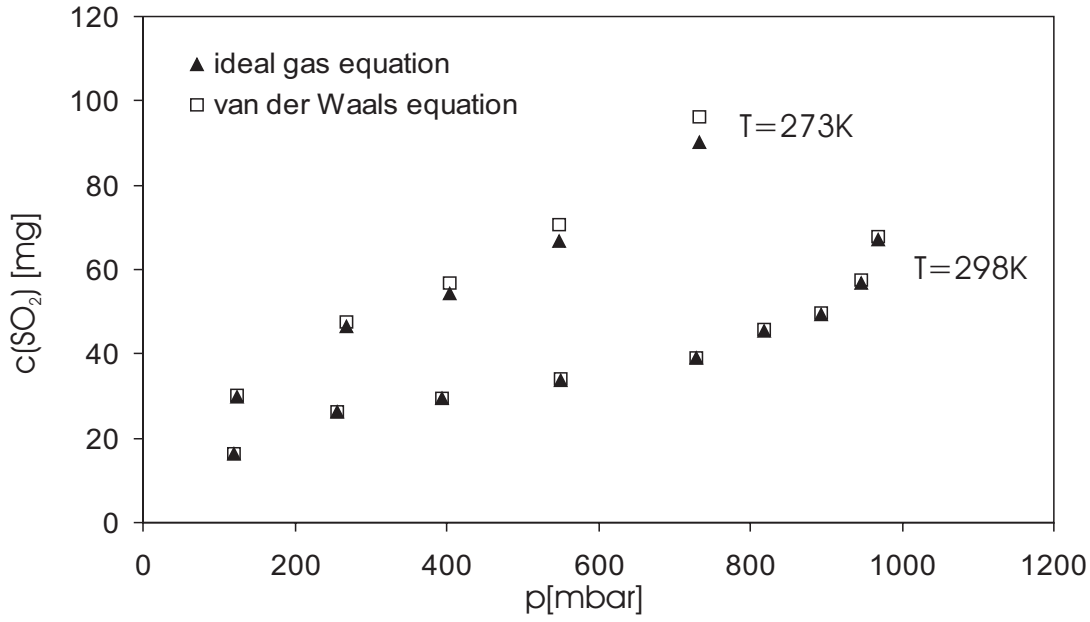

Figure 3.3: Comparison of the amount of adsorbed SO_2 at T=273K and T=298K as calculated from the ideal gas equation and the van-der-Waals equation, respectively

Sources of error

For multiple measurements the error distribution for an experimentally determined variable can be described by the *Gaussian distribution*[43]. The Gaussian distribution gives the statistical probability to find the variable in a given intervall $(\mu - x\sigma)$ to $(\mu + x\sigma)$ around the expected value μ, where x is any positive number and σ is the standard deviation (see Fig. 3.4):

In the interval $(\mu - \sigma)$ to $(\mu + \sigma)$ there are approx. 68% of all measured values
In the interval $(\mu - 2\sigma)$ to $(\mu + 2\sigma)$ there are approx. 95% of all measured values
In the interval $(\mu - 3\sigma)$ to $(\mu + 3\sigma)$ there are approx. 99.7% of all measured values

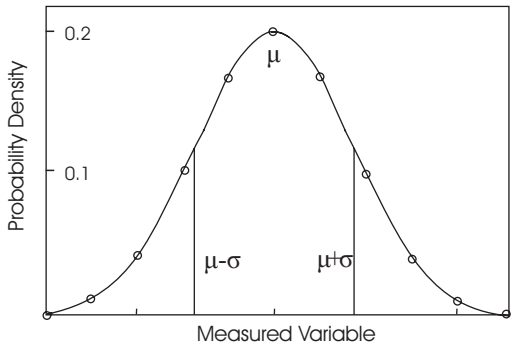

Figure 3.4: Gaussian distribution. σ: standard deviation; μ: expected value

However, these rules are only valid for an infinite number of measurements. For a limited number n of measurements the following parameters are in use:

$$\overline{x} = \frac{1}{n}\sum_{k=1}^{n} x_k \qquad \text{mean value} \tag{3.11}$$

$$\overline{s} = \sqrt{\frac{1}{n\,(n-1)}\sum_{k=1}^{n}(x_k - \overline{x})^2} \qquad \text{confidence interval} \tag{3.12}$$

The experimentally determined value then is given as

$$x = \overline{x} \pm t\,\overline{s} \tag{3.13}$$

where t is a correction factor, that accounts for the finite number of measurements. The correction factor depends on the number of measurements.
However, the final result, e. g. the number of adsorbed moles of SO_2 Δn, is not directly measured, but determined by calculation. Several error-containing variables enter this calculation:

Volume (V_1, V_2), pressure (p), temperature (T), surface area of the glass (A), density of the glass (ρ), weight of the glass (m).
Obviously, the errors of the individual variables contribute to the error of the resulting value. There are two approaches to calculate how the errors of the individual variables contribute to the error of the resulting value:
The ***linear error propagation*** and the ***Gauss error propagation***, respectively[43].
In the following calculations Gauss error propagation was used:
The quantity of interest derives from the mean values of the dependent variables:

$$\overline{f} = f\left(\overline{x}; \overline{y}; \overline{z}; \ldots\right) \tag{3.14}$$

The quantity of interest in this work is Δn:

$$\Delta n = f\left(\overline{V}; \overline{m}; \overline{\rho}; \overline{p}; \overline{A}; \overline{T}\right)$$

Δn is calculated with the van-der-Waals equation. However, for the error evaluation the van-der-Waals equation would be impracticable. Therefore, as the starting point for the Gauss error propagation the ideal gas equation was used.
The standard deviation is given as

$$\overline{s_f} = \left(\frac{\delta f}{\delta x}\overline{s_x}\right)^2 + \left(\frac{\delta f}{\delta y}\overline{s_y}\right)^2 + \left(\frac{\delta f}{\delta z}\overline{s_z}\right)^2 + \ldots \tag{3.15}$$

The result is then specified as

$$f = \overline{f} \pm \overline{s_f} \tag{3.16}$$

Further sources of error

Leakage
In addition to the errors mentioned in the section above, further "sources of error" emerged during my experiments.
The main problem that occured was the leak tightness. The coupling of the pressure gauge to the glass device posed some difficulties in the beginning, as all components had to be inert against SO_2. Another weak point is connected to the coupling of the stop cocks. They are lubricated with silicon paste (Baysilone-Paste, by BAYER), which is relatively inert against SO_2, but nevertheless seems to be corroded after some time. This is a problem as the experiments run over severall days.
When a leakage occurs the experiment had to be aborted, as it is not possible to correct for that kind of error.
Time
Adsorption is a diffusion-controlled process (see chapter 2), meaning that the gas molecules in principle adsorb as fast as they come into contact with the adsorbent. As the glass powder was not lose but compressed in the test tube, I

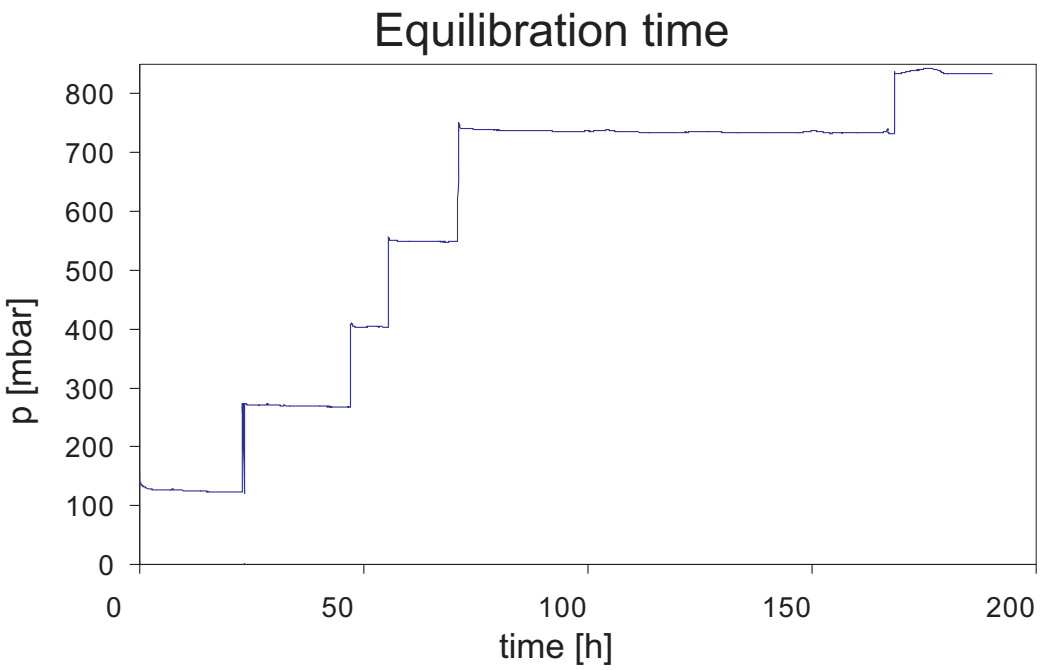

Figure 3.5: "Continuous" record of the pressure values over the time, as derived during an experiment at $t = 273K$.

first underestimated the equilibration time and thus obtained too low values of adsorbed gas.
For this reason I read out and stored the actual pressure value minute-by-minute via the interface of the pressure gauge. Figure 3.5 shows the plot of the pressure values read out during an experiment over the time. A plot of the discrete pressure values over the time makes it easy to identify the equilibration time, as the pressure values there reach a plateau (see Figure 3.5). Equilibration pressure was normally reached within a couple of hours (4-5 h).
The "continuous" record of the pressure values also helps to identify an occuring leackage.

X-ray Fluorescence (XRF) Spectroscopy

Principles When a sample is exposed to a hard x-ray source, the x-rays either can be scatterd through the material or adsorbed by the atoms. If the energy is high enough, an electron from the inner shells (e. g. 'core electron') is ejected out of its orbital. An electron from an outer shell then drops into that vacancy, releasing an x-ray photon whose energy is the difference between the binding energies of the involved shells, and is characteristic for each element. The emission of characteristic x-rays induced by irradiation with hard x-rays is called *X-ray Fluorescence*. Analysis using x-ray fluorescence is called *X-ray Fluorescence Spec-*

troscopy.

In principle there are two types of spectrometer:
Wavelength dispersive spectrometers, where the photons are seperated by diffraction on a single crystall before detection and energy dispersive spectrometers, that allow the determination of the energy of the photon when it is detected.

XRF measurements XRF spectroscopy during this work was used to determine the actual composition of the synthetic glasses (see Table 3.3, page 37) and to verify the presence of irreversibly bound sulfur (see Table 4.2 and Table 4.3 on pages 54f).
Measurements were carried out with the wavelength dispersive spectrometer *S4 Pioneer* by Bruker AXS GmbH with internal standard.
Sample preparation
First the glass powder was dried at 60°C. Then 6,0 grams of the powder was mixed with 1,2 grams of wax ("Lencowax"). The mixture was pressed to a pellet at 300 kN/m^2. Eventually XRF analysis was performed as a scan.

Chapter 4

Isothermal equilibrium experiments

4.1 Experiments at room temperature

4.1.1 Adsorption isotherm

The experiments at room temperature were conducted at pressures ranging from 38 mbar to 968 mbar. Adsorbent material was glass of rhyolitic, dacitic and andesitic composition (see Table 3.2).
In Figure 4.1 the adsorption isotherms for all 3 kinds of glass are superimposed. The form of the isotherms is very characteristic:
The amount of adsorbed gas first increases with pressure. At some pressure value it reaches a plateau and subsequently increases again. Comparing this behaviour with the classification of adsorption isotherms (see section 2.2.1) it is obvious, that it is described by type II adsorption. Type II adsorption is a physisorption process, including multilayer formation.

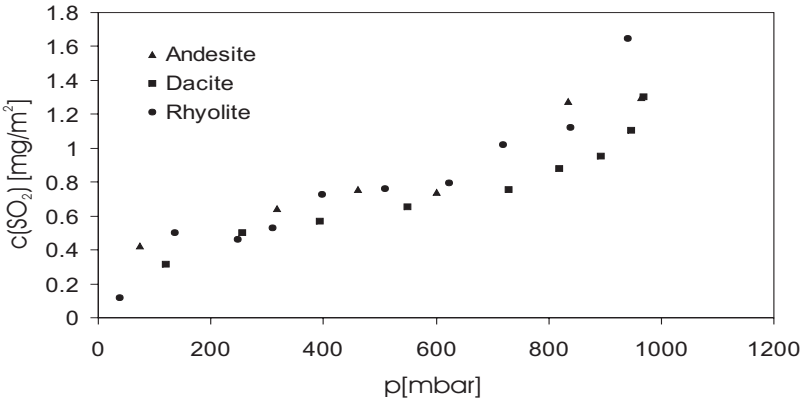

Figure 4.1: Isotherms for adsorption on rhyolitic, dacitic and andesitic glass

4.1.2 Adsorption-desorption isotherms

Figure 4.2 shows the adsorption-desorption isotherms for rhyolitic, dacitic and andesitic glass, respectively.

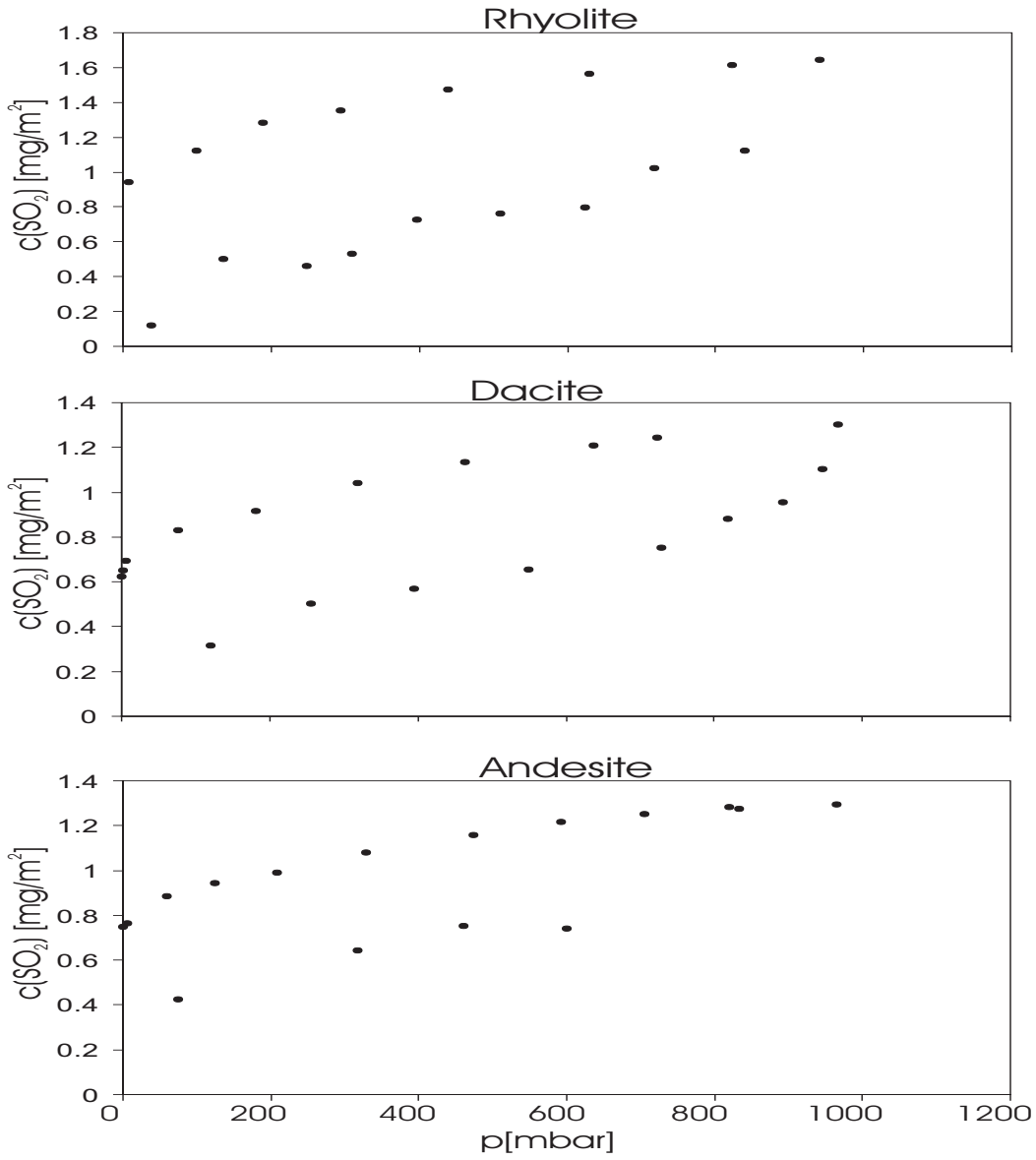

Figure 4.2: Adsorption-desorption isotherms for rhyolite, dacite and andesite, respectively

The adsorption branch of all three isotherms show type II behaviour. The desorption branches reveal 2 features, that do not correlate with type II adsorption:

Hysteresis Desorption shows a hysteresis-like behaviour. Generally this is associated with capillary condensation. Though type II adsorption is described as adsorption on non-porous solids, it still can have microporosity[19]. The *t*-curve method after de Boer et al. [16] provides a simple means to reveal the presence of porosity from nitrogen adsorption data. This method is based on the observation that for a wide variety of adsorbents, adsorption of nitrogen at liquid nitrogen temperature ($= 63 - 77$K) yields identical adsorption curves, if no capillary condensation occurs. Based on this assumption, de Boer et al. [16] suggested to use an universal adsorption curve (master curve) as a reference curve for texture determination. The master curve, alternatively *t*-curve, they determined experimentally for relative pressures between 0.1 and 0.75 (see Figure 4.3). They expressed the data in terms of an average thickness t of the adsorbed layer in Ångstrøm units (see Fig. 4.3), by assuming that the adsorbed layer behaves as a normal liquid nitrogen layer with its proper density at the given temperature [16].

A practical way to use this mastercurve is to plot experimental adsorption data as a function of the t-values, that can be derived from the t-curve. The resulting function V=f(t) (V is Volume of adsorbed N_2; t is average thickness of the adsorbed layer) gives a straight line through the origin, in case of "normal" multimolecular adsorption. Deviations from the straight line indicate capillary condensation.

Figure 4.4 shows the t-plot for adsorption of N_2 on andesitic glass, which is for all three glass compositions. As the curve is a straight line through the origin, there is no hint for microporosity.

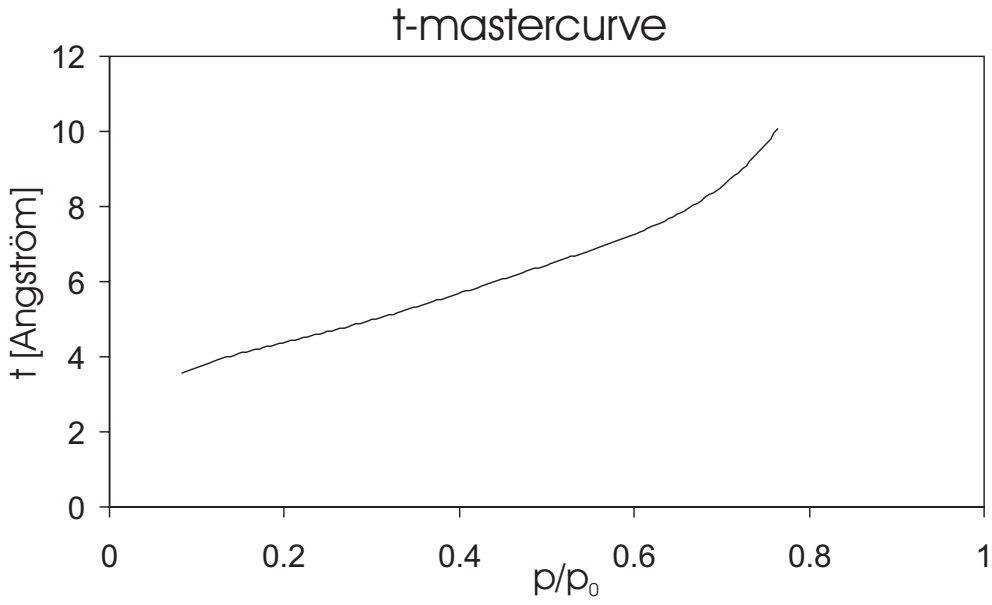

Figure 4.3: The experimental master curve for the adsorption of nitrogen at 78°K (redrawn after [16]).

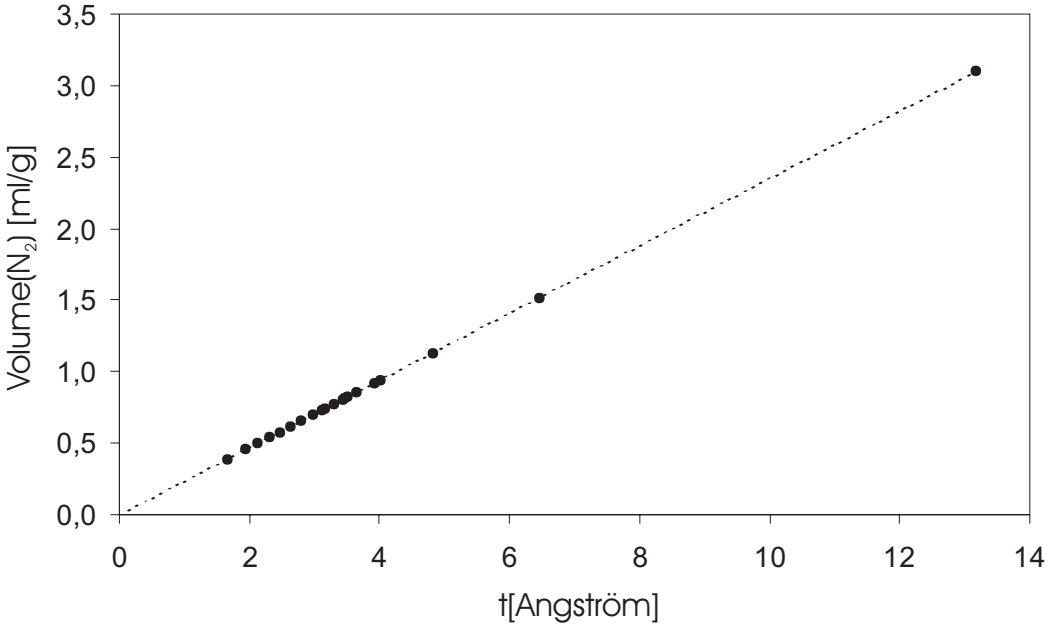

Figure 4.4: t-plot for the adsorption of N_2 on andesitic glass. The volume V of adsorbed N_2 is plotted against the layer thickness t.

Irreversibility A very decisive feature of adsorption of SO_2 on volcanic glasses can be seen at the low-pressure end of the desorption branches. Adsorption data at room temperature suggest, that remarkable amounts of SO_2 remain on the surface of the glass even after desorption (see Table 4.1). Taking the lower limit, then 30 wt% of the originally adsorbed SO_2 remains on the surface (see Table 4.3). XRF measurements confirm this (Table 4.2, 4.3)

Table 4.1: Amount of adsorbed SO_2 vs. amount of SO_2 remaining after desorption, as determined from the adsorption isotherms.

	adsorbed SO_2		pressure
	in mg/m^2	in wt%	in $mbar$
Rhyolite	1.645 ± 0.3217	0.389 ± 0.0390	940
Dacite	1.304 ± 0.1754	0.406 ± 0.0287	968
Andesite	1.297 ± 0.2214	0.336 ± 0.0282	965
	SO_2 after desorption		pressure
	in mg/m^2	in wt%	in $mbar$
Rhyolite	0.941 ± 0.2289	0.223 ± 0.0492	6.8
Dacite	0.626 ± 0.1591	0.195 ± 0.0372	0.9
Andesite	0.748 ± 0.2306	0.194 ± 0.0430	0.1

Table 4.2: Amount of SO_2 remaining after desorption, as determined from XRF measurements.

XRF measurements	
$a$mount of SO_2 remaining after desorption	
Rhyolite	2381 ± 328 ppm
Dacite	1286 ± 97 ppm
Andesite	783 ± 33 ppm

As physisorption is a completely reversible process, this behaviour can only be explained by assuming some chemical bonding of the SO_2 molecules. This assumption would also give an explanation for the hysteresis-like behaviour during desorption. Chemical interactions only can take place between the first layer of adsorbed molecules and the surface of the adsorbent. Hence it is reasonable to express the amount of irreversibly bound SO_2 in terms of the monolayer capacity V_m. In Table 4.4 the values for V_m for the different glasses versus the amount of permanently adsorbed SO_2 are listed. The V_m values were determined from the BET isotherms of the SO_2 adsorption data. It is obvious, that the values

Table 4.3: Amount of SO_2 remaining after desorption in % of the originally adsorbed SO_2. The values, that are listed among "XRF measurements", are calculated from the results in Table 4.2 including the final values for the amount of adsorbed gas, derived from the adsorption isotherms.

	*A*dsorption isotherms	*X*RF measurements
	remaining SO_2 in % of the originally adsorbed SO_2	
Rhyolite	57.227 ± 17.855	51.152 ± 12.234
Dacite	47.987 ± 13.804	35.108 ± 5.427
Andesite	57.678 ± 20.331	23.224 ± 4.067

derived from the adsorption of SO_2 vary from one glass composition to the other. The values for V_m derived from adsorption of nitrogen at the temperature of liquid nitrogen ($= 63 - 77$K) during the BET experiments do not depend on the composition of the respective glass. This argues for localized SO_2 adsorption in the first monolayer and thus would point to specific interactions with the surface sites.
V_m values delivered by SO_2 adsorption equal the amount of permanently bound SO_2 within the given errors, suggesting that the binding of nearly the whole first monolayer is irreversible.

Table 4.4: Monolayer capacity V_m derived from SO_2 adsorption at $t = 25°$C and N_2 adsorption respectively versus the amount of permanently adsorbed SO_2.

	$\boldsymbol{V_m}$in $\boldsymbol{cm^3/m^2}$		
	from SO_2 adsorption	from N_2 adsorption	permanent SO_2 in cm^3/m^2
Rhyolite	0.34	0.23	0.33 ± 0.08
Dacite	0.29	0.23	0.22 ± 0.06
Andesite	0.40	0.23	0.24 ± 0.08

Summarizing the results above, the isotherms for adsorption of SO_2 on volcanic glass provide evidence for both chemical and physical adsorption mechanisms:
(a) adsorption is partially irreversible; (b) isotherm type and the heat of adsorption is more characteristic for physical sorption.

4.2 Dependence on temperature

4.2.1 Adsorption on rhyolite at different temperatures

Experiments with rhyolitic glass were conducted at 150°C ($p = 118 - 538$ mbar), 25°C ($p = 38 - 940$ mbar), 0°C ($p = 0.1 - 471$ mbar), −20°C ($p = 75$ mbar) and −80°C ($p = 46$ mbar), respectively. In Figure 4.5 the corresponding adsorption isotherms are cumulatively plotted. For equal equilibration pressure at 150°C less gas is adsorbed than at 25°C. At 25°C less is adsorbed than at 0°C, where again less is adsorbed than at −80°C. Obviously the amount of adsorbed SO_2 increases with decreasing temperature.
The result at −20°C is not in accordance with the general observation that adsorption is enhanced at low temperature. For the given pressure (75 mbar) at −20°C less is adsorbed than at 0°C (see Figure 4.5). This is probably due to incomplete attainment of equilibrium, perhaps related to the sealing of pore space on the surface of the powder simply by the condensation of traces of water vapour.
In Figure 4.6 the percentage increase of adsorbed gas for the 0°C-isotherm in comparison with the 25°C-isotherm is depicted. The increase of adsorbed gas ranges from 100 % to 200 %.

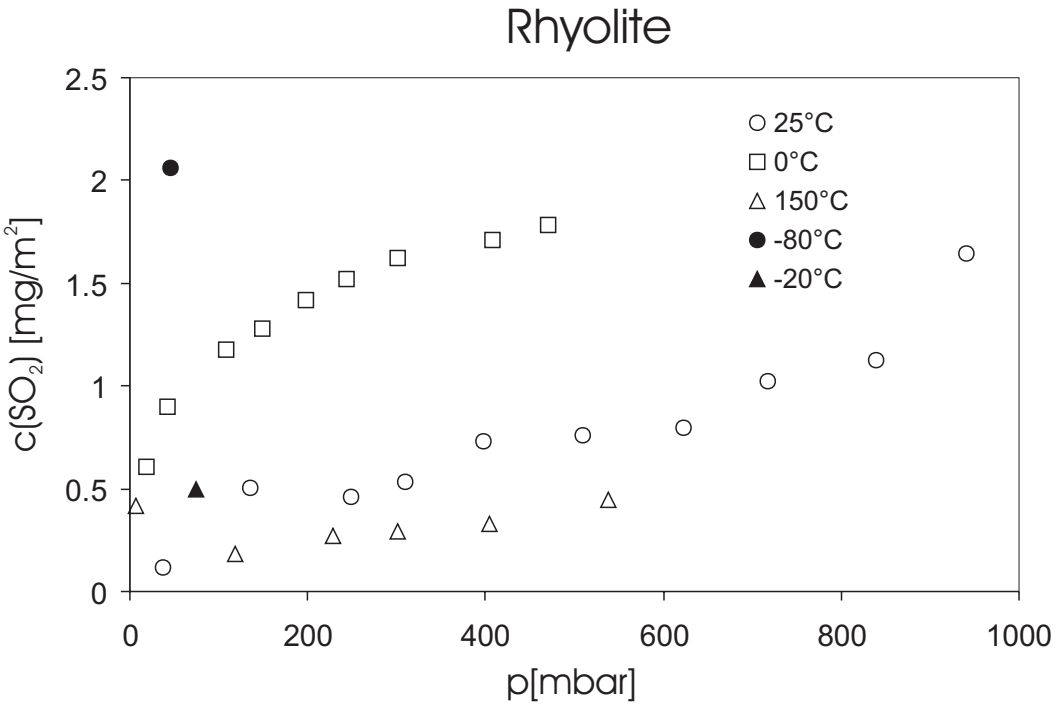

Figure 4.5: Adsorption isotherms for rhyolitic glass at different temperatures

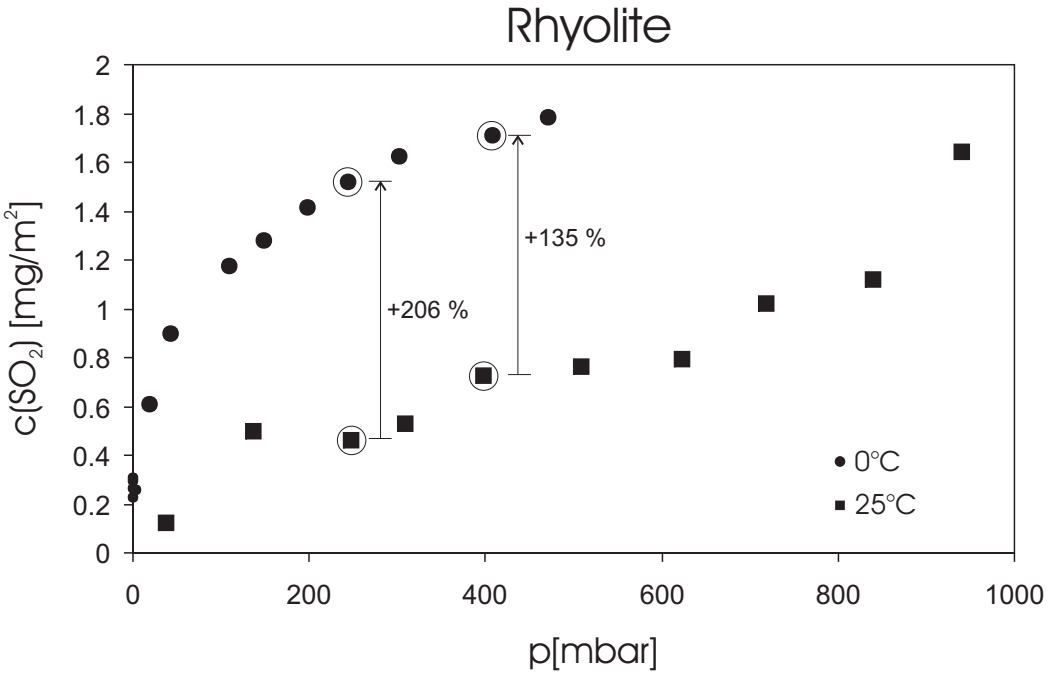

Figure 4.6: Temperature dependence of adsorption: Adsorption isotherms at $t = O°\mathrm{C}$ and $t = 25°\mathrm{C}$ for rhyolitic glass.

4.2.2 Adsorption on dacite at different temperatures

Adsorption experiments with dacitic glass were conducted at 0°C and 25°C. The pressure for the 0°C-isotherm ranges from 0.1 mbar to 732 mbar. The experiments at 25°C were conducted at pressures ranging from 120 mbar to 968 mbar.

The amount of adsorbed SO_2 is considerably higher at the deeper temperature (see Fig. 4.7), confirming the trend seen for adsorption on rhyolitic glass.

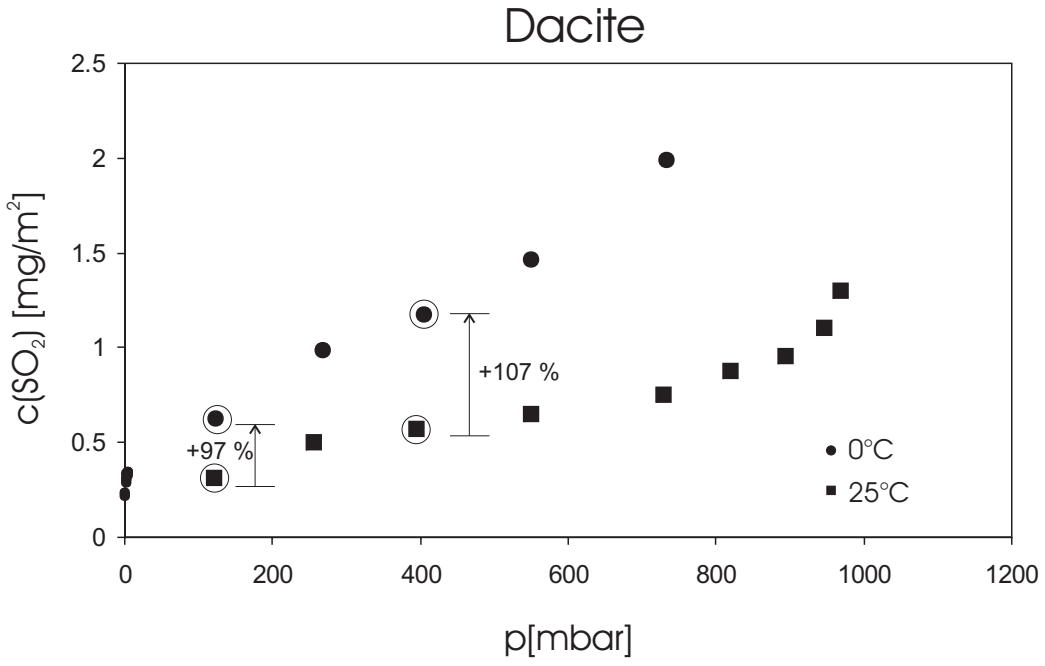

Figure 4.7: Isotherms at $t = 0$°C and $t = 25$°C for adsorption on dacitic glass.

4.2.3 Adsorption on andesite at different temperatures

Adsorption experiments with andesitic glass as the adsorbate were conducted at 25°C and at 0°C (see Figure 4.8). The experiments at 25°C cover the pressure range from 74 mbar to 965 mbar. The 0°C-isotherm includes values taken at pressures from 0.1 mbar to 984 mbar.

As for dacitic and rhyolitic glass adsorption is higher at the deeper temperature. The increase of adsorbed gas is in the order of several tens of wt%.

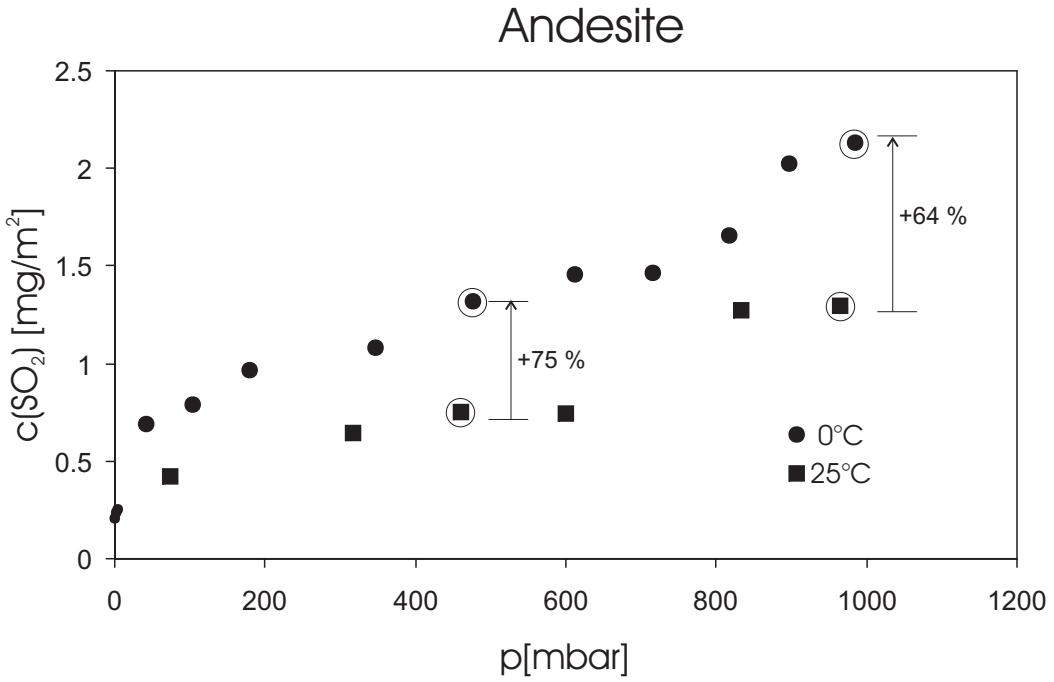

Figure 4.8: Temperature dependence of adsorption: Adsorption isotherms at $t = 0$°C and $t = 25$°C for andesitic glass.

4.2.4 The BET and Freundlich isotherms of adsorption

In chapter 2 different types of adsorption isotherm models for monolayer and multilayer adsorption are described.

BET model

The classical approach to describe multilayer adsorption is the BET isotherm. The experimental adsorption data were plotted according to the BET equation:

$$\frac{p}{V\,(p_0 - p)} = \frac{1}{V_m\,C} + \frac{(C-1)}{V_m\,C}\left(\frac{p}{p_0}\right) \tag{4.1}$$

$$\Longleftrightarrow$$

$$y = I + S\,x \tag{4.2}$$

V is the volume of adsorbed vapour at STP (e. g. 22.4 l/mol) in cm^3/g, V_m is the monolayer capacity at STP, p is the pressure in mbar, p_0 is the saturation vapour pressure and C is a constant.
A plot of $\frac{p}{V(p_0-p)}$ against $\frac{p}{p_0}$ gives an intercept I ($=\frac{1}{V_m\,C}$) and a slope S ($=\frac{C-1}{V_m\,C}$).

The experimental data were fitted to the BET equation at relative pressures p/p_0, between 0.05 and 0.35, when possible (see Fig. 4.9-4.12). In case of adsorption on rhyolite at 150°C the whole range was below that interval. In Table 4.5 the intercept I, the slope S, the C values and the values of V_m of the experimental data are listed. The numbers were derived using equation 4.1 and 4.2.
The V_m values obtained from the SO_2 experiments range from 0.24 to 0.40 cm^3/m^2, seemingly not correlated to temperature. The average of the values is one and a half times higher then the value obtained for nitrogen adsorption (average value: $0.33 cm^3/m^2$, N_2 value: 0.23 cm^3/m^2), suggesting that the capacity of the volcanic glasses for SO_2 adsorption is higher than for nitrogen adsorption.

Comparing adsorption at 25°C and at 0°C, the C values are always considerably higher at the lower temperature. The rise in all cases is approximately of the same magnitude. The parameter C is related to the magnitude of the adsorbent-adsorbate interaction energy [17], where high C values are related to high surface energies. Therefore the rise of the C value at lower temperature probably indicates some increase of the interaction intensity between the gas molecules and the glass surface. In contradiction to this assumption, the C value for adsorption at 150°C is considerably higher than for experiments at 0°C and 25°C. This might be because the range of relative pressure p/p_0 for that series is much lower than the range for which the BET method is supposed to deliver reliable results.

Table 4.5: BET constants for the adsorption of SO_2 on glasses. R^2 is a quality factor for the regression, ranging from 1 (perfect correlation) to 0 (no correlation).

BET Constants
–from SO_2 experiments–

	t in $°C$	**I**	**S**	**C**	$\boldsymbol{V_m}$in cm^3/m^2	$\boldsymbol{R^2}$
Rhyolite	150	0.004	0.70	190.62	0.24	0.87
	25	0.80	0.95	13.08	0.40	0.86
	0	0.008	0.69	93.4	0.32	0.99
Dacite	25	0.06	1.05	19.61	0.29	0.97
	0	0.017	1.07	65.86	0.34	0.98
Andesite	25	0.07	0.90	14.79	0.40	0.82
	0	0.012	0.90	72.02	0.29	0.99
from N_2 adsorption at liquid nitrogen temperature: $V_m = 0.23cm^3/m^2$						

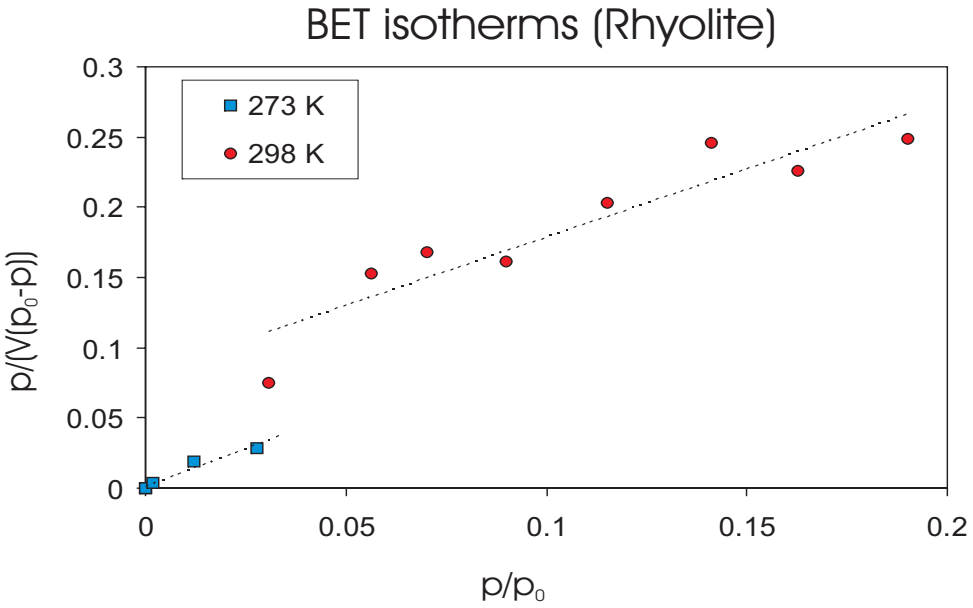

Figure 4.9: Experimentally determined BET isotherms for rhyolite glass, V is the volume of adsorbed vapour in cm^3/g, p is the pressure in mbar and p_0 is the saturation vapour pressure.

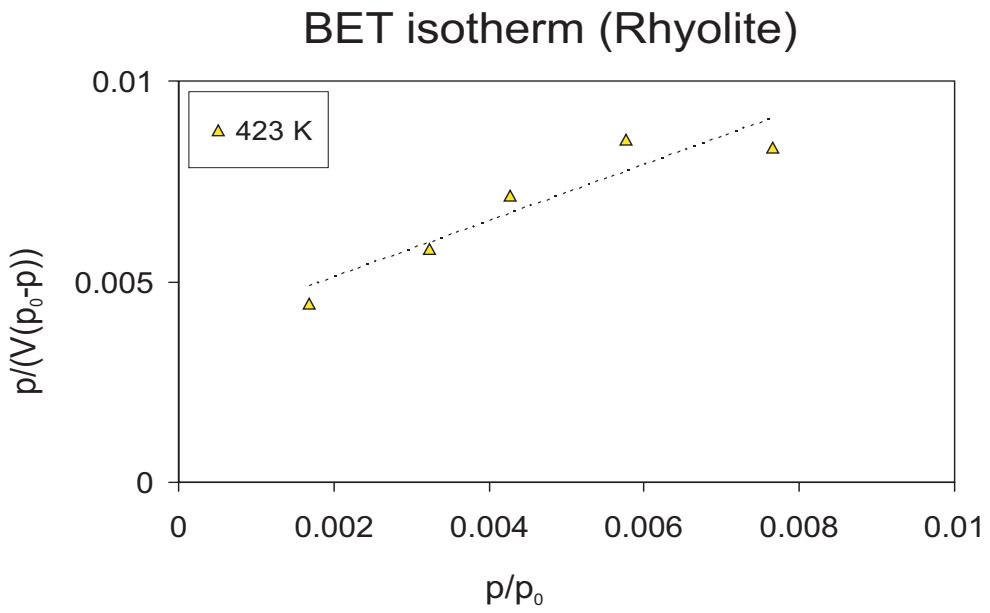

Figure 4.10: Experimentally determined BET isotherm for rhyolite glass, V is the volume of adsorbed vapour in cm^3/g, p is the pressure in mbar and p_0 is the saturation vapour pressure.

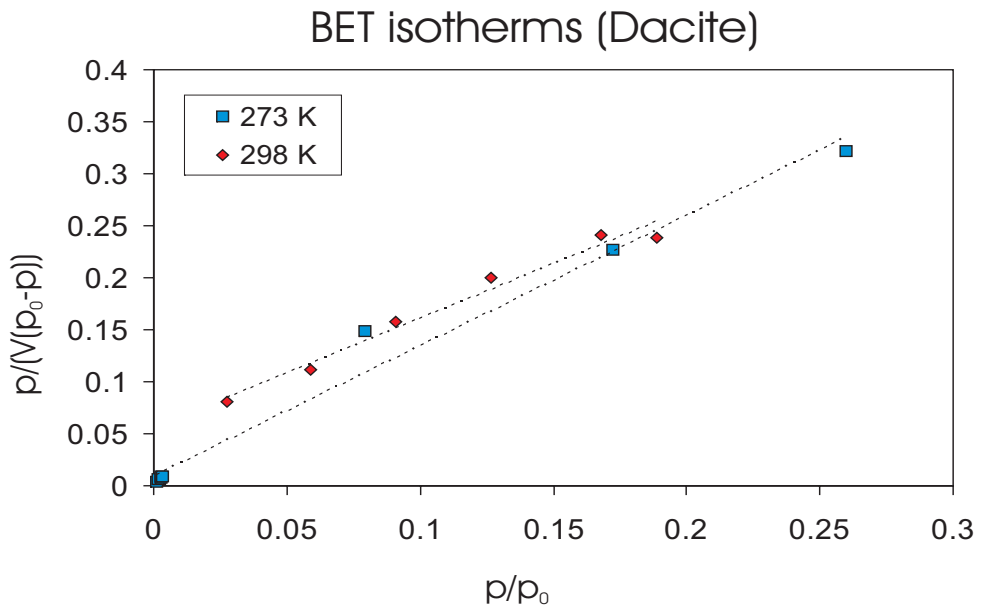

Figure 4.11: Experimentally determined BET isotherms for dacite glass, V is the volume of adsorbed vapour in cm^3/g, p is the pressure in mbar and p_0 is the saturation vapour pressure.

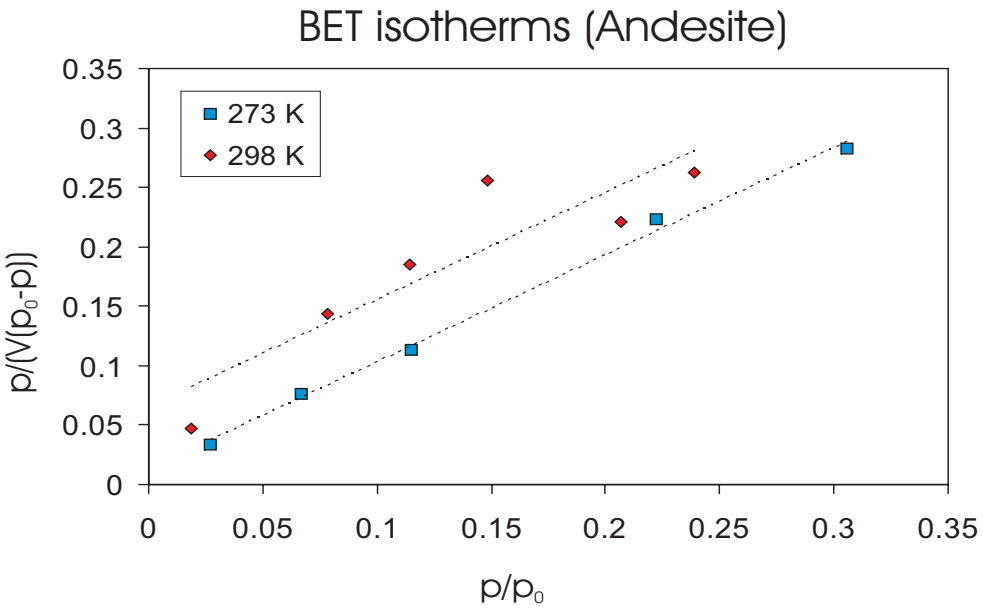

Figure 4.12: Experimentally determined BET isotherms for andesite glass, V is the volume of adsorbed vapour in cm^3/g, p is the pressure in mbar and p_0 is the saturation vapour pressure.

Freundlich model

In order to fit the Freundlich model the adsorption data were plotted according to the linearized Freundlich equation (also see equation 2.9):

$$\ln c = \ln k + \frac{1}{a} \ln p \tag{4.3}$$

$\frac{1}{a}$ and $\ln k$ are the Freundlich constants. The pressure p is given in mbars, the amount of adsorbed SO_2 c is in mg/m^2.

The experimental data were fitted over the whole given pressure range. The Freundlich isotherm was developed to describe monolayer adsorption. Nevertheless, the adsorption data fitted the model quite well (see Figures 4.13-4.16). As a good portion of the available dataset was recorded at pressures well above 100 mbar, the high pressure branch might be over emphasised. The exact numbers for the Freundlich constants, calculated from the experimental data (see Table 4.6) therefore, might be somewhat biased.

Table 4.6: The Freundlich constants for the adsorption of SO_2 on glasses. R^2 is a quality factor for the regression.

Freundlich Constants

–from SO_2 experiments–

	t in $°C$	$\mathbf{1/a}$	$\mathbf{\ln k}$	$\boldsymbol{R^2}$
Rhyolite	150	0.55	-4.33	0.96
	25	0.70	-4.51	0.93
	0	0.25	-1.01	0.93
Dacite	25	0.59	-4.01	0.93
	0	0.28	-1.47	0.95
Andesite	25	0.42	-2.76	0.86
	0	0.27	-1.37	0.93

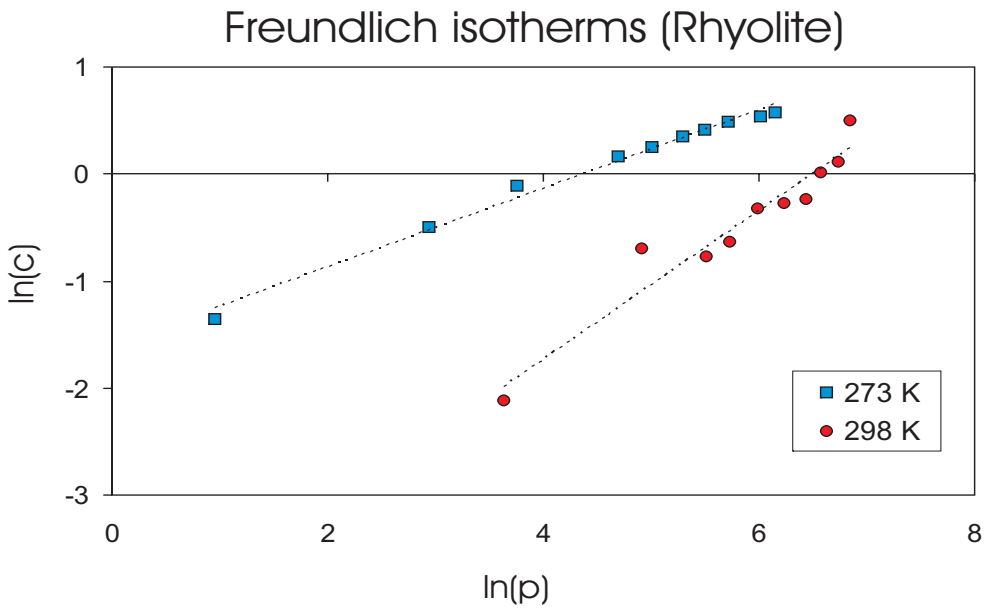

Figure 4.13: Experimentally determined Freundlich isotherms for the adsorption of SO_2 on rhyolite glass, where p is given in mbars and c is the amount of adsorbed SO_2 in mg/m^2.

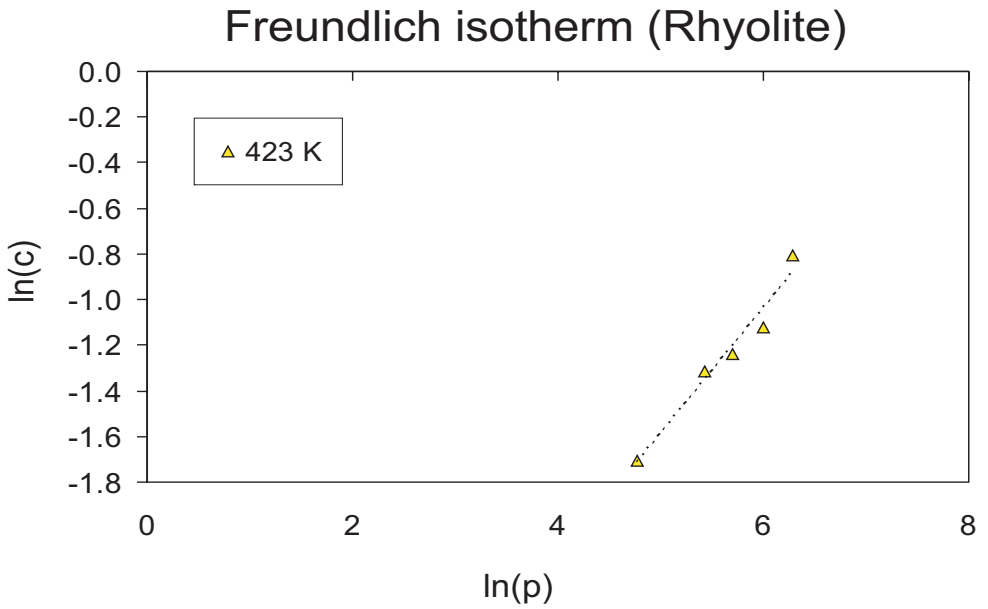

Figure 4.14: Experimentally determined Freundlich isotherm for the adsorption of SO_2 on rhyolite glass, where p is given in mbars and c is the amount of adsorbed SO_2 in mg/m^2.

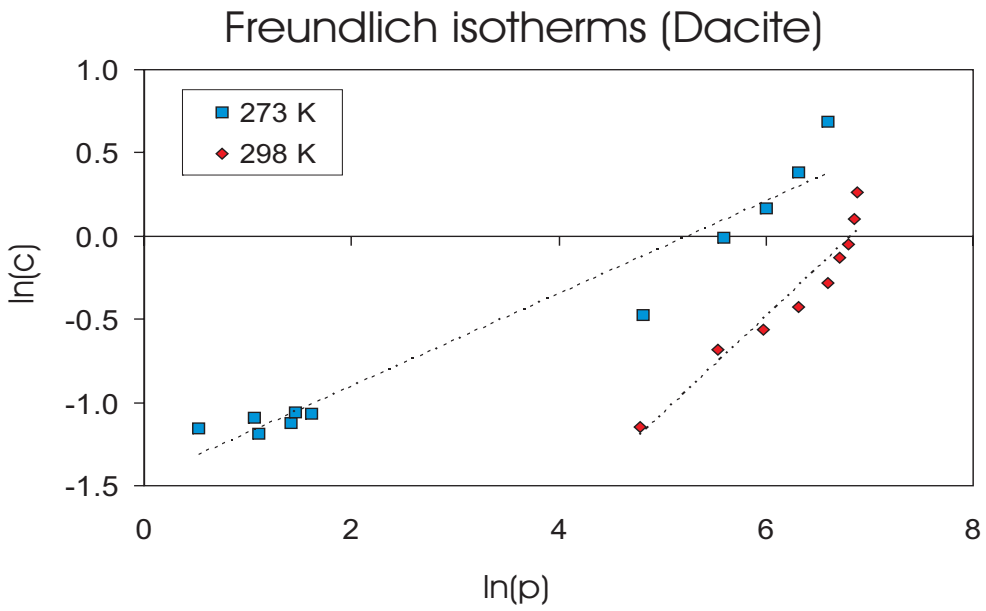

Figure 4.15: Experimentally determined Freundlich isotherms for the adsorption of SO_2 on dacite glass, where p is given in mbars and c is the amount of adsorbed SO_2 in mg/m^2.

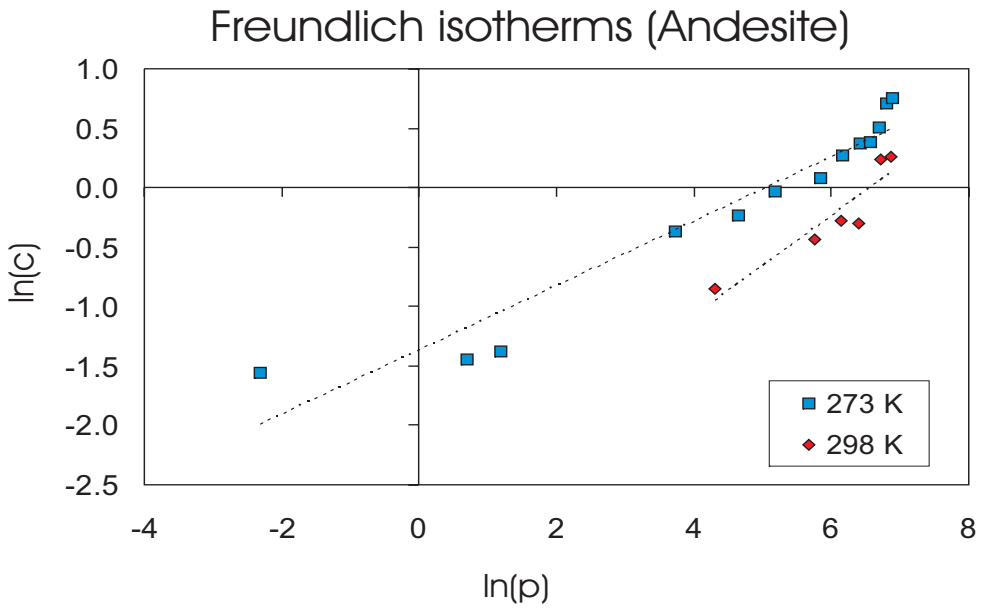

Figure 4.16: Experimentally determined Freundlich isotherms for the adsorption of SO_2 on andesite glass, where p is given in mbars and c is the amount of adsorbed SO_2 in mg/m^2.

4.2.5 Thermodynamic considerations

Adsorption of SO_2 on rhyolitic, dacitic and andesitic glass increases with decreasing temperature, revealing a typical feature for physisorption [23]. However, the percentage increase of adsorbed gas due to a given decrease of temperature depends on the actual equilibrium pressure (see Fig. 4.6, 4.7 and 4.8).
A more universal expression of the temperature dependence of the reaction can be derived by the *Gibb's free enthalpy* ΔG.

$$\Delta G = \Delta H - T\Delta S = -RT \ln(K) \tag{4.4}$$

where ΔH is the enthalpy of reaction, ΔS is the entropy of reaction, R is the gas constant, T is the temperature in Kelvin, K is the equilibrium constant.
For a general chemical reaction in equilibrium

$$a\,\mathrm{A} + b\,\mathrm{B} = c\,\mathrm{C} + d\,\mathrm{D}$$

the equilibrium constant K is defined by the activity coefficients a_i of the reactants and products as follows

$$K = \frac{a_C^c a_D^d}{a_A^a a_B^b} \tag{4.5}$$

The SO_2 in the free gas-phase is in equilibrium with the adsorbed layer, so the reaction can be described as

$$SO_{2(gaseous)} = SO_{2(adsorbed)}$$

The considering equilibrium constant than is given by the activity coefficients

$$K = \frac{a_{SO_{2(adsorbed)}}}{a_{SO_{2(gaseous)}}} \tag{4.6}$$

The activity of gases can be expressed in terms of their fugacity f. Assuming low gas pressure, the fugacity can be substituted by the partial pressure of the gas. The activity of the adsorbed SO_2 can be assumed to be proportional to its concentration. The equilibrium constant then is

$$K = z1 \cdot \frac{c_{SO_2}}{p_{equi.}^m} \tag{4.7}$$

where c_{SO_2} is the amount of adsorbed SO_2 per unit area; $p_{equi.}$ is the equilibrium pressure; z1 and m are constants.
The term $p_{equi.}^m$ allows for the number of adsorption sites being finite and derives from the Freundlich adsorption isotherm (see equation 2.9).
Introducing equation 4.7 in equation 4.4 yields

$$0 = \Delta H - T\Delta S + RT \ln\left(z1 \cdot \frac{c_{SO_2}}{p_{equi.}^m}\right) \tag{4.8}$$

Solving the equation for $\ln(c_{SO_2})$ gives

$$\ln(c_{SO_2}) = -\frac{\Delta H}{RT} + \frac{\Delta S - R\ln(z1)}{R} + m\ln(p_{equi.}) \quad (4.9)$$

$$\Longleftrightarrow$$

$$\ln(c_{SO_2}) = -\frac{\Delta H}{RT} + \frac{\Delta S}{R} - \ln(z1) + m\ln(p_{equi.}) \quad (4.10)$$

From equation 4.10 follows, that c_{SO_2} is proportional to $\exp(1/T)$. An isobar plot of $\ln(c_{SO_2})$ versus $1/T$ thus gives a straight line.
The slope A is given by

$$A = -\frac{\Delta H}{R} \quad (4.11)$$

ΔH is assumed to be a characteristic constant for the adsorption process [23], so the slope does not depend on pressure.
The intercept I_c is

$$I_c = \frac{\Delta S}{R} - \ln(z1) + m\ln(p_{equi.}) \quad (4.12)$$

Unlike the slope, the intercept depends on the actual pressure.

4.2.6 Extrapolation of adsorption data

In order to predict the amount of adsorbed gas at any temperature and any pressure, equation 4.10 may be rewritten as:

$$\ln(c_{SO_2}) = -\frac{\Delta H}{RT} + m\ln(p_{equi.}) + \frac{\Delta S}{R} - \ln(z1)$$

$$\Longleftrightarrow$$

$$\ln(c_{SO_2}) = A\frac{1}{T} + B\ln(p_{equi.}) + C \quad (4.13)$$

With the constant factors

$$A = -\frac{\Delta H}{R};\ B = m;\ C = \frac{\Delta S}{R} - \ln(z1)$$

Equation 4.13 can be solved by applying regression analysis.

Regression analysis statistically describes the dependence between a dependent variable (response variable) and the independent variable(s). Simple regression is used for problems, where the response variable is described by only one explanatory variable. Multiple regression is applied to fit models that are based on more than one independent variable.
The quality of a fit is described by the R-Square factor (R^2). R^2 is a means for the regression errors, ranging from 1 (perfect correlation between predicted and measured response variable) to 0 (no correlation). For detailed theory of multiple regression see textbooks as Aiken et al. [7].

Multiple Regression on the adsorption data

Using multiple regression, an adsorption model describing the experimental dataset was developed. The starting model for regression is based on the Freundlich model, developed in chapter 4.2.4 and is described by equation 4.13. From multiple regression adequate values for A, B and C were derived. The regression procedure was executed with Microsoft Excel ©, which is based on the method of least squares.

During the regression procedure all experimental data of the appropriate glass (e. g. rhyolite, dacite, andesite) were included. For rhyolite this includes adsorption data measured at 150°C, 25°C, 0°C, −20°C and −80°C. For andesite and dacite data measured at 25°C and 0°C were available.
The resulting regression variables (see Table 4.7) then completely describe equation 4.13, eventually allowing the amount of adsorbed SO_2 at optional pressure and temperature to be calculated.

Evaluation of the regression models The regression models, based on the three datasets yielded a quite good agreement between the values, estimated from the model and the measured values (see Figures 4.17, 4.18 and 4.19). The deviation between the measured amount of adsorbed gas and the calculated amount did not show any distinct dependence on temperature (see Fig. 4.20 – Fig 4.22).

Table 4.7: Thermodynamic model for the adsorption of SO_2 on glasses. The coefficients are derived by multiple regression according to equation 4.13. The pressure p is given in mbar; c is the amount of adsorbed SO_2 in mg/m^2 and T is the temperature in Kelvin.

Multiple regression									
$\ln c = -\frac{\Delta H}{R}\frac{1}{T} + \ln p + \frac{\Delta S}{R} - const.$ $\ln c = A\frac{1}{T} + B \ln p + C$									
Andesite				**Dacite**			**Rhyolite**		
	A	B	C	A	B	C	A	B	C
Value	1644.78	0.29	-7.43	2139.52	0.29	-9.32	909.75	0.21	-4.48
Errors	362.83	0.02	1.33	379.08	0.02	1.41	123.69	0.03	0.49
R^2	0.92			0.91			0.75		
error on $\ln c$	0.22			0.20			0.37		

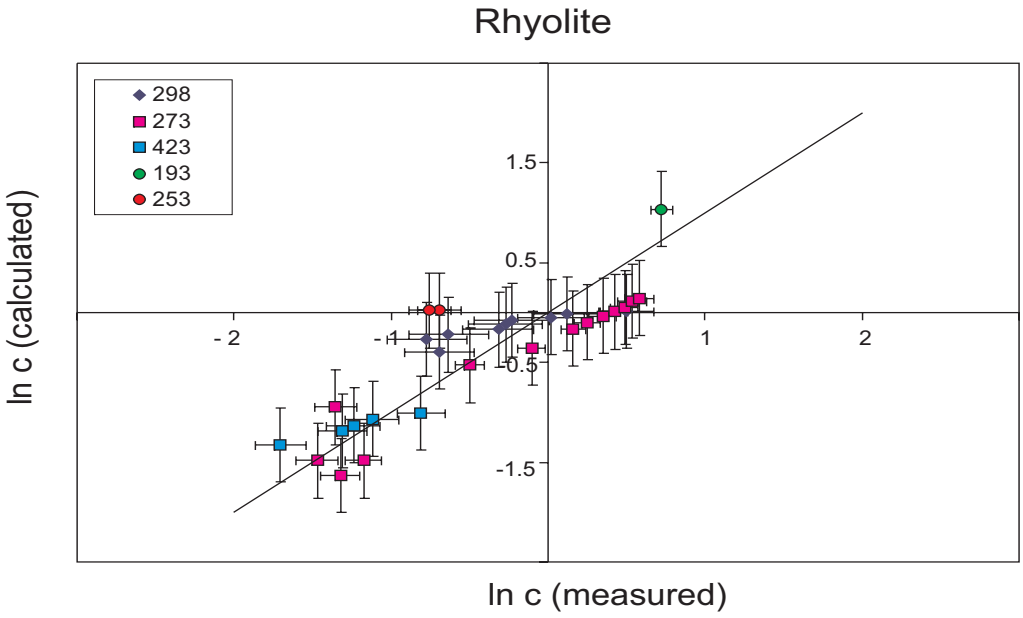

Figure 4.17: Multiple regression on adsorption data for SO_2 on rhyolite glass taken at -80°C, -20°C, 0°C, 25°C and 150°C. The amount of adsorbed SO_2 c is in mg/m^2. $R^2 = 0.75$

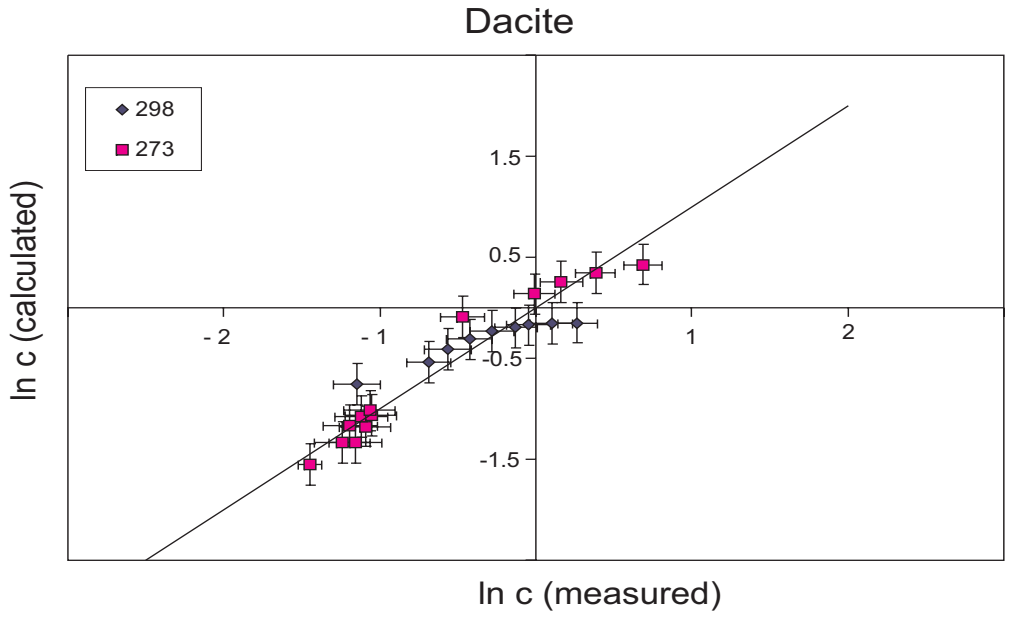

Figure 4.18: Multiple regression on adsorption data for SO_2 on dacite glass taken at 0°C and 25°C. c is in mg/m^2. $R^2 = 0.91$

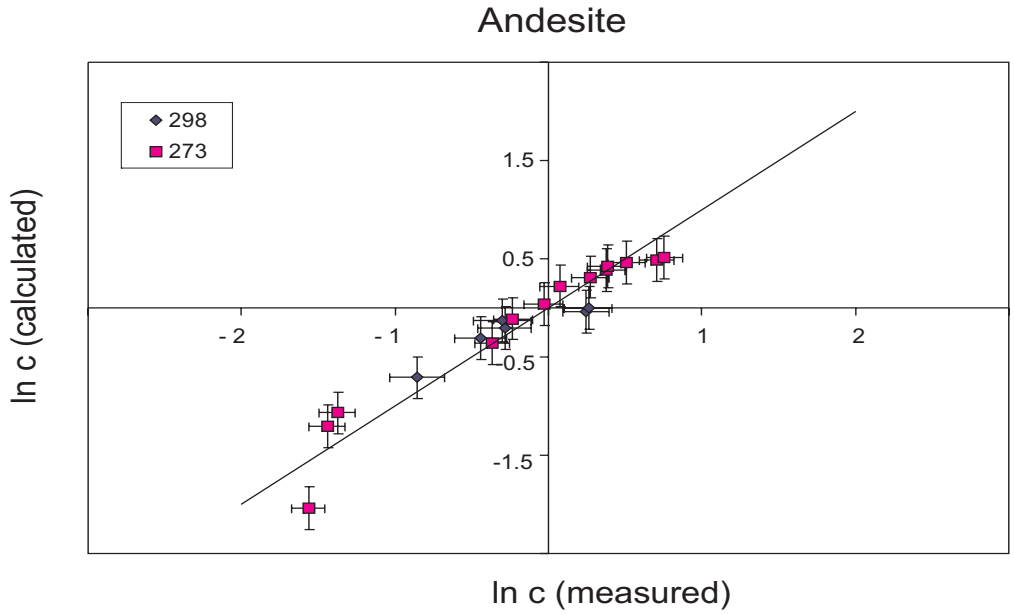

Figure 4.19: Multiple regression on adsorption data for SO_2 on andesite glass taken at 0°C and 25°C. $R^2 = 0.92$, c is in mg/m^2.

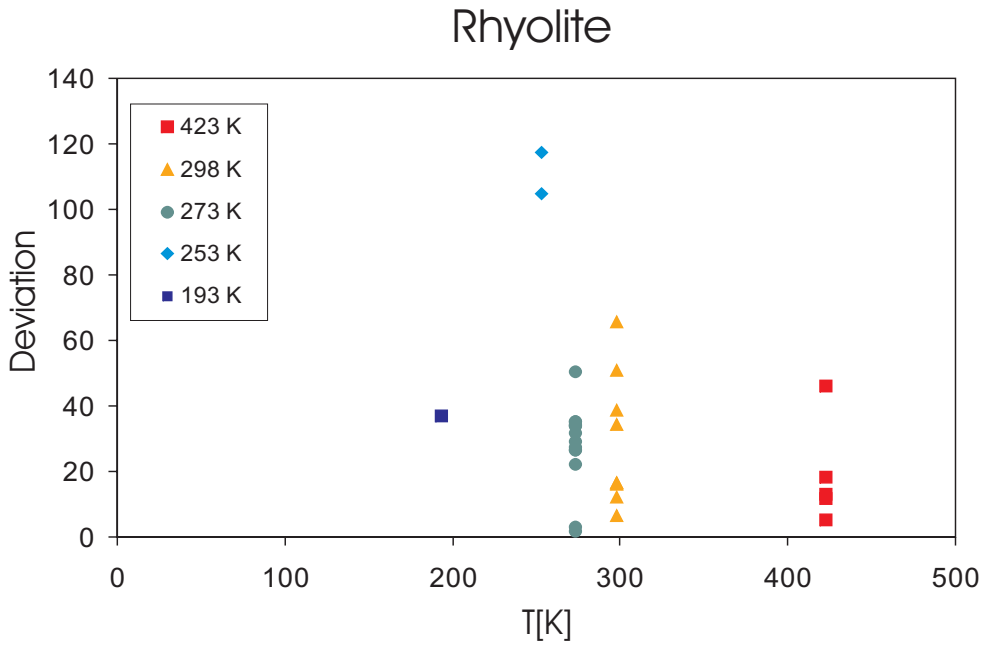

Figure 4.20: The deviation of the predicted amount (c_{pred}) of adsorbed gas from the measured amount (c_{meas}) at different temperatures. The dimensionless deviation is given as $|(c_{pred} - c_{meas})/(c_{meas}) \cdot 100\%|$

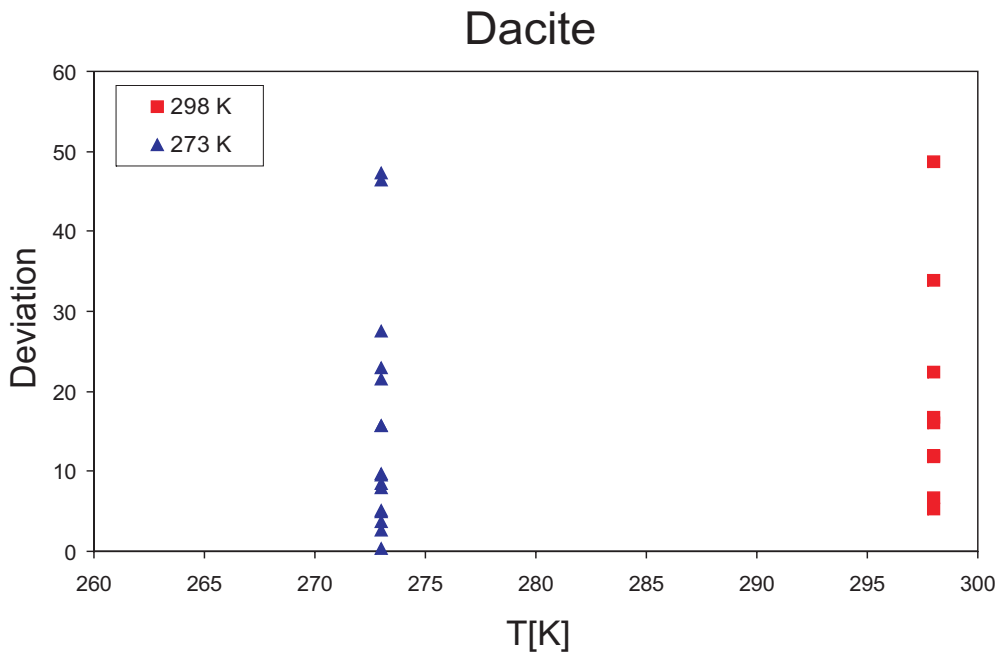

Figure 4.21: The deviation of the predicted amount (c_{pred}) of adsorbed gas from the measured amount (c_{meas}) at different temperatures. The dimensionless deviation is given as $|(c_{pred} - c_{meas})/(c_{meas}) \cdot 100\%|$

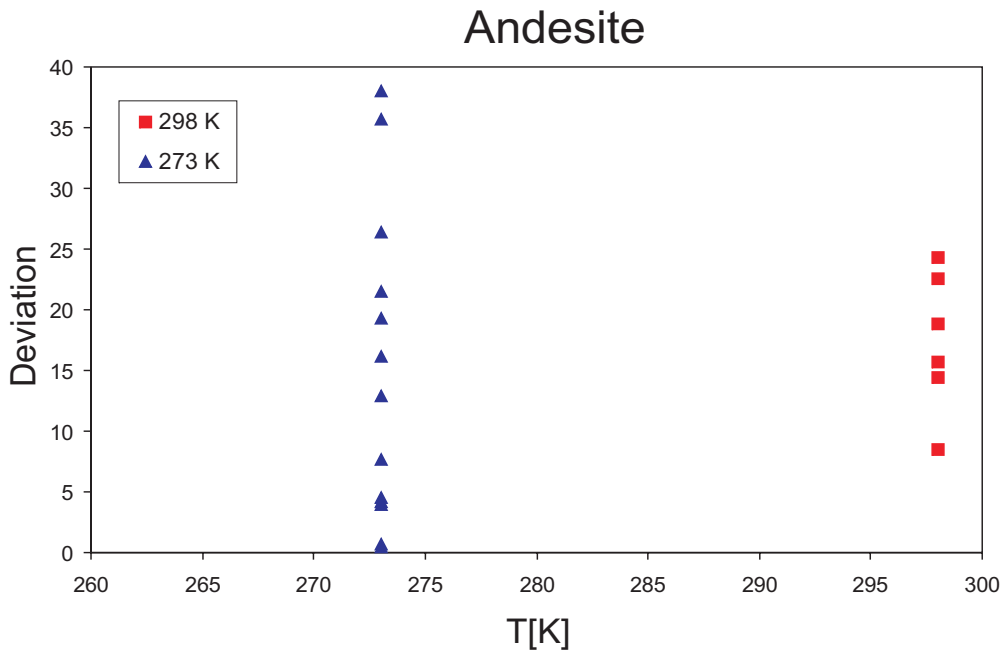

Figure 4.22: The deviation of the predicted amount (c_{pred}) of adsorbed gas from the measured amount (c_{meas}) at different temperatures. The dimensionless deviation is given as $|(c_{pred} - c_{meas})/(c_{meas}) \cdot 100\%|$

4.2.7 Correlation between solubility of SO_2 in water and the temperature dependence of adsorption

Since SO_2 is appreciably soluble in water, one may suspect that SO_2 adsorption is in fact due to the dissolution of SO_2 in a thin film of water on the glass surface. This hypothesis will be tested here.

The solubility of SO_2 in liquid water is also temperature dependent. It was tested whether there is a correlation between the solubility of SO_2 in water and the temperature dependence of adsorption. All experiments were conducted under dry conditions, e. g. before starting each experiment the probed glass powder was extensively exposed to vacuum conditions. Nevertheless, for the following consideration it was assumed that each powder grain may be covered by a monolayer of H_2O. As the available surface area of the glass powder was determined for each experiment, the total amount of water can be calculated. The amount of SO_2 potentially dissolved therein can be calculated from solubility data [5] of SO_2. In the temperature range from 0°C and 150°C the solubility of SO_2 in water steadily drops, having its maximum at 0°C. There are experimental results on the uptake of SO_2 onto ice at temperatures from −3°C to −60°C [15]. As the amounts are very small, the solubility for the experiments at −20°C and −80°C is negligible. In Table 4.8 the total amount of SO_2 potentially dissolved in the assumed monolayer of H_2O for the experiments with rhyolitic glass at 25°C, 0°C, −20°C and −80°C are listed. The numbers are overestimated, as the according solubility data refer to conditions at 1 bar. In none of the cited experiments such high equilibrium pressure was reached. Under these conditions, the amount of SO_2 that is soluble at the corresponding temperature, is two orders of magnitude lower than the measured values of SO_2-uptake. Therefore aqueous dissolution of SO_2 during the experiments is not likely to significantly contribute to adsorption.

Table 4.8: The amount of adsorbed SO_2 ($=c_{SO_2}$) at pressure p and temperature t in comparison with the theoretically solvable amount of SO_2 at the corresponding temperature ($c^t_{dissolved}$), alternatively at $t = 0$°C ($c^{0°C}_{dissolved}$). Based on the solubility of SO_2 in water at $p = 1$bar.

t	p/mbar	A_{powder}/m^2	c_{SO_2}/mg	c^t_{solved}/mg	$c^{0°C}_{dissolved}$/mg
25°C	940	42.68	70.23±7.03	1.17	2.86
0°C	471	51.10	91.32±6.78	3.42	3.42
-20°C	75	56.14	28.06±2.27	0	3.76
-80°C	46	73.02	150.70±2.69	0	4.89

4.3 Heats of adsorption

Physisorption is not only characterised by the type of the adsorption isotherm, but also by the corresponding heat of adsorption ΔH_A[26]. For physisorption ΔH_A is about -8 to $-40 kJ/mol$, which is in the same range as the heat of condensation for the gas. For chemisorption ΔH_A rises to about -60 to $-400 kJ/mol$. Equation 2.11 (see page 34) gives a simple means to evaluate the magnitude of ΔH_A from the BET isotherm of an adsorption experiment and from the heat of condensation of the vapor ΔH_L. In Table 4.9 the heats of adsorption ΔH_A^{approx}, derived from the BET isotherm of the SO_2 adsorption experiments at room temperature are shown. The values of ΔH_A^{approx} range from -13 to -14 kJ/mol, which is well within the order of the heat of condensation for SO_2 ($\approx 22 kJ/mol$ at $25°C$). This would be consistent with the type of isotherm observed, which is characteristic for physisorption.

Table 4.9: Heats of adsorption determined by equation 2.12 (see page 34).

	ΔH_A^{approx} in kJ/mol
Rhyolite	-13.99
Dacite	-13.90
Andesite	-13.30

The values for ΔH_A derived from equation 2.12 are only approximate and have to be varified.
In section 4.2.6 the data for adsorption on rhyolitic, dacitic and andesitic glass respectively, were fitted according to equation 4.13 by multiple regression. The heats of adsorption can easily be derived from the fitting results, listed in Table 4.7 (see page 69). The precoefficient A in Table 4.7, which describes the temperature dependence of adsorption, is defined as

$$A = -\frac{\Delta H_A}{R} \tag{4.14}$$

The resulting heats of adsorption $\Delta H_A^{regress}$ are listed in Table 4.10. The values are well within the range expected for physisorption.
In case of adsorption on dacite and on andesite the values for ΔH_A^{approx} match the values for $\Delta H_A^{regress}$ very well within the error bars. For adsorption on rhyolite the value of $\Delta H_A^{regress}$ is considerably smaller, this may be because unlike adsorption on andesite and dacite, adsorption on rhyolite not only involves data taken at medium temperatures (e. g. $0°C$, $25°C$), but also data taken at very low temperatures (e. g. $-20°C$, $-80°C$) and a relatively high temperature (e. g. $150°C$).

Table 4.10: Heats of adsorption, determined according to the results of multiple regression (see table 4.7)

	$\Delta H_A^{regress}$ in kJ/mol	error $[kJ/mol]$
Rhyolite	-7.56	1.03
Dacite	-17.79	3.15
Andesite	-13.68	3.02

4.4 Dependence on glass composition

In the preceding sections evidence for the dependence of adsorption on temperature was given. Generally, the amount of adsorbed gas strongly increases with decreasing temperature.
The dependence on the composition of the adsorbent is discussed below, based on experiments conducted with glasses of different composition.
In Figure 4.24 3 experimental data points for adsorption at room temperature are shown. The points represent adsorption on rhyolitic, dacitic and andesitic glass respectively. In the given pressure range (940 mbar – 965 mbar) dacitic and andesitic glass adsorbed almost the same amount of SO_2, whereas rhyolitic glass adsorbed 26 wt% more. The error bars range from ±13% to ±19% of the particular value. This example gives a first hint that the amount of adsorbed SO_2 depends on the composition of the glass.
To demonstrate the influence of the glass composition on adsorption, the amount adsorbed onto the different adsorbents was estimated from the corresponding relationship for equilibrium concentration (see Table 4.7) derived by multiple regression. The results show that the amount of adsorbed SO_2, at given pressure and temperature, depends on the composition of the adsorbent.
In Figure 4.23 the calculated isotherms for adsorption on rhyolite, dacite and andesite respectively are shown for 3 different temperatures (50°C, 10°C, -10°C). Obviously, the relative strength of adsorption on the three glasses changes with pressure and temperature (see Figure 4.23, 4.25).
A change in the sequence of adsorbents corresponds to the intersection of the isotherms. Therefore, the temperature and pressure, at which such changes take place, can be calculated mathematically. Figure 4.25 shows schematically, how the order of adsorbents changes within the temperature range from -80°C to 150°C. The considered pressure ranges from 0 to 1000 mbar. For low temperatures ($t \leq 10$°C) adsorption on dacite is strongest over a large pressure interval. At higher temperatures adsorption on rhyolite is strongest.

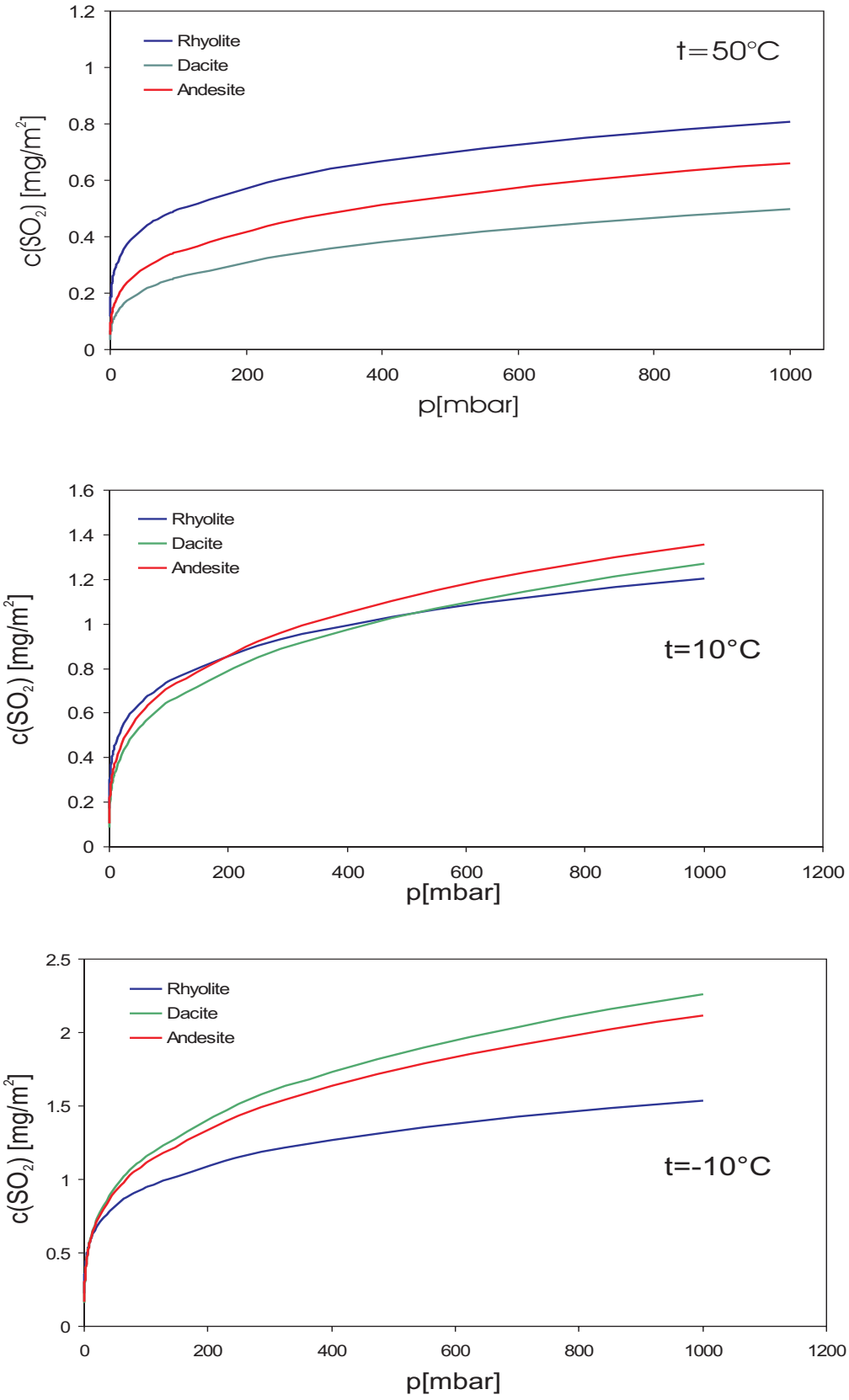

Figure 4.23: Adsorption isotherms, as calculated from multiple regression fits of experimental data (for parameters, see Table 4.7).

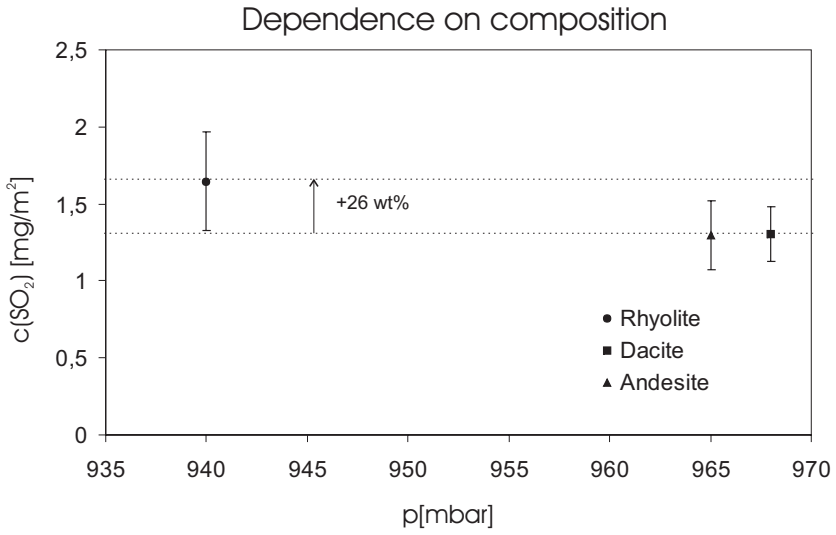

Figure 4.24: Adsorption at 25°C onto rhyolitic, dacitic and andesitic glass. Dacitic and andesitic glass adsorbed almost the same amount of SO_2, whereas rhyolitic glass adsorbed 26 wt% more. The error bars range from ±13% to ±19% of the respective value.

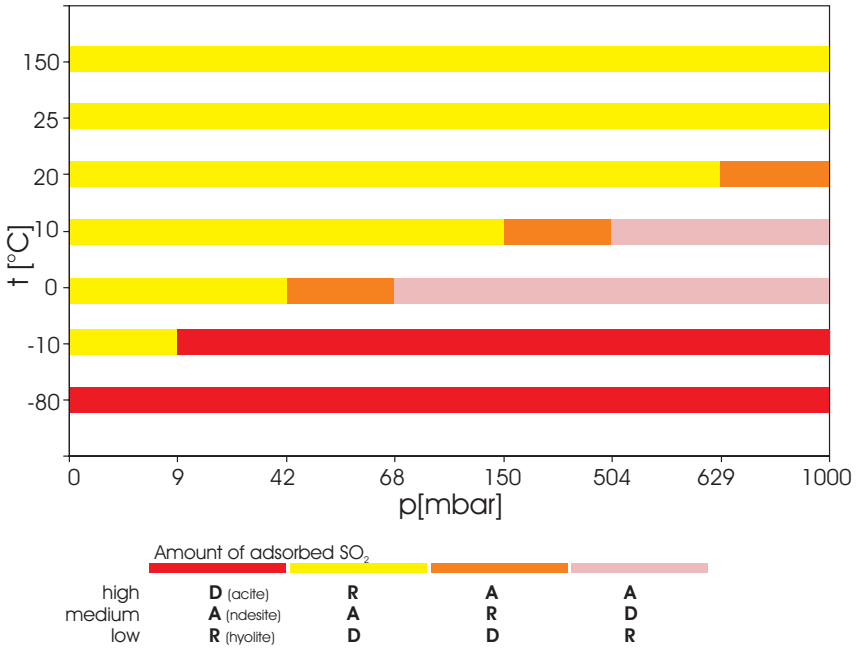

Figure 4.25: Relative strength of adsorption on rhyolite, andesite and dacite as a function of pressure and temperature. The designation of the bars in terms of colour indicate the sequence of adsorbents with respect to the amount of adsorbed gas. The qualitative sequence changes with temperature and pressure.

Chapter 5

Adsorption on natural volcanic glass

Adsorption on Lipari obsidian

Adsorption isotherm Two adsorption experiments at $t = 0°C$ on natural volcanic glasses were performed. In the first experiment Lipari obsidian served as the adsorbent. The formation of the Lipari obsidian is associated with calc-alkaline island arc volcanism of the Aeolian Islands [20]. Of them the island of Lipari is the largest one and is famous for its obsidian deposits. The Lipari obsidian is noted as an excellent secondary standard for the analysis of vitric tephra [20]. The chemical composition and its density is listed in Table 5.1.

Table 5.1: Electron microprobe analysis of the Lipari obsidian. Data were taken from [20].

density[a] g/cm^3	SiO_2	Na_2O	K_2O	FeO[b]	MgO	Al_2O_3	CaO	MnO
2.36	74.35	3.93	5.12	1.51	0.05	12.87	0.74	0.08

[a] own evaluation with hydrostatic balance
[b] FeO indicates total iron ($Fe_2O_3 + FeO$)

In Figure 5.1 the adsorption-desorption isotherm of the experiment is depicted. Obviously SO_2 is adsorbed readily. The isotherm shows some hysteresis-like behaviour. This feature is not as distinct as for adsorption at $t = 25°C$ on the rhyolitic, dacitic and andesitic samples (see Figure 4.2). However, for the synthetic glasses no adsorption-desorption isotherms for $t = 0°C$ are available.
Adsorption is not completely reversible.

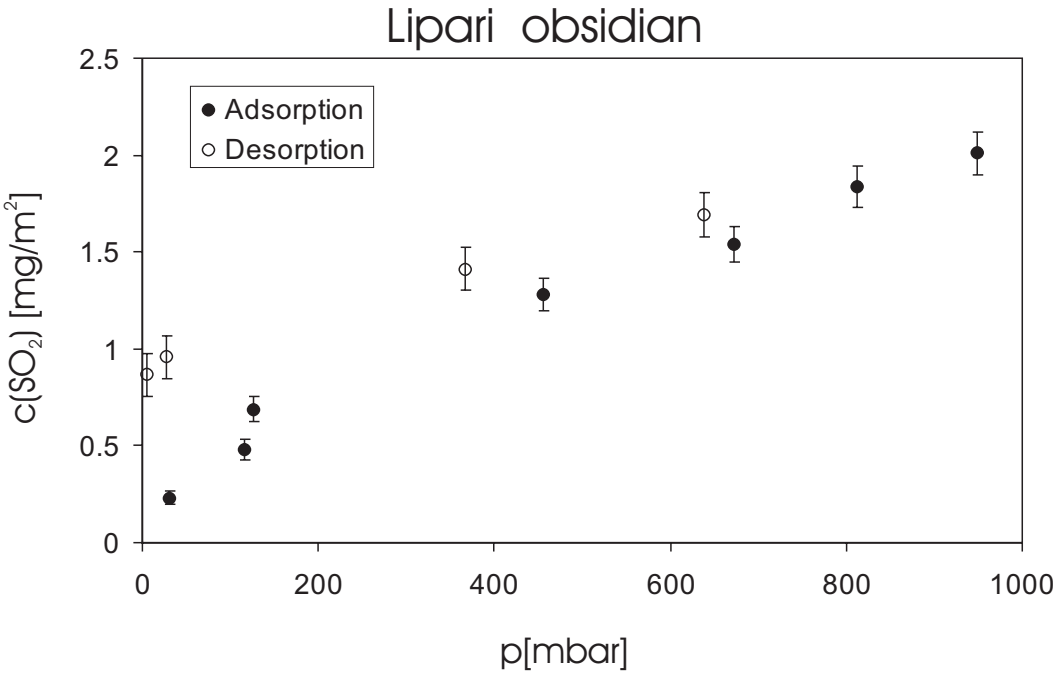

Figure 5.1: Adsorptionisotherm, with error bars, for adsorption of SO_2 on Lipari obsidian at $T = 273K$.

BET isotherm The data were fitted to the BET equation (equation 4.1, pp. 60) at relative pressures p/p_0 between 0.02 and 0.5. The calculated BET constant are listed in Table 5.4.
The V_m value is 0.33 cm^3/m^2 and equals the average V_m value derived from adsorption onto rhyolitic, dacitic and andesitic glass (see section 4.2.4). The C value, as a measure for the adsorbent-adsorbate interaction energy [17], for adsorption on the Lipari obsidian at 0°C is of the same magnitude as for adsorption at 25°C on the synthetic glass samples. The C values obtained from the 0°C isotherms for the synthetic glasses are significantly higher.

Freundlich isotherm The Freundlich constants are listed in Table 5.4. They were determined according to the linearized Freundlich equation (equation 2.10). The experimental data fitted the Freundlich isotherm very well, but as the data were recorded at relatively high pressures, the same constraints as for adsorption on synthetic glass have to be applied (see section 4.2.4).

Table 5.2: BET- and Freundlich isotherm parameters for SO_2 adsorption on Lipari obsidian. The notation of the listed BET constants is according to equation 4.2. The Freundlich constants are as quoted in equation 4.3. R^2 is a quality factor for regression, ranging from 1 (perfect correlation) to 0 (no correlation).

Lipari obsidian					
BET Constants					
t in $°C$	**I**	**S**	**C**	$\boldsymbol{V_m}$in cm^3/m^2	$\boldsymbol{R^2}$
0	0.041	0.62	16.00	0.33	0.9894
Freundlich Constants					
t in $°C$	$\boldsymbol{1/a}$		$\boldsymbol{\ln k}$		$\boldsymbol{R^2}$
0	0.62		-3.59		0.99

Heat of adsorpion ΔH_A For adsorption on Lipari obsidian only one isotherm is available. Therefore it is not possible to evaluate the heat of adsorption ΔH_A from temperature dependence of adsorption (equation 4.4), as done for adsorption on rhyolitic, dacitic and andesitic glass (see section 4.3).
The C value in the BET equation is related exponentially to the heat of adsorption. Although it does not yield a precise number for ΔH_A, it can be used as an order of magnitude estimate.

$$C \approx \exp \frac{\Delta H_A - \Delta H_L}{RT} \tag{5.1}$$

Applying equation 5.1 to the lipari adsorption data gives

$$\Delta H_A \sim -15 kJ/mol$$

This value is within the typical range for physisorption processes (see section 2.1).

Adsorption on trachyte obsidian

Adsorption isotherm The second experiment on natural volcanic glass was performed on hawaiian trachyte obsidian (Puu Waawaa obsidian). Puu Waawaa is located on the north slope of the Hualalai Volcano (Hawaii), 9.5 kilometers from the summit. Puu Waawaa is a cone of trachyte pumice, more than 1.5 kilometers in diameter. The trachyte lava flow is more than 270 meters thick and extends 9.5 kilometers northward from the cone. Scattered through the pumice are many blocks of black trachyte obsidian.
Its chemical composition and density is listed in Table 5.1. The adsorption experiment on the Puu Waawaa obsidian also was conducted at $t = 0°C$.

Table 5.3: XRF analysis of the Puu Waawaa obsidian. Data were taken from [14].

density[a]	SiO_2	Al_2O_3	Fe_2O_3[b]	MnO	MgO	CaO	Na_2O	K_2O	H_2O
$2.48 g/cm^3$	62.3	17.7	4.57	0.34	0.48	0.82	7.21	4.78	1.68

[a] own evaluation with hydrostatic balance
[b] Fe_2O_3 indicates total iron ($Fe_2O_3 + FeO$)

The adsorption-desorption isotherm of the experiment is shown in Figure 5.2. As for the experiments on synthetic glass and on lipari obsidian, the isotherm also shows hysteresis-like behaviour. After desorption to 3.3 mbar still about 50 wt% of the originally adsorbed gas (at $\sim$ 950 mbar) remained on the glass surface. Thus adsorption is not completely reversible.

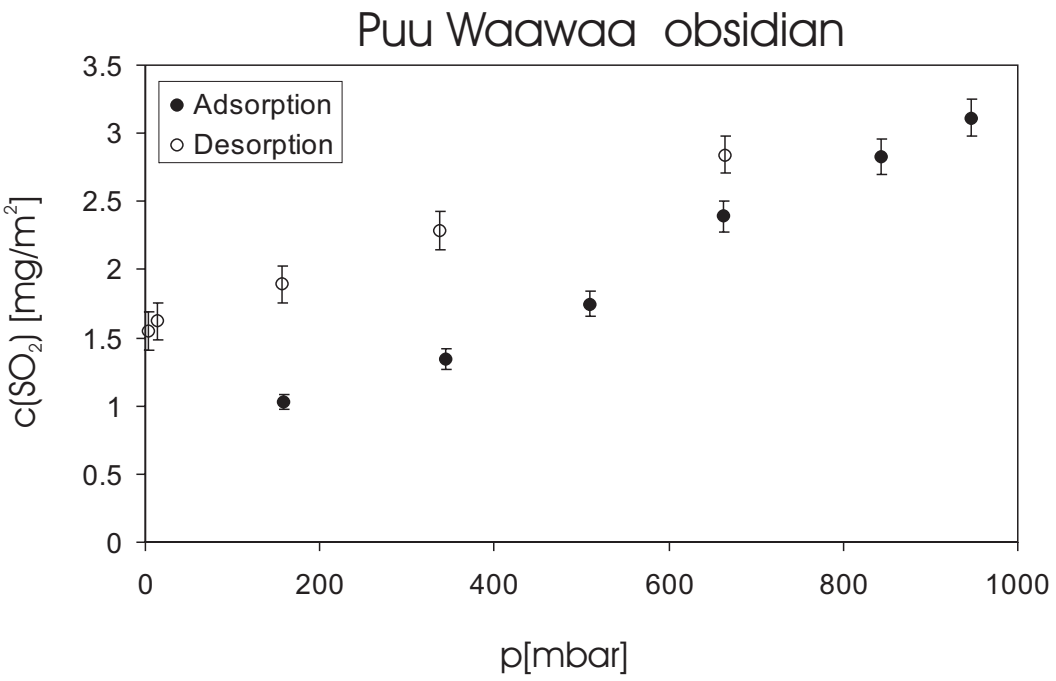

Figure 5.2: Adsorption isotherm for SO_2, with error bars, for adsorption on Puu Waawaa obsidian at $T = 273K$.

BET isotherm The data were fitted to the BET equation at relative pressures p/p_0, between 0.02 and 0.5. The calculated BET constants are listed in Table 5.4.
The V_m value is 0.47 cm^3/m^2. It is higher than the average value derived from adsorption on the synthetic glass samples and on the Lipari obsidian (in each case: $V_m = 0.33cm^3/m^2$). The C value for adsorption on the Puu Waawaa obsidian at 0°C is of the same magnitude as for adsorption on the Lipari obsidian.

Freundlich isotherm The Freundlich constants (see Table 5.4) were determined according to the linearized Freundlich equation. The experimental data fitted the Freundlich isotherm very well. As they were recorded at relatively high pressures, the same constraints as for adsorption on synthetic glass have to be applied (see section 4.2.4).

Heat of adsorpion ΔH_A The heat of adsorption ΔH_A can not be evaluated from the temperature dependence of adsorption, as the experiment was conducted only at one specific temperature.
Evaluating the magnitude of ΔH as a first order approximation, from the C value of the BET equation, according to equation 5.1 gives

$$\Delta H_A \sim -15kJ/mol$$

This value for ΔH suggests a strictly physisorptional process.

Table 5.4: BET- and Freundlich isotherm parameters for SO_2 adsorption on Pu Waawaa obsidian. The notation of the BET- and Freundlich constants is as described in equation 4.2 and equation 4.3. R^2 is a regression quality factor.

Pu Waawaa Obsidian					
BET Constants					
t in $°C$	**I**	**S**	**C**	$\boldsymbol{V_m}$ in cm^3/m^2	$\boldsymbol{R^2}$
0	0.029	0.56	20.10	0.47	0.9791
Freundlich Constants					
t in $°C$	$\boldsymbol{1/a}$		$\boldsymbol{\ln k}$		$\boldsymbol{R^2}$
0	0.64		-3.32		0.95

Chapter 6

Volcanic plumes

6.1 Introduction

Volcanic plumes are mainly produced during explosive eruptions. They are composed of a mixture of particles, volcanic gases, water and air. In most cases the initial bulk density of the mixture is higher than the ambient air. The initial ascent of the plume is due to the momentum gained by gas exsolution. Density decreases, as atmospheric air is entrained into the gas thrust region (see Fig. 6.1) by the development of turbulent eddies at the margins of the plume [37]. The gas is heated by the solids and expands, resulting in a decrease of the plume's density with height. In the convective phase of the plume, its density becomes less than that of the surrounding atmosphere, resulting in buoyancy [12]. The gas thrust region may extend for tens of kilometers into the atmosphere. Due to the entrainment of air the width of the plume steadily increases, whereas its temperature decreases, and so does the density difference to the surrounding air [12]. Eventually the plume's density and the density of the ambient atmosphere are the same [37]. At a level of neutral buoyancy, H_b (Fig. 6.1) the material starts to spread laterally. Nevertheless, the maximum plume height H_t is higher than H_b due to the excess momentum the plume has, when it reaches the level of neutral buoyancy [12]. The region between H_b and H_t is called umbrella region (see Fig. 6.1), where the plume spreads laterally.
The behaviour of volcanic plumes is controlled by the amount and composition of gases, the rate of magma discharge, the vent geometry [12]. Some plumes are maintained over relatively long periods of time by a continuous discharge of material, whereas some plumes form discrete injections into the atmosphere [12].

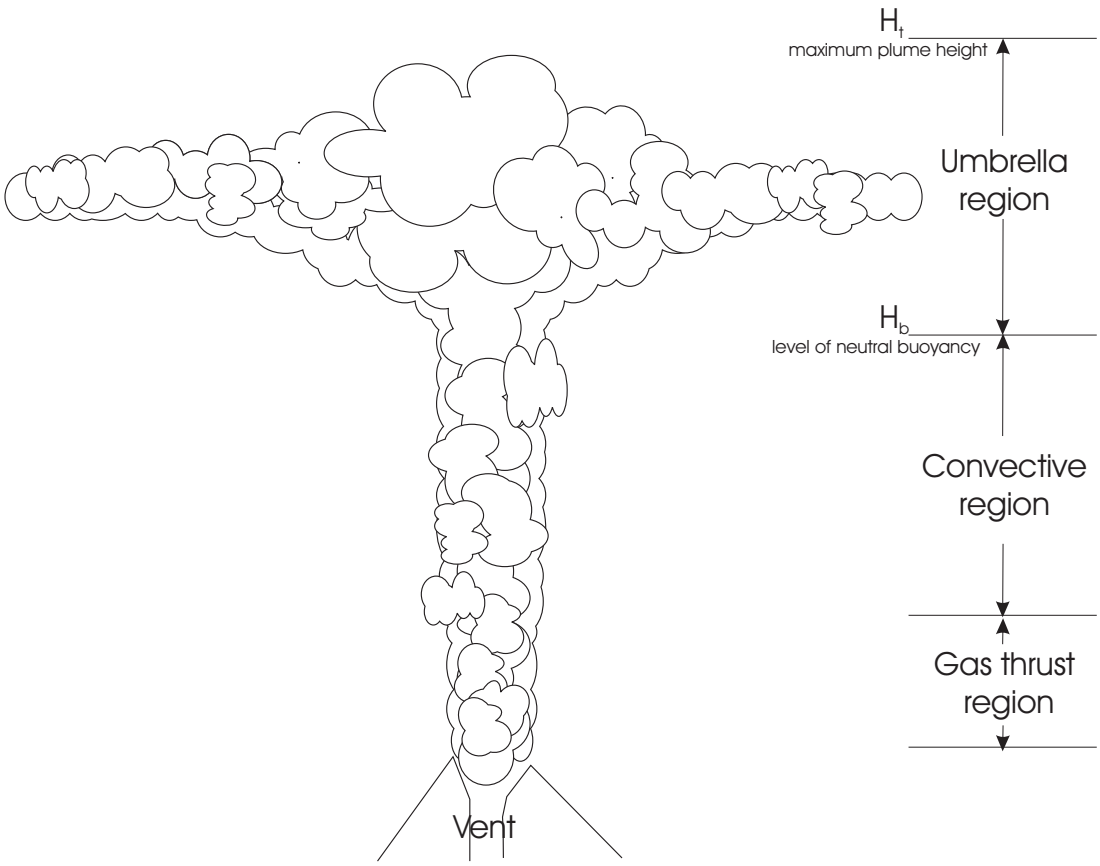

Figure 6.1: Sketch of the different regions of a volcanic eruption column.

6.2 The gas thrust- and convective region of a model plume

For evaluating a general framework for the adsorption conditions in an eruption column, this section presents a simple temperature-height model of a plume. The development of the partial pressure of the SO_2 is calculated as well.

6.2.1 Temperature-height model

For estimating the development of the temperature with height in the gas thrust- and convective region (see Fig. 6.1), it is necessary to be aware of some starting parameters, concerning the physical nature of the plume and its environment. An overview on the parameters is given in Table 6.1.

Table 6.1: Parameters used for calculating the development of temperature with height of an eruption column.

parameter		*value*	*remarks*
Starting temperature of mixture	T_0	1000K	
Starting gas mass fraction	σ	0.03[40]	
Starting composition of gas fraction			see Table 6.2
Temperature-height model of standard atmosphere			see Figure 6.2
Heat capacity of the ash	$c_p^{Ash}(T)$	$\sim 1200 J/kg/K$	see Table 6.4
Heat capacities of the gaseous components	$c_p^{Gas}(T)$		see Table 6.3
Entrainment coefficient	ϵ	0.09[37]	

Heat content of the mixture
It is assumed that the thermal energy of the solids and the gas is conserved. The pyroclasts in the mixture are assumed to be very fine-grained, so that the heat transfer between the particles and the gas in the column is very rapid and thermal equillibrium is achieved within seconds. The mixture is modeled to ascend as one phase of uniform temperature and velocity. The heat content of the starting plume is defined by the starting temperature T_0 (=1000K) of the gas and the ash, the according heat capacities and the starting gas mass fraction σ (=0.03).
The starting mixture
The composition of the starting gas fraction is according to Table 6.2. The heat capacities of the gases ($c_p^{Gas}(T)$) are listed in Table 6.3. The ash is assumed to be

of rhyolitic composition, according to Table 3.1. The exact heat capacity of the ash fraction ($c_p^{Ash}(T)$) then was calculated by the partial molar heat capacities of the oxides as listed in Table 6.4.

Table 6.2: Equilibrium compositions of high-temperature volcanic gas. Adapted after Symonds et al. [39]. The concentration of the listed species is given in mole%.

Site	Date	H_2O	CO_2	SO_2	HCl
Merapi	1979	88.87	7.07	1.15	0.59

Table 6.3: The temperature dependent heat capacities of the gaseous components relevant for the model plume.

	Temperature range [K]	c_p in $cal/mol/grd$
H_2O[2]	298-1500	$7.256 + 2.298 * 10^{-3}T + 2.83 \times 10^{-7}T^2$
CO_2[1]	298-1500	$5.152 + 15.224 \times 10^{-3}T - 9.681 \times 10^{-6}T^2 + 2.319 \times 10^{-9}T^3$
SO_2[5]	173-1673	$8.1704 + 6.6820 \exp(-1957.326/T^{1.25})$
HCl[3]	200-2000	$7.053 - 0.8712 \times 10^{-3}T + 1.916 \times 10^{-6}T^2 - 0.5635T^3$
dry air[4]	173-1773	$-2 \times 10^{-7}T^2 - 0.0016T + 6.5076$

Entrainment of air

Calculating the heat content of the ascending plume makes it necessary to take into account the entrainment of ambient air. Entrainment causes a change in the gas mass fraction and a compositional change of the gaseous part of the plume. It also results in cooling the column. Below it is assumed, that the entrainment is independent from the size of the plume. This corresponds to the motion of a simple buoyant plume in a uniform environment (e. g. the density of the surrounding fluid does not vary with height)[37]. In this case the radius of the plume b increases linearly with height above the source z [37]:

$$b = \frac{6\epsilon}{5} z \tag{6.1}$$

ϵ is the entrainment coefficient, and is a measure of the efficiency of mixing of the plume with ambient air.

With the assumption that the system admits a self-similar flow the plume spreads with an constant angle θ, where

$$\tan\theta = 6\epsilon/5 \tag{6.2}$$

Table 6.4: Coefficients of partial molar heat capacities of oxides in silicate glasses: $C_{Pi} = a_i + b_i T + c_i T^{-2} + d_i T^{1/2}$ $[J/mol/K]$. *A*dapted after [30]

	a_i	$10^3 b_i$	$10^{-5} c_i$	d_i	$\Delta T^a[K]$
SiO_2	127.200	-10.777	4.3127	-1463.9	270-1600
Na_2O	70.884	26.110	-3.5820	0	270-1170
K_2O	84.323	0.731	-8.2980	0	270-1190
CaO	39.159	18.650	-1.5230	0	270-1130
MgO	46.704	11.220	-13.280	0	270-1080
Al_2O_3	175.491	-5.839	-13.470	-1370	270-1190

[a]Temperature interval of the experimental data used to derive C_{Pi}

In the gas thrust region a number of models for the entrainment of air have been developed. The simplest model is to assume that the gas thrust region is fully mixed and entrains with $\epsilon = 0.09$ [37]. For the convective region the entrainment coefficient is taken to be constant 0.09.

Standard atmosphere

The temperature of the "diluted" plume depends on the temperature development of the surrounding atmosphere. Therefore the temperature variation with height of a standard atmosphere model [37] is used as one input parameter (see Fig. 6.2).

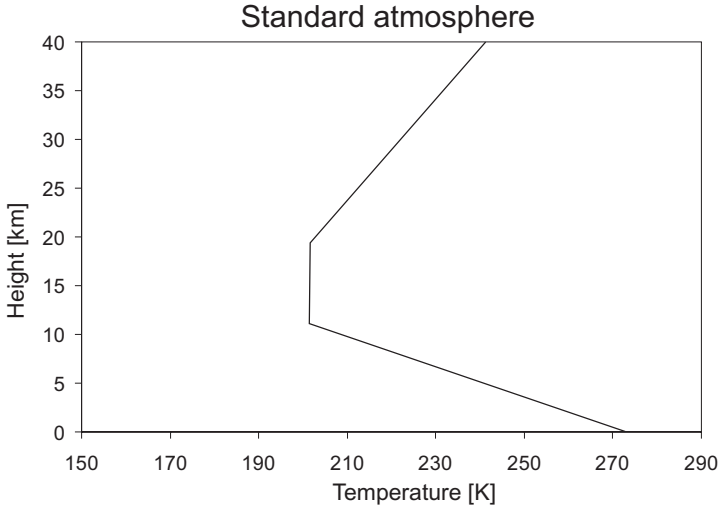

Figure 6.2: Temperature variation with height in the standard atmosphere according to [37]

Temperature-height model of the eruption column.
In Figure 6.3 the development of temperature with the height of the modeled gas/ash plume is shown and compared to the temperature pattern of a gas-only plume. Due to the heat content of the ash the gas/ash plume cools down much more slowly than the gas-only plume.

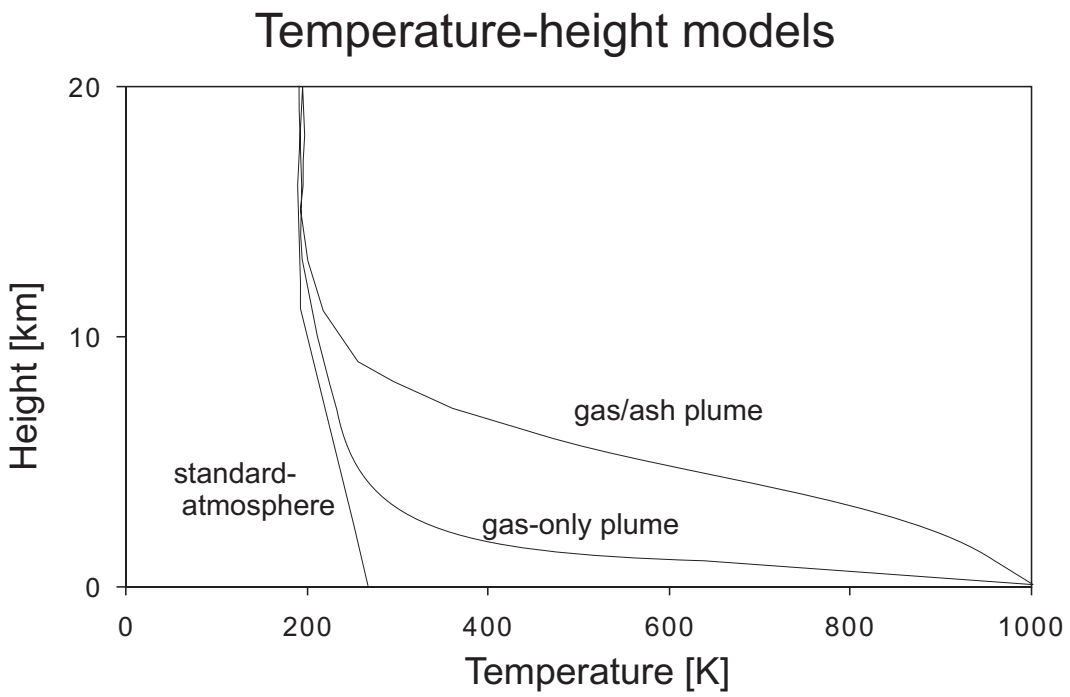

Figure 6.3: The temperature profil of the modeled gas/ash plume, the gas-only plume and the standard atmosphere.

6.2.2 SO_2 partial pressure

The partial pressure of the $SO2$ as a function of temperature and ascending height is shown in Figure 6.4. Also the partial pressure drops relatively fast at the given starting conditions of the plume.

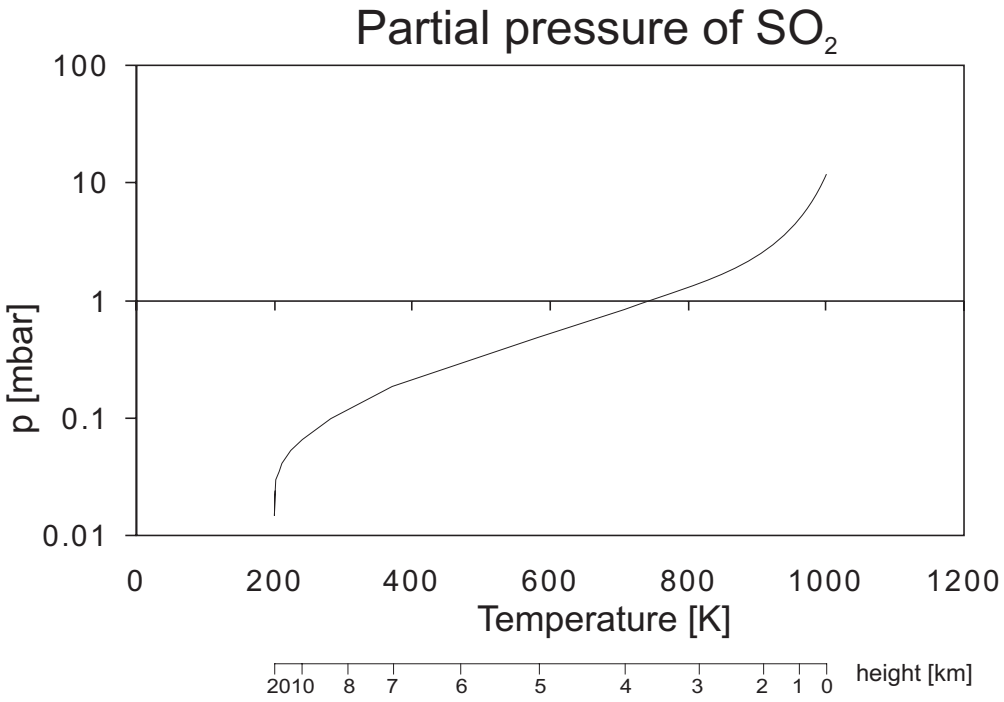

Figure 6.4: The development of the partial pressure of SO_2 as a function of the temperature and the height above the vent, respectively.

6.3 The umbrella region of a model plume

When the convecting eruption column reaches its height of neutral bouyancy H_b (see Figure 6.1) it is driven upwards by its inertia [37] to its maximum height H_t. When the eruption column reaches H_t it begins to flow downward. Eventually it is spreading laterally around its height of neutral buoyancy forming an intrusion that is referred to as the umbrella cloud [37].

6.3.1 Temperature-time model

The development of temperature with time in the umbrella cloud is investigated in the following section.
A compilation of the required parameters is given in Table 6.5.

Table 6.5: Key-parameters used for calculating a temperature model of an umbrella cloud.

parameter		***value***	***remarks***
Column height	H,(H_t)	$\sim 9km$	depends on u_0,b_0
Velocity at vent	u_0	$100m/s$	arbitrary
Vent radius	b_0	$100m$	arbitrary
Temperature of the column at H_t	T_1(t=0)	$\sim 260K$	see Fig. 6.1
Depth of the umbrella cloud	ΔH		time dependent
Volume of the umbrella cloud	V	$\sim 14km^3$	constant
Radius of the umbrella cloud	R		time-dependent
Umbrella shape factor	λ	0.8[37]	constant
Heat transfer coefficient	α	$6W/m^2/K$[44]	

Column height *H*
The height of the eruption column was calculated using equation 6.3 [37].

$$H = 5\left(\frac{gQ}{\rho_e C_0 T_a}\right)^{1/4} N^{-3/4} \tag{6.3}$$

where ρ_e (kg/m^3) is the density of the environment (standard atmosphere: $1.25kg/m^3$); C_0 $(J/kg/K)$ is the initial specific heat of the eruption mixture; T_a is the ambient temperature; g is the gravitational acceleration (m/s^2); N is related to the stratification in the environment; Q is the total energy flux due to the hot pyroclasts.

The stratification in the environment is defined relative to the adiabatic stratification, and is given by

$$N^2 = \frac{g\Gamma}{T_1}(1 + \eta_a) \tag{6.4}$$

Γ is the lapse rate of the atmosphere (e. g. the adiabatic rate of decrease of temperature in the atmosphere); η_a is the ratio of the absolute temperature gradient to the lapse rate; T_1 is a reference temperature (e. g. the ground temperature). The thermal energy flux Q is defined by

$$Q = C_0(T_0 - T_a)\beta_0 u_0 \, b_0^2 \tag{6.5}$$

β_0 is the initial bulk density of the mixture; u_0 is the velocity at the vent; b_0 is the vent radius.
Solving equation 6.3 in consideration of equations 6.4 and 6.5 yields that the column height of the model plume described in section 6.2 is about 9 km (see Table 6.5). For calculating the temperature profile of an umbrella cloud model, the maximum column height is important as it defines starting parameters as the starting temperature $T_{t=0}$, the initial radius R_0 of the umbrella cloud and therefore its volume V_0.

Volume and radius of the umbrella cloud model

In the most common situation the umbrella plume is supplied by a time-dependent mass flux as $Q(t) = Q_0 t^b$ [37]. Where $b = 0$ corresponds to continuous emplacement, $b > 0$ implies an increase of the supply rate with time and $b < 0$ implies, that the supply rate decreases with time. The radius of the umbrella cloud then is given by

$$R^3 = R_0^3 + \frac{3\lambda N Q t^{b+2}}{\pi(b+2)(b+1)} + \frac{3\lambda N V_0 t}{\pi} \tag{6.6}$$

where R_0 is the plume radius and V_0 is the volume at $t = 0$; λ is a dimensionless constant, which accounts for the shape of the plume.

Discrete volcanic explosion

Assuming an instantaneous volcanic eruption, equation 6.6 reduces to

$$R^3 = R_{H_s}^3 + (3\lambda V N(\pi)t \tag{6.7}$$

R_{H_s} is the radius of the plume at height H_t. To a first approximation R_{H_s} is

$$R_{H_s} = 0.2H_t \tag{6.8}$$

In Figure 6.5 the radius as a function of time for an umbrella cloud, as arising from the model plume as described in section 6.2, is depicted.
In case of discrete eruptions the mass and volume of the plume are supposed to be conserved as it expands laterally [37]. It is assumed that entrainment is negligible. Under these conditions, the volume of the umbrella cloud relates to the radius and depth:

$$V = \pi R^2 \Delta H = \text{constant} \tag{6.9}$$

with R is according to equation 6.7. The depth ΔH of the cloud can be described as

$$\Delta H = 0.24 H_t - 8 b_0 \tag{6.10}$$

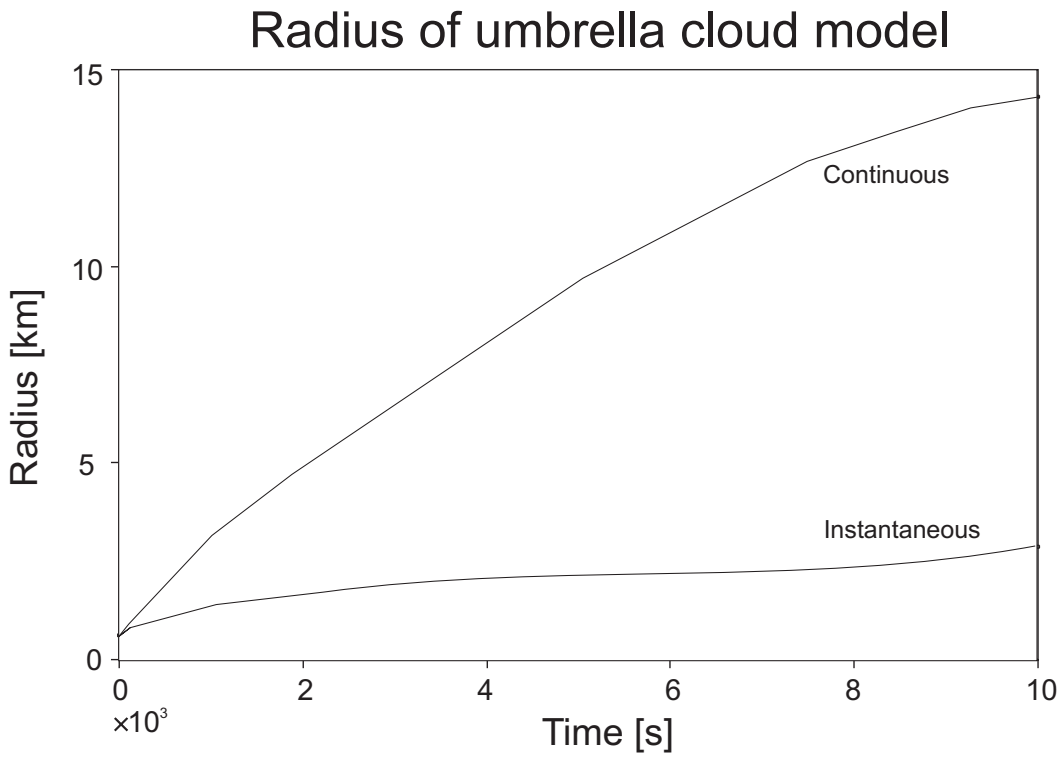

Figure 6.5: Theoretical curves on radius as a function of time for the umbrella cloud. The radius grows more rapidly for a continuous than for an instantaneous source.

Temperature of the umbrella cloud model as a function of time
The umbrella cloud model is based upon the database for the model of the ascending plume (section 6.2). For calculating the temperature of the umbrella cloud model as a function of time, a discrete volcanic eruption is assumed. In this case, the plume is assumed to be emplaced instantaneously. The radius of the umbrella cloud then is given by equation 6.7 and 6.8 respectively, and its volume is given by equation 6.9.
The evolution of temperature of the umbrella cloud with time was estimated applying *Newton's law of cooling*

$$P = \alpha A (T_1 - T_2) \tag{6.11}$$

where P is the heat flux [W]; α is the surface heat transfer coefficient $[W/m^2/K]$; T_2 is the temperature of the fluid and T_1 is the temperature of the body (surface area: A; mass: m_1; heat capacity: c_1), which is immersed in the fluid.
Newton's law of cooling states, that the rate of cooling of a body with surface A and initial temperature T_1, that is immersed in a fluid of temperature T_2 is proportional to the difference between the temperature of the surface of the body and the temperature of the fluid. In case when T_2 is constant and there is no additional heat supply to the immersed body, Newton's law of cooling can be reformulated:

$$T(t) - T_2 = (T_1(t) - T_2)exp\left(-\frac{\alpha A}{m_1 c_1}t\right) \tag{6.12}$$

$T(t)$ is the adjusted temperature of the body at time t.

The approach here was to treat the umbrella plume as a body immersed in the surrounding atmosphere. This assumption is justified, as the dimensions of the intruding body is small as compared to the surrounding fluid. The surface area of the plume, that enters equation 6.12, was calculated assuming cylindrical spread of the cloud. The initial dimensions thereby were defined by the starting radius R_{H_s} (equation 6.8) and the initial depth of the cloud ΔH (equation 6.10). Applying equation 6.7, assuming constant volume, gives the surface area as a function of time.
The development of temperature in the umbrella cloud with time is depicted in Figure 6.6. The temperature drops to ambient atmospheric temperature at 9 km altitude ($\sim 208K$) within less than 3 hours.

6.3.2 SO_2 partial pressure

SO_2 partial pressure without adsorption

The partial pressure of SO_2 in the umbrella cloud is assumed to be the same, as in the ascending plume at height H_t as no entrainment is supposed to occur during the umbrella cloud formation. The ascending height of the model plume was calculated to be $H_t = 9km$. The SO_2 partial pressure in the umbrella cloud then follows from Figure 6.4 to be $0.07mbar$.

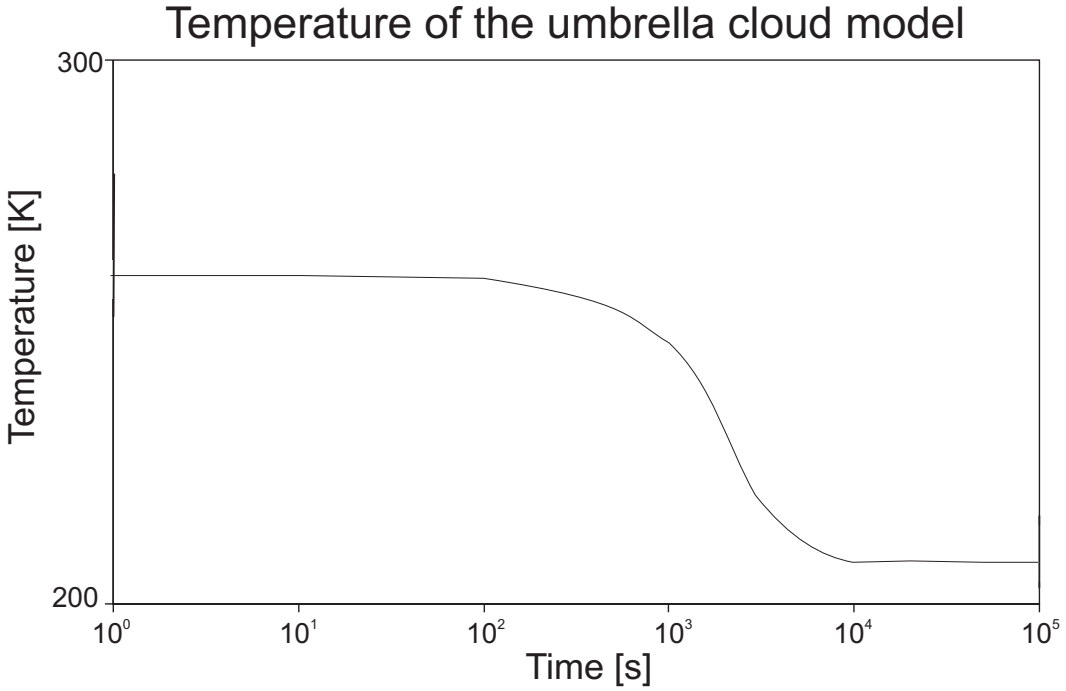

Figure 6.6: The temperature of the umbrella cloud model as a function of time.

6.4 Adsorption of SO_2 in the plume

6.4.1 Adsorption in the plume model

In the sections 6.2 and 6.3 the temperature and pressure conditions for adsorption occuring during a volcanic eruption were evaluated. For the cited plume model, the partial pressure of SO_2 drops rapidly while the plume is ascending. At its maximum ascent height ($H_t = 9km$) the partial pressure p is less than $0.1mbar$ (p=0.07 mbar). When the plume is starting to spread laterally and to form an umbrella cloud, the temperature drops fast to ambient stratospheric temperature, while the partial pressure of SO_2 remains constant, as no entrainment is allowed for.
The prevailing temperature-pressure constraints in the umbrella cloud make physisorption of SO_2 probable. The amount of SO_2 that is expected to be adsorbed in the plume can be calculated.
Adsorption in the ascending eruption column is neglected. In fact the temperature-pressure conditions in the eruption column reach values that are likely to allow for physisorption to some extent, but as the partial pressure of SO_2 drops very fast during the ascent of the column it is likely that at the same time desorption takes place. Also, the time available for adsorption in the ascending plume is very short ($\sim$ 90 sec.) and not comparable with the time available in the umbrella cloud (several hours, days). Following these considerations only adsorption in the

umbrella cloud at the lowest temperature was taken into account.
In the calculation it has to be taken into account, that the partial pressure of SO_2 in the cloud drops successively due to adsorption. So the amount of adsorbed SO_2 was calculated iteratively (see Table 6.6), using the results of the regression models for adsorption (see Table 4.7, p. 69) each with adopted values for the prevailing partial pressure of SO_2. Eventually, the total amount of adsorbed SO_2 is defined by the magnitude of available ash surface. In Figure 6.7 the estimated grain size distribution of the Mount St. Helens eruption in 1980 is illustrated [13]. Based on the depicted distribution and the given starting gas mass fraction σ (see Table 6.1) the total surface area of the suspended ash was evaluated, assuming no ash was driven out of the plume by sedimentation so far. In Table 6.7 the percentage of the total amount of adsorbed SO_2 relative to the total amount of SO_2 in the plume is given. The amount of SO_2 in the plume is determined by the starting gas composition (see Table 6.2). As derived in chapter 4.4 the amount of adsorbed gas is dependent on the composition of the adsorbent. As expected for low temperatures, ash of dacitic composition adsorbes the most, ash of andesitic and rhyolitic composition following (also see Figure 4.25).
Independent from the composition the calculation for the model plume suggests, that all of the originally emitted SO_2 could be adsorbed under the given conditions.

Table 6.6: The Table shows schematically how the amount of adsorbed SO_2 was calculated iteratively, taking into account that the pressure drops due to adsorption.

n(SO_2)total in plume	n(SO_2)iteratively removed	n(SO_2)remaining	p(SO_2)	n(SO_2)adsorbable at p(SO_2)	remainder
A(mole)	B_1(mole)	$A - B_1$	$\rightarrow p_1$ $= f(A-B_1)$	C_1(mole) $= f(p_1)$	$B_1 - C_1$
from starting composition	adjusted in steps		from Waals equation	from regression model	
	.	.	.	.	.
	.	.	.	.	.
	.	.	.	.	.
A(mole)	B_n(mole)	$A - B_n$	$\rightarrow p_n$	C_n(mole)	$B_n - C_n$ =0
$B_n - C_n = 0 \leftrightarrow A - B_n$ was adsorbed $\leftrightarrow p_n$ is equilibrium pressure					

Table 6.7: The total amount of adsorbed SO_2 at the final temperature-, pressure conditions in the model plume, relative to the total amount of SO_2 in the plume.

$p = 0.07\ mbar;\ T = 208\ K$	
adsorbent	amount of adsorbed SO_2 (% portion of the total amount)
Rhyolite, Dacite, Andesite	$\approx 100\%$

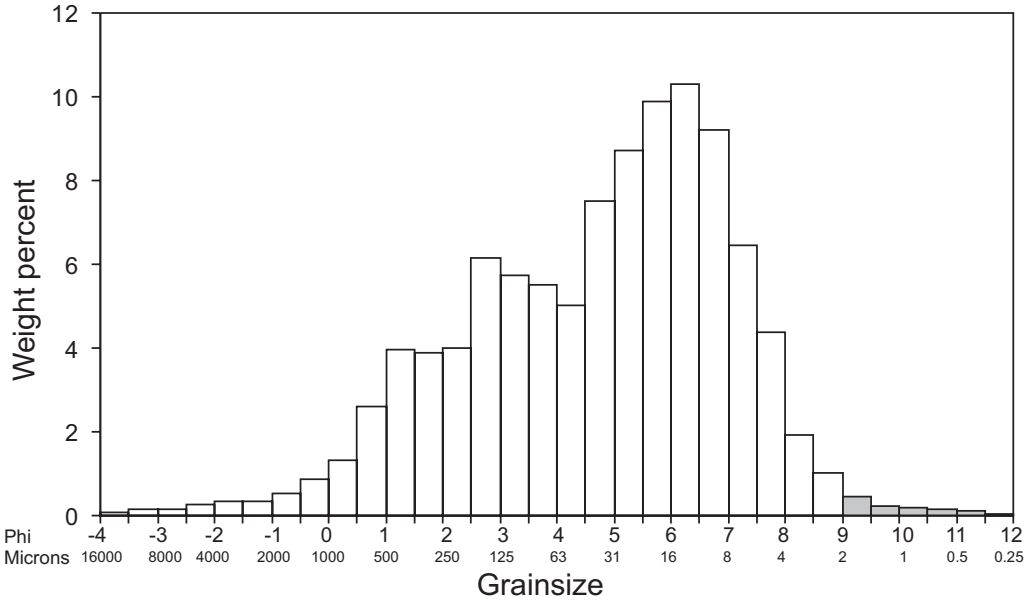

Figure 6.7: The estimated total grain size distribution of the Mount St. Helen eruption in 1980 (adapted after [13]). The ash fall deposit is within the area 0-500 km from the source. The shaded columns are added and are based on applying a Gauss Model to the depicted grain size distribution.

6.4.2 Factors controlling adsorption in a plume

The total amount of adsorbed SO_2 depends on the total surface area of the ash suspended in the plume, which again results from the starting gas mass fraction σ in the eruption column.
Moreover, the relative amount of adsorbed SO_2 (e. g. the adsorbed amount, compared to the total amount in the plume) dependes on the initial SO_2 content x_{SO_2} in the volcanic gas, where x_{SO_2} is given as $x_{SO_2} = n_{SO_2}/n_{Gas}$.

In the following, changes in the total amount of adsorbed SO_2 depending on σ and x_{SO_2} are described.
All calculations refer to the 'same' plume, as described in sections 6.2 and 6.3,

deviating only in σ and x_{SO_2} from it.

Varying gas mass fraction σ

A decrease in $\sigma = m_{Gas}/m_{Ash}$ results in an increase of ash mass in the plume and thus in an increase of the total surface area of the ash suspended in the plume (see Fig. 6.8). However, a variation in σ not only has an effect on the available surface area of the ash in the plume, but indirectly also influences the partial pressure at which adsorption takes place:
From equation 6.5 it follows, that the column height of the plume, among others, depends on the initial bulk density β_0 of the gas/ash-mixture. The higher the gas mass fraction σ is, the higher the bulk density β_0. Consequently, σ has an effect on the column height H_t, such that an increase of σ results in a decrease of H_t. As the partial pressure of SO_2 mainly drops during the ascent of the plume due to dilution, it follows that the lower H_t is, the higher is the final partial pressure of SO_2 in the plume.
However, that effect is of minor importance, the decisive factor is the ash surface, that is available for adsorption. Consequently, a decrease in σ results in an increase of adsorbed gas (see Fig. 6.9 and Fig. 6.10).
In Figure 6.9 σ varies from 0 to 0.3 to clearly show the influence of the gas mass fraction on the amount of adsorbed SO_2. Nevertheless, from geological considerations values for σ ranging up to 0.1 are more reasonable because the amount of dissolved volatiles in the orignal magma will always be below 10% (see Fig. 6.10).

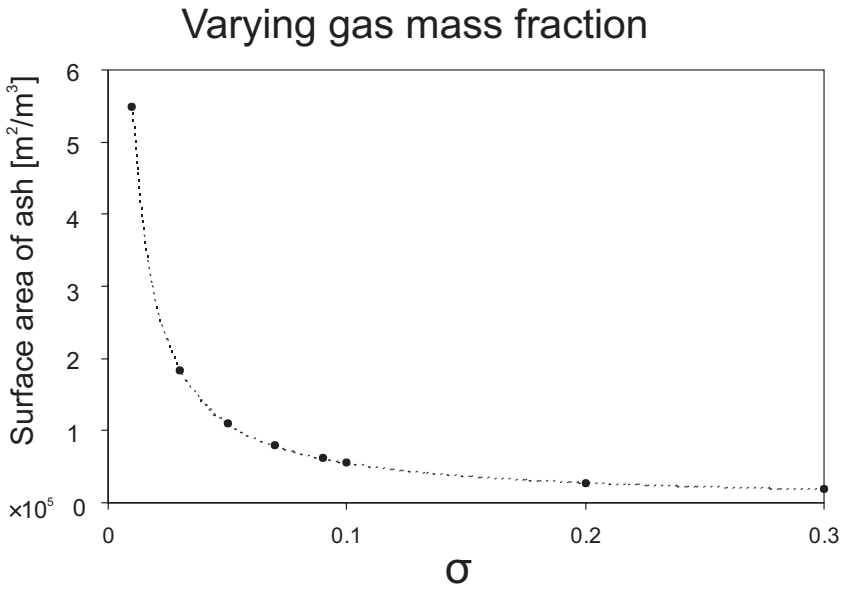

Figure 6.8: Variation of the relative ash surface area of the suspended ash in the plume model with varying gas mass fraction σ. The numbers were normalized to a starting volume of the plume $V_{plume}^{start} = 1m^3$, with $V_{Plume}^{Start} = V_{Gas} + V_{Ash}$

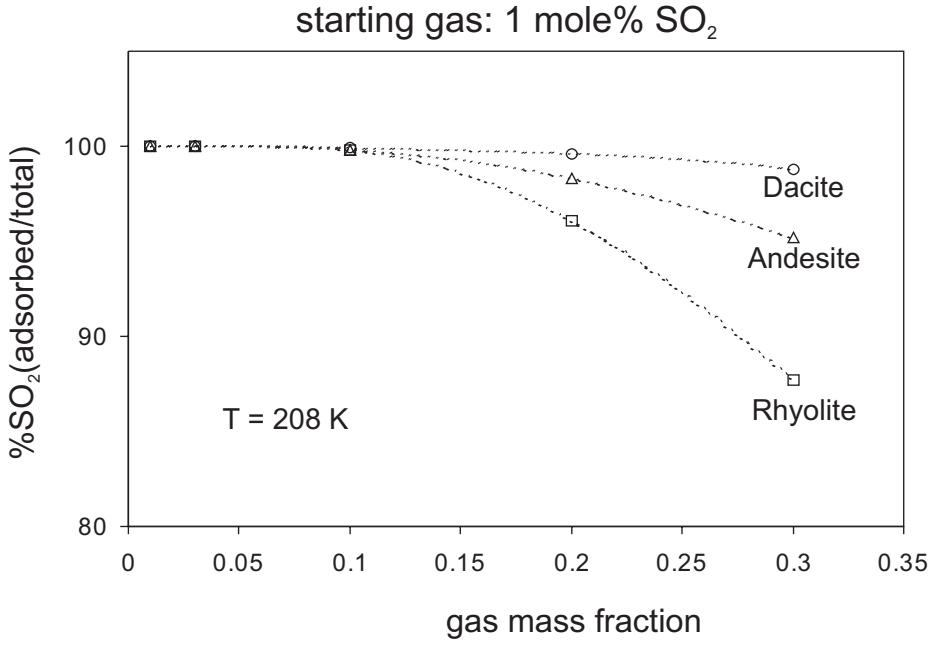

Figure 6.9: The fraction of adsorbed gas relative to the total amount of SO_2 in the plume, against the gas mass fraction σ.

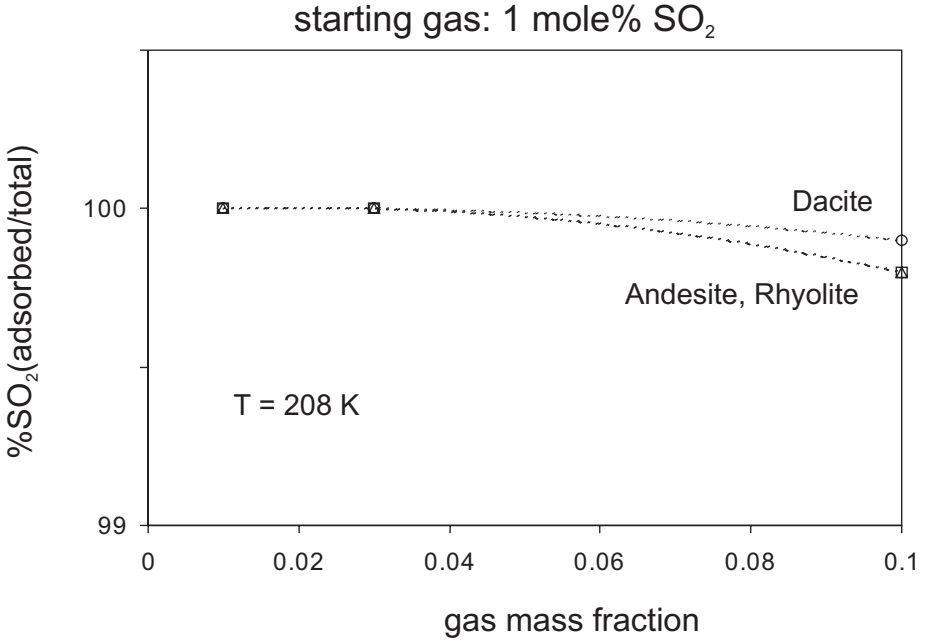

Figure 6.10: Enlarged detail of Figure 6.9. The fraction of adsorbed gas relative to the total amount of SO_2 in the plume, against the gas mass fraction σ.

Variation of x_{SO_2}

The higher the molar fraction of SO_2 in the starting gas mixture x_{SO_2} ($x_{SO_2} = n_{SO_2}/n_{Gas}$), the higher is the partial pressure of SO_2 in the ascending eruption mixture and consequently, the higher is the final partial pressure, controlling adsorption. The concentration of adsorbed gas (c_{SO_2}) is correlated via a potential function to the partial pressure (p_{SO_2}) at which the adsorption takes place (see Table 4.7, page 69). According to the regression models for the glasses (see Table 4.7), the concentration of adsorbed SO_2 approximately is proportional to $p_{SO_2}^{0.3}$:

$$c_{SO_2} \sim p_{SO_2}^{0.3} \leftrightarrow c_{SO_2} \sim n_{SO_2}^{0.3} \tag{6.13}$$

From equation 6.13 follows, that an increase in the amount of SO_2 in the plume by a factor ξ only can result in an increase of the amount of adsorbed SO_2 by a factor $\xi^{0.3}$:

$$\begin{aligned} n_{SO_2} &\mapsto \xi \cdot n_{SO_2} \\ &\Leftrightarrow \\ c_{SO_2} &\mapsto \xi^{0.3} \cdot c_{SO_2} \end{aligned}$$

According to the preceding considerations it follows, that the higher the molar fraction of SO_2 in the starting gas, the less is the percentage fraction of adsorbed SO_2, relative to the totally available amount in the eruption column. In Figure 6.11, the molar fraction of SO_2 in the starting gas mixture varies, as well as in their gas mass fractions.

This is an important result. It implies that eruptions releasing the same total amount of SO_2 can have very different effects on climate, depending on wether the SO_2 is strongly diluted by water vapour or relatively concentrated. If the SO_2 is very diluted in the volcanic gas, it will be nearly completely adsorbed by the volcanic ash and accordingly, the impact of such eruptions on the environment is likely to be small. On the other hand, if the SO_2 concentration in the volcanic gas is high, only part of it will be adsorbed and a much stronger impact of the eruption on climate is expected. If one compares two eruptions releasing the same total amount of SO_2, the one releasing more water vapour will probably be more explosive. However, since the dilution of the SO_2 by water vapour makes surface adsorption on ash more feasible, the eruption will have a smaller impact on climate than a smaller eruption that releases less total volatiles but the same amount of SO_2. SO_2 adsorption on ashes therefore is a decisive factor in controlling the environmental input of volcanic eruptions. In particular, it can explain why atmospheric cooling does not necesseraly correlate with the magnitude of the eruption or the total amount of sulfur release.

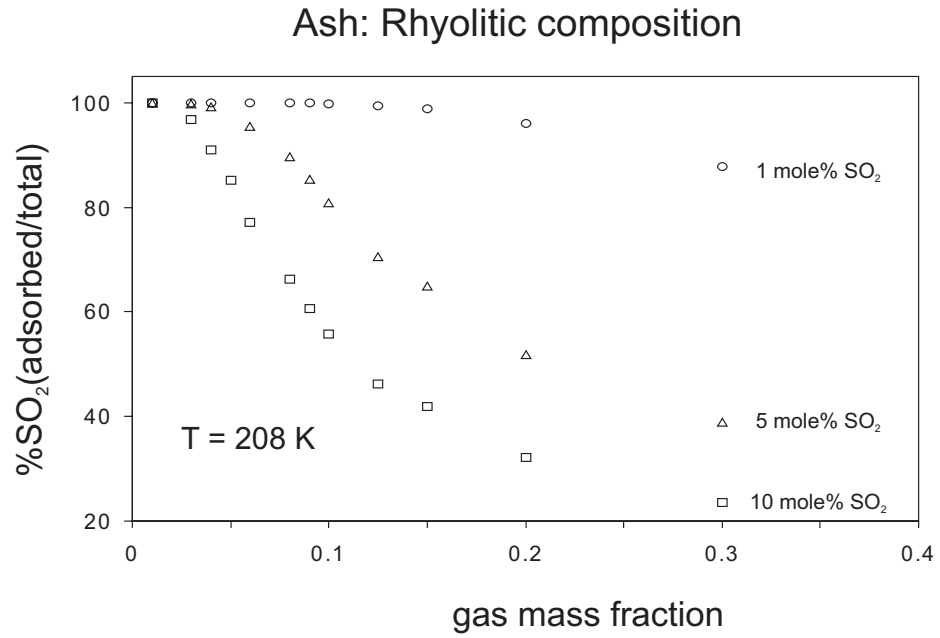

Figure 6.11: The percentage fraction of adsorbed gas relative to the total amount of SO_2 in the plume versus the gas mass fraction σ. The different graphs refer to different contents of SO_2 in the starting gas mixture.

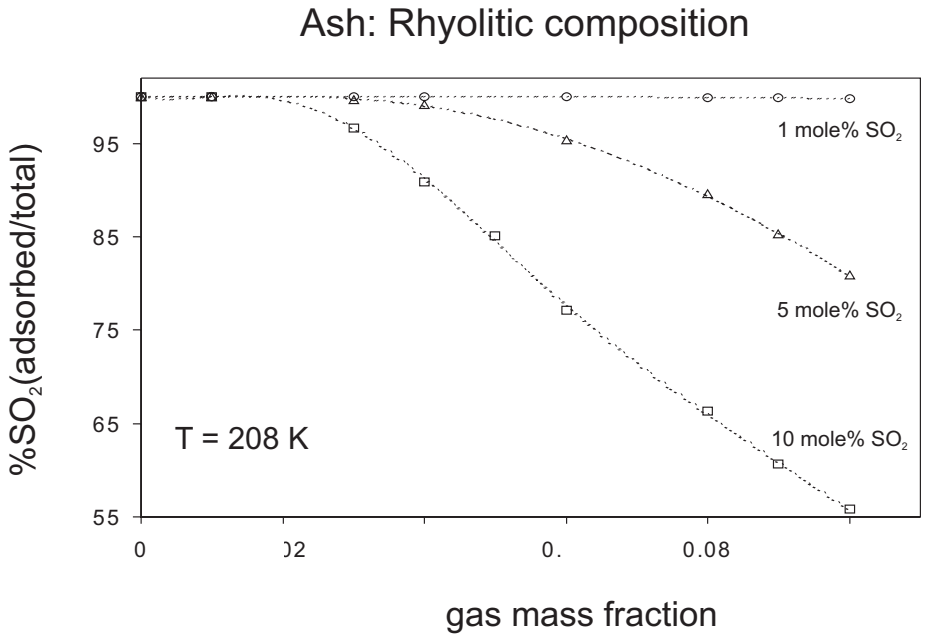

Figure 6.12: Enlarged detail of Figure 6.11. The percentage fraction of adsorbed gas relative to the total amount of SO_2 in the plume versus the gas mass fraction σ. The different graphs refer to different contents of SO_2 in the starting gas mixture.

The preceding model calculations have shown, that during volcanic eruption considerable amounts of SO_2 could be scavenged from the eruption column by adsorption on volcanic ash.
The assumption, that all ash in the model is available as glassy material, does not entirely reflect natural processes, but is justifiable, because glass shards are likely to be the most abundant component in the fine grain size fraction of natural volcanic ashes[13]. These fine grain sizes are responsible for most of the surface area of the ash.
A principal limitation for the model calculations might be due to the application of the regression models for adsorption (see chapter 4.2.6) to 'natural' plumes, as the regression models derive from experiments, that were all performed in a pure SO_2 atmosphere. One might argue, that under natural conditions, a multitude of gaseous components compete for the available adsorption sites on the ash surface. Among the most abundant constituents of volcanic gases (see Table 1.1) the most likely to adsorb notably on the surface of volcanic ash is water vapour[17]. However, it can be assumed, that during the experiments each powder grain of the probed glass powder was covered by a thin layer of adsorbed H_2O[21], as the powder was produced under atmospheric conditions, e. g. atmospheric moisture. It is therefore reasonable to assume that the experimental data are realistic for the process occuring in natural plumes.

The model above assumes a homogeneous distribution of ash and volcanic gases. If some phase separation occured in the plume, concentrating ash particles in only a part of the plume, the extent of SO_2 adsorption could be reduced.
An other restriction to the model might be that for the development of the umbrella region of the plume no entrainment is allowed (see section 6.3). This is a commonly adopted assumption[37]. It implies, that the partial pressure of SO_2 will never fall below a final value as calculated in section 6.3.2. Considering a residence time of the SO_2-cloud of several days, weeks and months, the partial pressure of the gas will fall below this cited value. This implies, that some portion of the SO_2 desorbes again and is released to the atmosphere.
This effect, that the mass of measured SO_2 often increases for 1-2 days, independent of any volcanic contribution already was observed during SO_2 measurements by TOMS (Total Ozone Mapping Spectrometer)[8].
This also implies, that the reliability of remote measurements of SO_2 is restricted, as far as it does not incorporate the scavenging of SO_2 by adsorption on the surface of volcanic ash.

Chapter 7

Geological implications

In the following chapter the geological implications of SO_2 adsorption in a historical explosive eruption, the 1980 Mt. St. Helens eruption, are estimated. The constraints for adsorption of SO_2 were derived from estimates of the total impact of gas and mass of the considering eruption (see Table 7.1). In Table 7.2 parameters, such as the estimated gas mass fraction, the column height and the partial pressure of SO_2 in the umbrella region of the plume of the Mt. St. Helens eruption, are listed. The number for the gas mass fraction was derived directly from the parameters characterizing the total impact of the eruption as listed in Table 7.1. Based on the gas mass fraction and the composition of the volcanic gas (see Table 7.1) the numbers for the column height H_t and the partial pressure of SO_2 (e. g. p_{SO_2}) were derived according to the algorithms used for developing the plume model in chapter 6.

Table 7.1: Composition of the volcanic gas during the Mt. St. Helens eruption. The concentration of the listed species are given in mole%. Mass volume is given as **D**ense**R**ock**E**quivalent.

Site	Date	H_2O[a]	CO_2[a]	SO_2[a]	HCl[a]	total SO_2[b]	mass volume (DRE)[c]	magma composition[b]	ρ
St. Helens	1980	91.58	6.64	0.29	0.59	1.0 Mt	0.25 km^3	dacite	2.3g/cm^3

[a] [39]
[b] [18]
[c] [34]

Table 7.2: Mt. St. Helens eruption parameters mainly derived from the parameters listed in Table 7.1.

	T_0 [a]	σ [b]	H_t [c]	p_{SO_2} [d]	T_{ads} [e]	A_{Ash} [f]
St. Helens	1000	0.2	7	0.03	201	$1.12 \cdot 10^{10}$

[a] Starting temperature of the mixture in K, arbitrary.
[b] Gas mass fraction, derived from numbers in Table 7.1.
[c] Column height in km according to eq. 6.3.
[d] Partial pressure of SO_2 at height H_t in mbar.
[e] Temperature in K, assumed for the adsorption process.
[f] Surface area of ash in km^2

A limitation of this approach arises from the assumption, that the total mass of erupted gas and magma is due to a single continuous eruption. It neither takes into consideration the period of the eruption, nor does it allow for discontinuous input, nor does it reflect the complex processes taking place during the eruption. The temperature T_{ads} decisive for the amount of adsorbable SO_2 was not derived from the estimated column height, as it was suggested in section 6.4.1. Instead it was assumed, that the column height exceeded the calculated height of 7 km, as with such a low column height the plume is supposed to collapse rapidly. The surface area of ash A_{Ash} that is listed in Table 7.2 was calculated from the total impact of mass of the eruption (see Table 7.1), adopting the grain size distribution depicted in Figure 6.7.
The following model calculation intends to show the possible effects of adsorption of SO_2 particularly with regard to the evaluation of remote measurements of SO_2.
Starting point is the assumption, that the amount of SO_2 detected during an eruption does not show the total impact of SO_2, as it does not incorporate the amount of SO_2, that was removed from the atmosphere by being adsorbed on the surface of the ejected ash. Consequently, the amount detected by remote measurements only represents some portion of the total impact, namely the portion, that was not removed by adsorption. Due to that approach, the number listed as 'total SO_2' in Table 7.1 was assumed to represent the non-adsorbed portion of SO_2 only. Based on the regression model for adsorption onto dacite (see Table 4.7) it was estimated how much SO_2 originally should have been injected into the atmosphere, to give the amount of the 'total SO_2' as the remainder ($\leftrightarrow$ 1 Mt) of the assumed adsorption of the gas. Two values for the resulting 'original amount' of SO_2 were calculated and are listed in Table 7.3. The values refer to different values of ash surface, available for adsorption. The first value assumes, that 100 % of the surface area of ash that is listed in Table 7.2 actually is available to adsorption, whereas the second value assumes, that the surface area of ash that

is suspended is less. In line with the model calculation, the estimated amount of originally released SO_2 ($\leftrightarrow$8–9 Mt) clearly exceeds the amount remaining detectable in the atmosphere ($\leftrightarrow$1 Mt) by severalfold (see Table 7.3), independent of the presumed value for the surface area.

The estimated amount of adsorbed SO_2 is supposed to partly desorb again, for example when the partial pressure of SO_2 drops due to dilution. Adsorption experiments at room temperature suggest, that the binding of nearly the whole first monolayer is irreversible (see section 4.1.2). From the BET constants, that were derived from the adsorption experiments (see Table 4.4), the amount of SO_2, necessary to give a monolayer coverage of the suspended ash, was calculated (see values for $V_m(A_{Ash})$ in Table 7.3). Accordingly, it was assumed, that after some time, the originally adsorbed SO_2 desorbes again, except for the first monolayer, and is released to the atmosphere again. The according values for the amount of releasable SO_2 (see Table 7.3) range from 0–1 Mt, depending on the underlying value of the surface area of ash. The amount of releasable SO_2 particularly supports the idea, that the known effect, that the mass of measured SO_2 often increases for 1-2 days[8], can be described in terms of adsorption- and desorption processes. The results of the model calculation also imply, that the reliability of remote measurements of SO_2 is restricted, as far as it does not incorporate the scavenging of SO_2 by adsorption on the surface of volcanic ash.

Table 7.3: SO_2 balance of the Mt. St. Helens eruption. The amount of adsorbed SO_2 was calculated by applying the regression model for adsorption on dacite (see Table 4.7) to $p_{SO_2} = 0.03$ mbar and $T_{ads} = 1000$ K, accounting for the successive drop of the partial pressure of SO_2 in the cloud due to adsorption (see diagram in Table 6.6). The amount of releasable SO_2 is based on the assumption, that a monolayer of SO_2 ($V_m(A_{Ash})$) was adsorbed irreversibly.

% of A_{Ash}[a]	$V_m(A_{Ash})$[b]	SO_2 adsorbed[c]	'original' SO_2[d]	SO_2 releasable[e] (after some time)
100%	8 Mt	8 Mt	9 Mt	0
80%	6 Mt	7 Mt	8 Mt	1 Mt

[a] surface area of the ash, as % portion of the total surface area A_{Ash}, listed in Table 7.2
[b] total monolayer capacity of the given ash surface at STP, with $V_m = 0.25 cm^3/m^2$
[c] total amount of adsorbed SO_2
[d] originally exhausted amount of SO_2, before adsorption
[e] amount of SO_2 that could be released to the atmosphere after some days, due to desorption

Bibliography

[1] Kohlenstoff. In Gmelin-Institut für anorganische Chemie und Grenzgebiete, editor, *Handbuch der anorganischen Chemie.*, volume C.

[2] Sauerstoff. Lfg. 5. In Gmelin-Institut für anorganische Chemie und Grenzgebiete, editor, *Handbuch der anorganischen Chemie.* Springer, Berlin, 1963.

[3] Chlor. Ergänzungsband Teil B; Lfg. 1. In Gmelin-Institut für anorganische Chemie und Grenzgebiete, editor, *Handbuch der anorganischen Chemie.* Springer, Berlin, 1968.

[4] Sauerstoff. Lfg. 4. In Gmelin-Institut für anorganische Chemie und Grenzgebiete, editor, *Handbuch der anorganischen Chemie.* Springer, Berlin, 1969.

[5] Schwefel. Ergänzungsband 3. In Gmelin-Institut für anorganische Chemie und Grenzgebiete, editor, *Handbuch der anorganischen Chemie.* Springer, Berlin, 1980.

[6] C. D. Ahrens. *Meteorolgy today.* West Publishing Company, 1994.

[7] L. S. Aiken and S. G. West. *Multiple regression.* Sage, 2001.

[8] G.J. Bluth, W.I. Rose, and S. Guo. The role of TOMS in understanding the fates of volcanic emissions. In *American Geophysical Union, Fall Meeting 2003*, 2003.

[9] S. Brunauer. *The adsorption of gases and vapors.*, volume 1. Princeton university press., Princeton, NJ, 1945.

[10] S. Brunauer, P. H. Emmett, and E. Teller. Adsorption of gases in multimolecular layers. *J. Am. Soc.*, 1938.

[11] M. Bursik and R. S. J. Sparks. The concentration of ash in volcanic plumes, inferred from dispersal. In *US Geological Survey Bulletin, Report B2047*, pages 19–29, 1994.

[12] S. C. Carey and M. Bursik. Volcanic plumes. In *Encyclopedia of Volcanoes*, pages 527–544. H. Sigurdsson, 2000.

[13] S. N. Carey and H. Sigurdsson. Influence of particle aggregation on deposition of distal tephra from the may 18, 1980, eruption of Mount St. Helens volcano. *J. Geophys. Res.*, 87:7061–7072, 1982.

[14] D. Claque and W. A. Bohrson. Origin of xenoliths in the trachyte at Puu Waawaa, Hualai volcano, Hawaii. *Contr.Min.Pet.*, 108:439–452, 1991.

[15] M. H. Conklin and R. C. Bales. SO_2 uptake on ice spheres: Liquid nature of the ice-air interface. *J. Geophys. Res.*, 98:16851–16855, 1993.

[16] J. H. de Boer, B. C. Lippens, J. C. P. Broekhoff, A. van den Heuvel, and T. J. Osinga. The t-curve of multimolecular N_2-adsorption. *Journal of Colloid and Interface Science*, 21:405–414, 1966.

[17] P. Delmelle, F. Villiéras, and M. Pelletier. Surface area, porosity and water adsorption properties fo fine volcanic ash particles. *Bull. Volcanol.*, 67:160–169, 2005.

[18] R. G. Grainger and E. J. Highwood. Changes in stratospheric composition, chemistry, radiation and climate caused by volcanic eruptions. In *Volcanic degassing*, volume 213, pages 329–347. Geological Society, 2003.

[19] S. J. Gregg and K. S. W. Sing. *Adsorption, surface area and porosity.* Academic Press., London, 1982.

[20] J. B. Hunt, P. D. Clift, C. Lacasse, T. L. Vallier, and R. Werner. 7th Interlaboratory comparison of electron probe microanalysis of glass geochemistry. In *Proceeding of the ocean drilling program, scientific results*, volume 152, pages 85–91, 1998.

[21] H. Keppler and M. Rauch. Water solubility in nominally anhydrous minerals measured by FTIR and H MAS NMR: the effect of sample preparation. *Phys. Chem. Minerals*, 27:371–376, 2000.

[22] M. T. Leu. Heterogeneous reaction of N_2O_5 with H_2O and HCl on ice surfaces: Implications for antarctic ozone depletion. *Geophys. Res. Let.*, 15(8):851–854, 1988.

[23] R. I. Masel. *Principles of adsorption and reaction on solid surface.* John Wiley & Sons, Inc., 1996.

[24] M. P. McCormick, L. W. Thomason, and C. R. Trepte. Atmospheric effects of the Mt Pinatubo eruption. *Nature*, 37:399–404, 1995.

[25] M. J. Mills. Volcanic aerosols and global atmospheric effects. In *Encyclopedia of Volcanoes*, pages 941–943. H. Sigurdsson, 2000.

[26] D. Myers. *Surfaces, interfaces, and colloids. Principles and applications.* John Wiley & Sons, Inc., 1999.

[27] D. M. Pyle. How did the summer go? *Nature*, 393:415–417, 1998.

[28] D. M. Pyle. Sizes of volcanic eruptions. In *Encyclopedia of Volcanoes*, pages 263–269. H. Sigurdsson, 2000.

[29] M. R. Rampino and S. Self. Sulphur-rich volcanic eruptions and stratospheric aerosols. *Nature*, 310, 1984.

[30] P. Richet. Heat capacity of silicate glasses. *Chemical Geology*, 62:111–124, 1987.

[31] A. Robock. Volcanic eruptions and climate. *Rev. of Geophys.*, 38(2):191–219, 2000.

[32] W. I. Rose. Scavenging of volcanic aerosol by ash: Atmospheric and volcanologic implications. *Geology*, 5:621–624, 1977.

[33] A. M. Sarna-Wojcicki, S. Shipley, R. B. Waitt, D. Dzurisin, and S. H. Wood. Areal distribution, thickness, mass, volume and grain size of air-fall ash from six major eruptions of 1980. *U. S. Geological Survey Professional Paper*, P 1250:577–600, 1981.

[34] B. Scaillet, J. Luhr, and M. R. Carroll. Petrological and volanological constraints on volcanic sulfur emissions to the atmosphere. In *Volcanism and the earth's atmosphere*, pages 11–54. American Geophphysikal Union, 1991.

[35] M. R. Schoeberl and et. al. Investigation of chemical and dynamical changes in the stratosphere up to and during the eos observing period. In *Progress Report on EOS IDS*, 1995.

[36] S. Self, J.-X. Zhao, R. E. Holasek, R. C. Torres, and A. J. King. The atmospheric impact of the 1991 mount pinatubo eruption. In *Fire and Mud. Eruptions and Lahars of Mount Pinatubo, Philippines.*, pages 1089–1111. Phillipine Institute of Volcanology and Seismolog & University of Washington Press, 1996.

[37] R. S. J. Sparks, M. I. Bursik, S. N. Carey, J. S. Gilbert, L. S. Glaze, H. Sigurdsson, and A. W. Woods. *Volcanic Plumes.* John Wiley & Sons Ltd, 1997.

[38] J. Stix and H. Gaonac'h. Gas, plume, and thermal monitoring. In *Encyclopedia of Volcanoes.* H. Sigurdsson, 2000.

[39] R. B. Symonds, W. I. Rose, G. J. S. Bluth, and T. M. Gerlach. Volcanic-gas studies: Methods, results and applications. *Rev. Min.*, 30:1–60, 1994.

[40] A. Tabazadeh and R. P. Turco. Stratospheric chlorine injection by volcanic eruptions: HCl scavenging and implications for ozone. *Science*, 260:1082–1085, 1993.

[41] H. S. Taylor. The activation energy of adsorption processes. *J. Am. Soc.*, 1931.

[42] C. Textor, H. Graf, C. Timmreck, and A. Robock. Emissions from volcanoes. In *Emission of chemical compounds and aerosols in the atmosphere.* Kluwer academic publisher, 2003.

[43] J. Topping. *Fehlerrechnung.* Physik-Verl., Weinheim, 1975.

[44] H. Vogel, editor. *Gerthsen Physik.* Springer-Verlag, Berlin Heidelberg, 1995.